Structuring the hydrodynamics of the Elbe estuary

Master thesis

UNIVERSITY OF TWENTE.

Nelen & Schuurmans

Version 10-10-2024

K. Korporaal, S2279304
Civil Engineering & Management

Master thesis

Supervisors:
Dr. Ir. P.C. Roos
Dr. Ir. E.M. Horstman
Dr. N.D. Volp
Ir. M. Siemerink
Ir. O. Baltus

Figure front page: Elbe estuary (GEODUS, n.d.)

Preface

This report marks the completion of my Master's in Civil Engineering and Management at the University of Twente. Over the past six months, I have worked hard to complete my research on "Structuring the hydrodynamics of the Elbe estuary". The primary goal was to explore whether a structured model with a subgrid captures the estuarine hydrodynamics accurately and computationally efficient, while also assessing how different model settings and schematizations influence the simulated hydrodynamics and computational performance.

I had the privilege of conducting my research at Nelen & Schuurmans in Utrecht, where I gained valuable experience working in an engineering consultancy environment. I would like to thank Olof Baltus, Nicolette Volp, and Martijn Siemerink for their invaluable guidance throughout this process. Their insights during our weekly meetings greatly enhanced my research, and their feedback significantly improved this thesis. I am also grateful to all my colleagues at Nelen & Schuurmans who contributed to my work.

From the University of Twente, I want to thank Pieter Roos and Erik Horstman for their support and guidance during this process. Pieter Roos introduced me to this research topic early on, this gave me the confidence that I could successfully execute this type of research.

I am also grateful to the Federal Waterways Engineering and Research Institute (BAW) in Germany for providing the measurement data used in this research. This data was crucial for setting up the model and validating my results. Therefore, I would thank the team of the BAW for their valuable contribution.

Throughout this research, I have gained knowledge about estuarine hydrodynamics, particularly in the context of the Elbe estuary. I have also increased my modelling skills using 3Di and deepened my understanding of conducting scientific research. These past six months have been challenging, and I am especially thankful for the support and encouragement from my family and friends, which kept me motivated to the end. After countless hours of work and travel, I am pleased to finally complete my thesis.

I hope you enjoy reading my thesis.
Karla Korporaal
Leeuwarden, 10-10-2024

Abstract

Estuaries serve crucial roles, such as acting as navigation routes that link the sea to harbours. Understanding the complex hydrodynamics of estuaries is essential for managing these vital systems, especially when planning interventions or assessing risks. Numerical models are useful tools that simulate estuarine hydrodynamics, offering insights into processes like tidal movements and water level changes. They can predict critical conditions, such as water levels during storm surges, essential for flood risk assessment (Boehlich & Strotmann, 2008). Various numerical models exist which can simulate estuarine hydrodynamics, each with settings that influence their accuracy and computational efficiency (Bomers et al., 2019; Bounagui et al., 2003).

One distinction among numerical models is whether they incorporate the subgrid method. This method offers significant advantages in estuarine modelling, including enhanced computational efficiency and the ability to model partly dry/wet computational cells (Casulli, 2009; Volp et al., 2013). Research on the Elbe estuary, Germany, has shown that unstructured grids with subgrids improve accuracy and efficiency, but combining a structured grid with a subgrid has not been explored thoroughly. This study investigates whether a model with a structured grid and subgrid can accurately and efficiently capture estuarine hydrodynamics, and how factors like tidal boundary, grid width, time step, grid refinements, roughness values, and river discharge impact simulation results. This research uses the 3Di software, which supports structured grids with subgrids and continues to use the Elbe estuary as study area.

Instead of using a non-spatially and temporally varying tidal boundary, a more realistic spatially and varying tidal boundary, consisting of multiple 1D boundaries, was implemented. This boundary better captured small-scale water level variations in the sea region, while its accuracy in the upstream regions was similar to the simulation with a non-spatially varying tidal boundary. The settings of the 1D boundaries affected the total in- and outflow volumes and momentum, influencing hydrodynamics across the estuary in both timing and magnitude. To enhance natural flow patterns and prevent unrealistic high velocities and water levels an extra line of computational cells was added at the boundary.

Next, an analysis on grid width and time step was conducted. Increasing the grid width reduced tidal ranges in the river due to increased numerical diffusion, while larger grid widths resulted in unexpectedly larger tidal ranges in the sea area. Further research is needed to understand this effect. Larger time steps increased tidal ranges and delays, as they fail to capture certain

small-scale processes that would otherwise lead to energy dissipation. Ultimately, larger grid widths or time steps reduce computational time but affect accuracy negatively.

Instead of using an uniform grid width, applying grid refinements can enhance both model accuracy and computational efficiency. Strategically placing refinements in complex flow areas, such as the river widening and main navigation channel, can improve the hydrodynamic results. A coarse grid can be used in open sea regions if critical areas are properly refined. While refinements enhance accuracy in specific regions, they can also increase computational time if the number of computational cells increases. Thus, balancing grid width and refinements is essential. For the Elbe estuary, refining the navigation channel is crucial.

Finally, the bottom roughness and river discharge were systematically varied to assess their effects on hydrodynamic results. Lower roughness values led to larger tidal ranges due to reduced energy dissipation. Additionally, river boundary influence was greater during low tide, when tidal forces are weaker. Increased river discharge raised water levels, but its effect decreased with distance from the river boundary.

In conclusion, this research show that model settings and schematizations significantly affect simulated estuarine hydrodynamics and computational efficiency. The 3Di subgrid model shows promise for large-scale estuarine studies, as it accurately captured the hydrodynamics of the Elbe estuary with discrepancies of less than 10 cm compared to measurements, while requiring just 5 minutes of computational time for a 15-day simulation.

Table of Contents

Preface **2**

Abstract **4**

1 Introduction **8**
1.1 Relevance of estuaries 8
1.2 Characteristics of estuaries 8
1.3 Hydrodynamic numerical modelling 10
1.4 3Di software 14
1.5 Knowledge gap 15
1.6 Objective and research questions 16
1.7 Report outline 16

2 Study area: The Elbe estuary **18**

3 Methodology **22**
3.1 Phase 1: Model setup 23
3.2 Phase 2: Defining cases 27
3.3 Phase 3: Comparison strategy 32

4 Results Q1: Spatially and temporally varying tidal boundary condition **34**
4.1 Connection node storage area and boundary channel length 34
4.2 Tidal "tub" 39
4.3 Validation of applied boundary conditions 39

5 Results Q2: Grid width and Time step **42**
5.1 Grid width 42
5.2 Time step 47
5.3 Combination time step and grid width 50

6 Results Q3: Local grid refinements **52**
6.1 Port of Hamburg 52
6.2 River widening, river/sea division and navigation channel 56

6.3 Combining findings 61

7 Results Q4: Roughness values and River discharge 66
7.1 Roughness values 66
7.2 River discharge 69

8 Discussion 72
8.1 Impact of subgrid 72
8.2 Impact of boundary settings 73
8.3 Impact of grid width, grid refinements and time step setting 74
8.4 Impact of roughness value and river discharge 75

9 Conclusion and Recommendations 76
9.1 Conclusion 76
9.2 Recommendations for future research 79

References 83

A Details of the methodology 84
A.1 Phase 1: Subgrid 84
A.2 Phase 2: Defining cases 87

B Q1: Spatially and temporally varying boundary condition 88
B.1 Connection node storage area 88
B.2 Boundary channel length 91
B.3 Performance check on applied boundaries 93

C Q2: grid width and time step analysis 96
C.1 grid width 96
C.2 Time step 98

D Q3: Local grid refinements 102
D.1 Port of Hamburg 102
D.2 River widening 104
D.3 River sea connection 108
D.4 Navigation channel 112
D.5 Combination 114

E Q4: Roughness values and river discharge 118
E.1 Roughness values 118
E.2 river discharge 121

Chapter 1

Introduction

1.1 Relevance of estuaries

Estuarine environments are important for various reasons. They have environmental, commercial and cultural significance. Firstly, they fulfil essential environmental functions, including water purification by settlement of sediments and absorption of nutrients (Barbier et al., 2011; Ostroumov, 2006). Additionally, they have a role in the regulation of the climate system by exchanging gases between water, sediment and the atmosphere (Thrush et al., 2014). Moreover, estuaries have a rich biodiversity, where numerous fish species can be found (Elliott et al., 2007; Potter et al., 2015; Vasconcelos et al., 2011).

Secondly, estuaries function as navigation routes, linking the sea to the harbours near the river entrances (Jiang et al., 2012). This accessibility is essential for various maritime activities, including fishing and cargo transportation, which significantly contribute to the economic value of the surrounding areas (Thrush et al., 2014). Therefore, estuaries also have a commercial function. For instance, in the case of the Elbe estuary, cargo ships navigate to the Port of Hamburg, the third largest harbour in Europe, making it a hub for regional and international trade (Shipsgo, 2023).

Thirdly, they have a cultural significance, by functioning as a recreational place offering opportunities for activities, such as sailing and swimming (Thrush et al., 2014).

1.2 Characteristics of estuaries

Estuarine environments, as highlighted in the previous section, have multiple environmental, commercial and cultural benefits. However, their complex and dynamic nature makes understanding their behaviour challenging. To manage and protect these environments, it is crucial to first identify their characteristics and dynamics. This understanding forms the basis for developing accurate models to simulate estuarine behaviour under various conditions.

Estuarine ecosystems are widespread across the globe. According to Elliott and McLusky (2002) and Potter et al. (2010), a distinction can be made between estuaries in the northern and the southern hemisphere based on freshwater inflow and salinity. Northern estuaries receive consistent river input, leading to fluctuating but hyposaline conditions, while southern estuaries, with limited inflow, can become hypersaline due to evaporation and may periodically close off from the sea.

Estuarine environments are defined as transitional waters, which are the waters between land and sea, for example, lagoons, bays, and deltas (Elliott & Whitfield, 2011; Telesh & Khlebovich, 2010). According to Telesh and Khlebovich (2010), typical estuarine environments contain brackish water. Estuarine ecosystems have a unique blend of characteristics, due to the transition of marine water to freshwater. Therefore, estuarine areas are seen as ecosystems on their own and not part of the marine or freshwater ecosystems (Elliott & Whitfield, 2011). In the estuarine environment, a salinity gradient appears at this transition. The key characteristic of an estuary is the mixing of salt water and fresh water. The maximum mixing takes place in the middle part of the estuary. The upper estuary is mainly dominated by freshwater and the lower estuary is marine-dominated (Whitfield & Elliott, 2011) (Figure 1.1).

Estuarine environments can be classified using its tidal characteristics. An estuary can be micro, meso or macro tidal. This depends on the tidal range within the estuary. It is important to know the tidal range in the estuary to get insight in the hydrodynamics of the estuary, particularly important for flood risk management strategies. An estuary is microtidal if the tidal range is less than 2 meters, mesotidal if the range is between 2 and 4 meters and macrotidal if the range is larger than 4 meters (Leonard & Reed, 2002; Short, 1991; Tweedley et al., 2016). There can be tidal asymmetry in an estuary, implying that the duration and magnitude differ between flood and ebb tidal flow (Gong et al., 2016). A system is flood dominant if the tide is shorter rising than falling and has higher flood than ebb velocities (Herrling et al., 2021). If it is the other way around the system is ebb dominant.

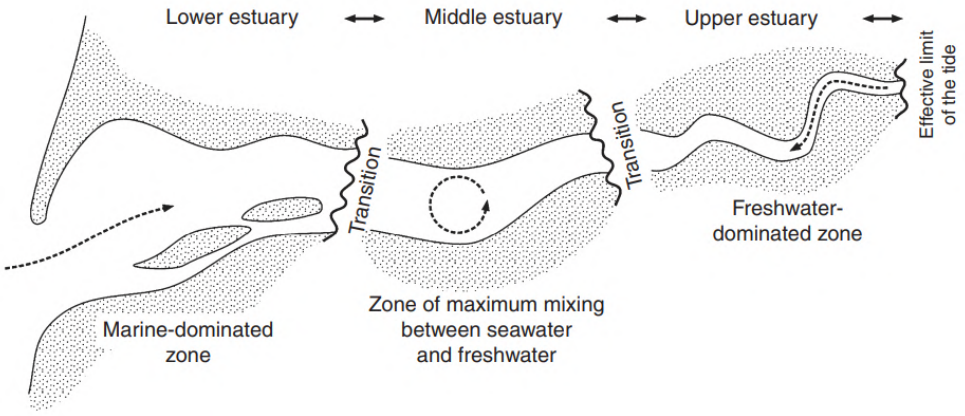

Figure 1.1: Schematic representation of a 'standard' estuary (Whitfield & Elliott, 2011)

1.3 Hydrodynamic numerical modelling

Building on the understanding of estuarine characteristics, the next step is to translate this knowledge into predictive tools. Hydrodynamic modelling is essential for simulating and analyzing estuarine behaviour. These models can simulate future scenarios, such as nautical water depths during low river flows (Jiang et al., 2012) or water levels during storm surges, crucial for flood risk management in the hinterland (Boehlich & Strotmann, 2008). The insights gained from these simulations serve as invaluable resources for stakeholders in the study area, aiding in informed decision-making and risk management.

A hydrodynamic numerical model creates an idealized representation of the hydrodynamics in the natural system. As noted by Levins (1966), developing such models requires balancing accuracy with computational efficiency. Setting up a model involves key decisions, such as spatial resolution, the physical processes to include, and the methods for solving the flow equations, all affecting both model's accuracy as computational efficiency.

The flow equations describe how water flow over time and space, providing insights into the dynamics of the system. To facilitate this, a grid framework divides the spatial domain into a finite set of cells, allowing these equations to be solved numerically. In the following section, different grid structures and their respective advantages and disadvantages in capturing the complex dynamics of estuaries will be explored.

1.3.1 Grid structures

Different grid structures exist, and the choice of which to use depends on several factors. Key criteria influencing grid selection include the complexity of the bathymetry, which may necessitate finer resolution for accurate flow representation. Computational time is also a critical consideration; while finer grids enhance accuracy in regions of interest, they can increase simulation time and resource demands. Balancing these factors is essential for selecting the appropriate grid structure (Lane et al., 1999).

The three main grid structure types used are structured, unstructured and hybrid grids (Figure 1.2). Within structured grids, two variants exist: rectilinear and curvilinear grids. Rectilinear grids have grid lines parallel to the Cartesian coordinate system, resulting in rectangular cells (Sang & Li, 2007). If the grid lines are uniformly distributed over the axis then the cells are squares, this is called a uniform grid (He et al., 1996). A uniform grid has perfect orthogonality. Orthogonal grids not only reduce computational time, but also enhance model accuracy due to a reduction in numerical diffusion compared to non-orthogonal grids (Bomers et al., 2019; Kernkamp et al., 2011). On rectilinear grids local grid refinement can be applied, allowing for increased resolution in specific areas of interest (Alakashi & Basuno, 2014). However, complex geometries can still be difficult to capture with rectilinear grids.

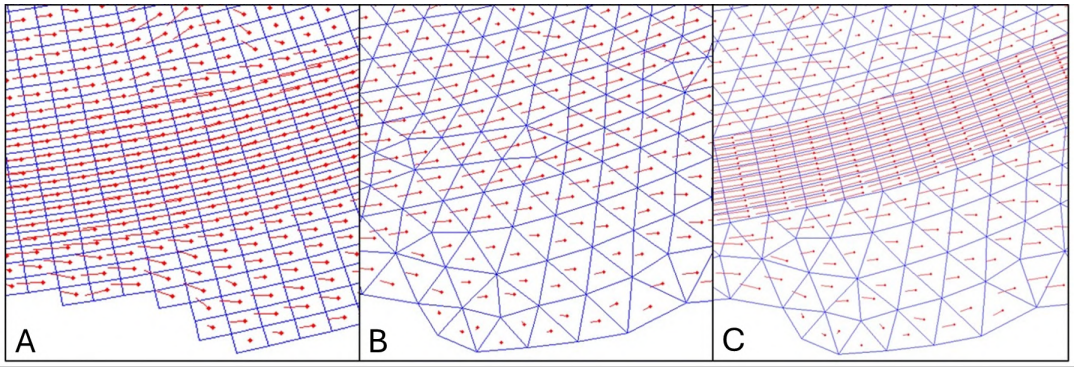

Figure 1.2: Example of grid types, A: structured grid, B: unstructured grid, C: hybrid grid (Bomers et al., 2019)

The quad-tree method is one of the existing local grid refinement techniques. This method divides each computational cell into four quadrants, while ensuring that neighboring cells differ in size by no more than a factor of two (Stelling, 2012). Smaller grids can be applied in areas with high interest, while larger grids can be applied in areas requiring less details (Dahm et al., 2014), an example is illustrated in Figure 1.3. By applying finer grids only where necessary, the quad-tree method optimizes computational time.

The second variant of structured grids are curvilinear grids, where the cells align with the bank lines of a river (Morianou et al., 2016). This grid design allows for stretching along the river's main channel (Lai, 2010) and provides higher resolution in the inner bends of the river (Bomers et al., 2019), as shown in Figure 1.4. However, curvilinear grids are less effective at capturing geometric features like bifurcations, and local grid refinement will also increase the resolution of the main channel (Bomers et al., 2019; Lai, 2010).

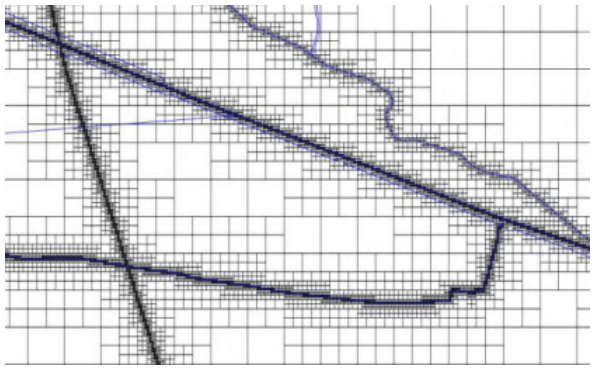

Figure 1.3: Local refinement using the quad-tree method (Dahm et al., 2014)

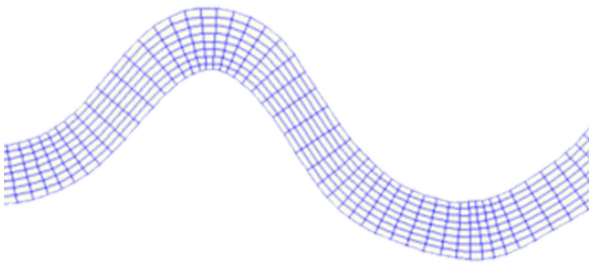

Figure 1.4: Curvilinear grid example (Bomers et al., 2019)

Alternatively, an unstructured grid often contains triangular-shaped cells (Figure 1.2), allowing for the most flexibility (Lai, 2010). Unstructured grids can capture complex geometries, but their accuracy relies on the alignment of the grid (Zhang et al., 2012). Also unstructured grids require high computational times (Klingbeil et al., 2018). Furthermore, it is not possible to stretch the triangles in the flow direction.

Finally, a hybrid grid combines the strengths of structured and unstructured grids (Bomers et al., 2019) (Figure 1.2). This grid optimises computational time while having high accuracy in certain areas of interest. However, it is not suitable for all models, as not all software supports the combination of different grid types because of their complexity (Sang & Li, 2007).

1.3.2 Subgrid

Within grid structures, a subgrid can be applied. This can be useful if high-accuracy bathymetric data is available. When a model, without subgrid, is created with high resolution bathymetric data, the computational cells may become very small if this same resolution is applied. This will result in many computational cells, increasing the computational time of the model (Bounagui et al., 2003). The use of a subgrid method can mitigate this problem.

The subgrid method is based on the idea that water levels vary more gradually than the bathymetry. The water level and bathymetry are assumed to be uniform in a computational cell in most hydrodynamic models without subgrid, to achieve this the bathymetry is averaged on a grid cell resulting in a less accurate bathymetry, as illustrated in Figure 1.5. If a subgrid is applied, the bathymetry can vary within a computational cell (Casulli, 2009), as shown in Figure 1.6.

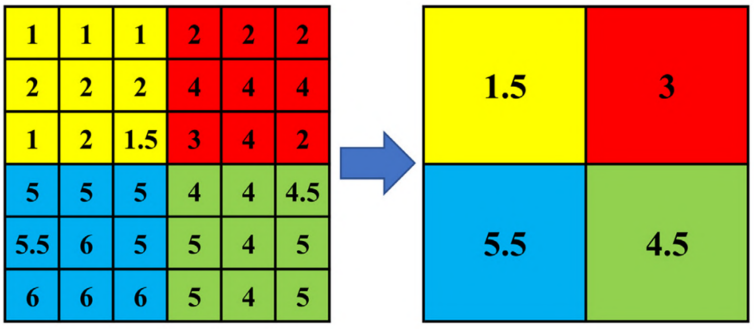

Figure 1.5: Example of data averaging from 36 to four computational cells, resulting in a lower accurate bathymetry for a model without subgrid (Wijaya et al., 2023)

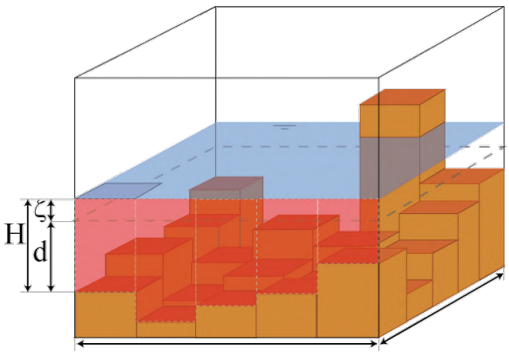

Figure 1.6: Subgrid (orange) with a high-resolution bathymetry and a coarse computational cell (blue) (H = water depth, ζ = water level, d = bed level, dotted line = reference level) (Volp et al., 2013)

The overall quality of flow representation can improve with the use of a subgrid, when the same computational grid resolution is applied, as demonstrated by Volp et al. (2013). This is because volumes and cross-sectional areas are calculated using high-resolution bathymetric data (Casulli, 2009). The increased accuracy achieved through the subgrid method enables the use of a coarser computational grid. This coarser grid utilizes fewer computational cells, reducing computational time compared to models without subgrid refinement, while using the high-accuracy bathymetric data (Volp et al., 2013). Similar to the bathymetric data, friction parameters and infiltration properties can also be assigned to the subgrid (Stelling, 2012; Volp et al., 2013).

Another advantage, next to a reduction in computational time, is that the subgrid method allows for partially dry or wet computational cells. Models without a subgrid include computational cells in the flow equations only if the cell is wet, as determined by the flooding threshold; otherwise, the cells are assumed to be dry (Casulli, 2009). These cells may stay dry while in reality the cell is partly wet for example, so there can be an under or overestimation of the water volume at that location compared to reality. If the bathymetry within a computational can vary, this can result in a partially dry or wet cell.

1.4 3Di software

In this research, the Elbe estuary will be simulated with the hydrodynamic modelling software 3Di, provided by Nelen & Schuurmans (n.d.). The 3Di software contains a 2DH hydrodynamic model, which uses a structured grid in combination with the subgrid method (section 1.3.2). Local grid refinement can be implemented using the quad-tree method.

The depth-averaged velocity (u, v) will be defined in the x- and y-direction (Figure 1.7b). This approach is suitable for estuarine modelling since the dominant flow patterns are horizontal, and the main interest of the research is the horizontal spatial variations in flow velocities and water levels. In the 2DH model, water levels depend on the x and y location.

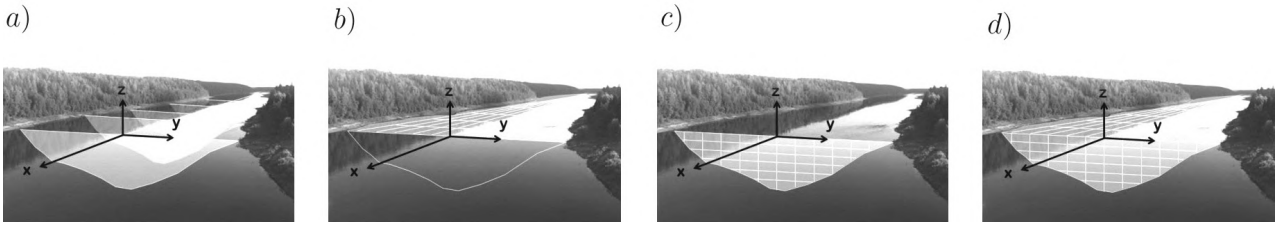

Figure 1.7: Schematization (a) 1D, (b) 2DH, (c) 2DV, (d) 3D model (Winckler, 2015)

The structured grid is staggered, where water levels are placed at cell centers and velocity variables are defined at cell edges (Figure 1.8). The hydrodynamics are calculated using the conservation of mass and momentum, assuming constant water density and hydrostatic pressure that depends only on water depth, both independent of temperature or salinity variations. The Coriolis effect is not included in the 3Di model.

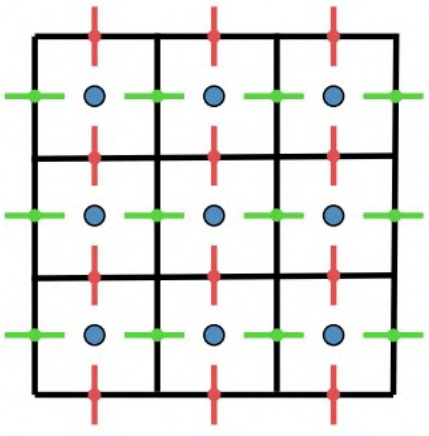

Figure 1.8: Staggered grid for a 2D model, velocities are defined on the red and green lines and water levels on the blue points (Lee & O'Sullivan, 2007)

1.5 Knowledge gap

One of the key choices in setting up a model is choosing a grid type. Unstructured grids are often preferred over structured grids in estuarine modelling due to their flexibility in achieving finer resolution, especially useful in areas with complex geometries, such as irregular coastlines commonly found in estuarine systems (Lai, 2010; Zhang et al., 2012). These complex geometries and irregular coastlines are harder to represent accurately with a structured grid (Alakashi & Basuno, 2014). Therefore, it is generally preferred and faster to apply an unstructured grid.

However, the application of a subgrid method can change this balance. As mentioned in section 1.3.2, the subgrid method enhances hydrodynamic accuracy by incorporating high-resolution bathymetry. This allows for the use of a coarser computational grid, reducing computational time compared to models without subgrid, while still maintaining similar accuracy in flow computations (Volp et al., 2013). Furthermore, the subgrid method enables the modelling of partly dry/wet computational cells, which is important in estuarine systems (Casulli, 2009; Volp et al., 2013). This capability allows for more accurate representation of coastlines within each computational cell, compared to models without subgrid. Additionally, using the quad-tree method, local refinement becomes possible, which can enhance the model's accuracy by placing fine grid in areas with high interest and larger grid cells in areas with lower interest, which improves computational efficiency. These capabilities make the subgrid method suitable for estuarine modelling. Moreover, these capabilities reduce the advantages that unstructured grids traditionally have over structured grids in estuarine modelling.

The Federal Waterways Engineering and Research Institute (BAW), responsible for waterways in Germany, currently uses an unstructured model with subgrid in the Elbe estuary, demonstrating good agreement in hydrodynamic results and improved computational efficiency compared to the traditional unstructured models (Sehili & Lang, 2014).

However, no thorough research has investigated the combination of a subgrid with a structured grid in the Elbe estuary. This combination holds the potential to further optimize both model accuracy and computational efficiency, but currently it is unknown if it captures estuarine hydrodynamics accurately. Additionally, no comprehensive analysis has been conducted on how various model settings, in conjunction with a subgrid, affect the accuracy of hydrodynamic results. The 3Di software is particularly suitable for this purpose, as it employs a structured grid in combination with a subgrid.

1.6 Objective and research questions

The objective of this research is to evaluate how combining a structured grid with a subgrid method enhances the accuracy and computational efficiency of estuarine modelling in the Elbe estuary. This research will explore if the structured model with subgrid captures the estuarine hydrodynamics accurately and computationally efficient, together with how various model settings and schematizations impact the simulated estuarine hydrodynamics and computational time. The study will use 3Di to conduct these analyses in the Elbe estuary.

To achieve the above research objective, four research questions will be answered:

Q1 How do the settings of a spatially and temporally varying tidal boundary condition affect the simulated estuarine hydrodynamics throughout the model domain?

Q2 How do grid width and time step settings affect the simulated estuarine hydrodynamics throughout the model domain and the computational time required for a simulation?

Q3 How do the location and extent of local grid refinements affect the simulated estuarine hydrodynamics throughout the model domain and the computational time required for a simulation?

Q4 How do the variations in uniform roughness values, as well as the inclusion/exclusion of upstream river discharge, influence the simulated estuarine hydrodynamics throughout the model domain?

This research focuses on the entire Elbe estuary in Germany, a large system that allows for an extensive analysis of its hydrodynamics, without the need to examine other estuaries in this study. The analysis will be conducted solely using 3Di. Since 3Di is a two-dimensional, depth-averaged (2DH) model, the impact on vertical flow structures will not be examined. Additionally, this study will concentrate solely on hydrodynamics within the estuary.

1.7 Report outline

In Chapter 2, the Elbe estuary will be introduced. This will be followed by the methodology in Chapter 3, including model setup, simulation cases and comparison criteria. Chapter 4 elaborates on the tidal boundary, relating to research question 1. Chapter 5 investigates the influence of grid width and time step, corresponding to research question 2. Chapter 6 discusses the influence of local grid refinements, relating to research question 3. In Chapter 7, the results for research question 4, which examines the influence of river discharge and roughness values, will be presented. In Chapter 8 the results and methods of this research will be discussed. Finally, Chapter 9 will provide the conclusion and recommendations based on the findings of this research.

Chapter 2

Study area: The Elbe estuary

The study area of this research is the Elbe estuary, which is situated in the north of Germany in the Northern hemisphere (Figure 2.1). The Elbe estuary has a open connection to the North Sea and receives fresh water input through the river Elbe.

The estuary stretches from Cuxhaven on the southern bank and Friedrichskoog on the northern bank (Elbe-km 724) up to the weir inland in Geesthacht (Elbe-km 586) (S. Hein et al., 2021). The Elbe-km indicates the distance of the location to the origin of the Elbe. The Elbe estuary, further shown in Figure 2.2, can be divided into three parts. The upper Elbe estuary is less than 10 m deep and reaches from Elbe-km 586 until Elbe-km 610. The middle Elbe estuary, reaches from Elbe-km 611 until Elbe-km 625 and the lower estuary is from Elbe-km 626 until the sea. The river mouth widens between Elbe-km 695 and 724 to a width of 17.5 km (Boehlich & Strotmann, 2008).

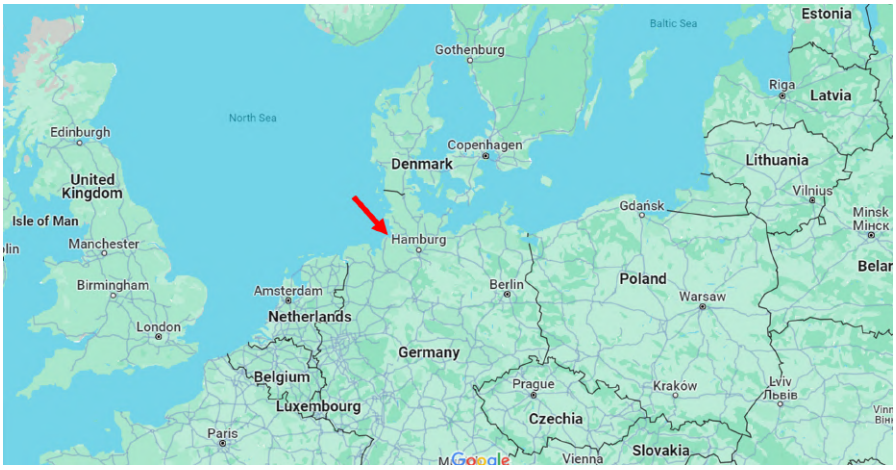

Figure 2.1: Map of northern Europe, red arrow indicates location of the Elbe estuary (Google Maps, 2024)

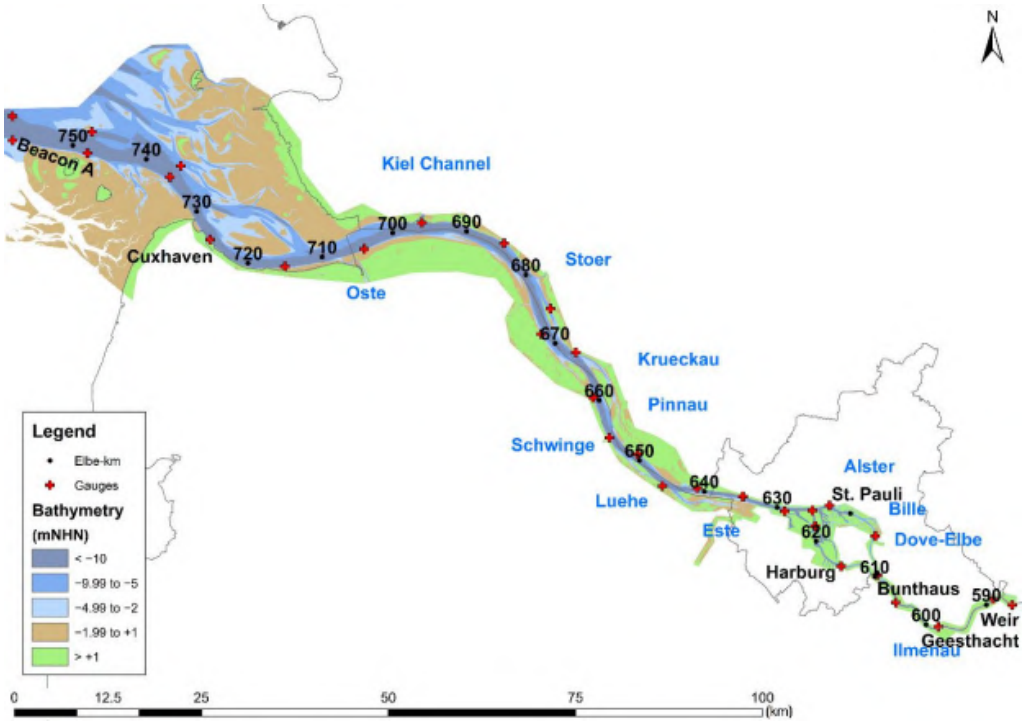

Figure 2.2: Map of the Elbe estuary, with colours indicating the bed levels compared to the mNHN (German Normalhöhennul, which is equal to NAP), numbers refer to Elbe-km (S. Hein et al., 2021)

.

The estuary receives inflow from the river Elbe. The Elbe River basin ranks as the fourth largest river basin in Central and Western Europe, covering an area of 148.268 km^2. 66% of the basin lies within Germany, with the remaining portion in the Czech Republic, Austria, and Poland. The Elbe originates in the Giant Mountains located in Poland and is 1100 km long (ICPER, 2016). The runoff regime is characterized by rain and snow, causing a seasonal variation in the Elbe discharges (Bartl et al., 2009; S. Hein et al., 2021).

According to S. Hein et al. (2021) the most characteristics discharge values measured at Neu Darchau (Elbe-km 536) for the time series 2000 to 2018 are:

- Mean discharge: 674 m^3/s
- Lowest observed discharge: 162 m^3/s (16 August 2015)
- Highest observed discharge: 4080 m^3/s (11 June 2013)

The Elbe estuary is connected to the North Sea. The water levels of the North Sea are determined by tidal forcing and wind set-up, resulting in varying water levels in the Elbe estuary (Muller-Navarra & Bork, 2011). Additionally, the salinity levels within the estuary fluctuate, but the salinity level remains lower than that of natural seawater. The Elbe estuary can be classified as a partially to well-mixed estuary (Zorndt et al., 2011).

The tidal variation in water levels is mainly influenced by the semi-diurnal lunar tide (M2), originating from the moon's forcing, and the semi-diurnal solar tide (S2), originating from the sun's forcing. The tidal amplitude and periods of these tides are shown in Table 2.1. The maximum tidal range in the Elbe estuary is measured around 120 km from the sea near St.Pauli in Hamburg (Figure 2.3) (H. Hein et al., 2014). According to Zorndt et al. (2011), the Elbe estuary is a mesotidal and flood-dominant estuary.

	Period (h)	Amplitude (m)
M2	12.42	1.5
S2	12	0.3

Table 2.1: Period and amplitude of the semi-diurnal tides M2 and S2 in the Elbe estuary, according to H. Hein et al. (2014)

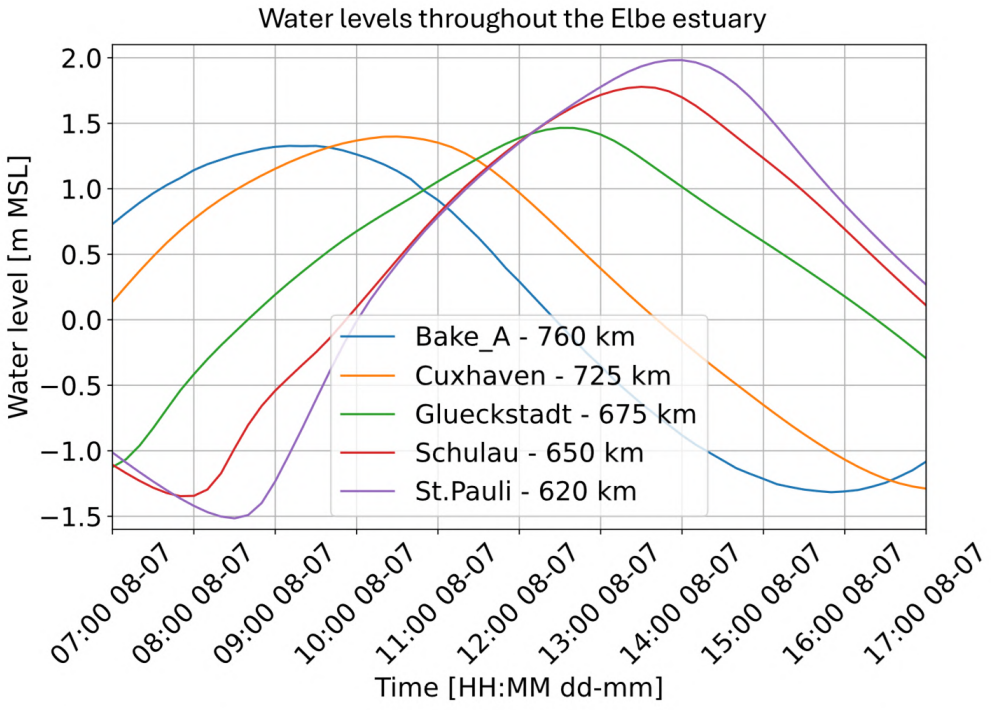

Figure 2.3: Example of a tidal curve of the Elbe on 8 July 2006 at different locations, where Bake A is located at sea and St.Pauli in Hamburg and km indicate the Elbe-km.

Figure 2.4 shows a notable transition occurring in the bed elevation at kilometre 615, from the sea up to this location dredging is taking place (Li et al., 2014). This topographic step acts as a partial reflector of the tidal current, reflecting about 75% of the total tidal wave (Sohrt et al., 2023).

The weir (Elbe-km 586) acts as a total reflector (S. Hein et al., 2021), implying that no tidal wave occurs upstream of this weir (Sohrt et al., 2023). Such reflections within an estuary can induce resonance, a phenomenon arising when the system's length corresponds to a quarter of the tidal wavelength (or an odd multiple of that). This quarter-wavelength resonance is not observed in the Elbe estuary (S. Hein et al., 2021), but there are signs that resonance can happen in the future if the water depth increases, for example due to dredging or sea level rise (Sohrt et al., 2023).

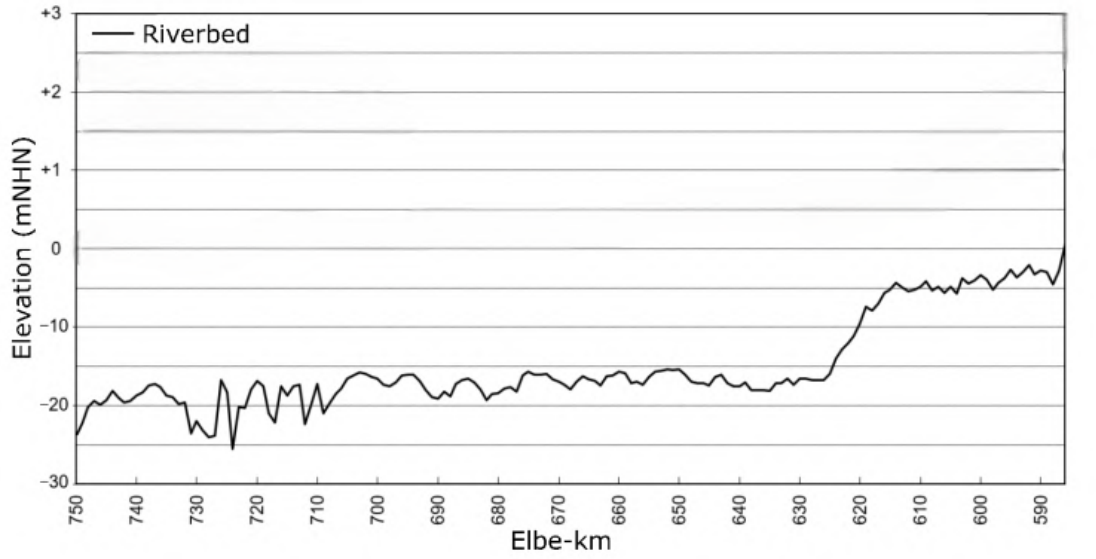

Figure 2.4: Fairway averaged bathymetry of the Elbe estuary between 2000 and 2018 (S. Hein et al., 2021)

Chapter 3

Methodology

The research methodology consists of three phases: (i) model set-up, (ii) define cases, and (iii) modelling and comparison. After the model is set up and the cases are defined, the cases related to each research question are implemented and analyzed. Following each research question, the base case is updated based on the outcomes to improve accuracy and efficiency, and this updated base case is used for the set of cases of the next research question. This iterative process ensures systematic refinement of the model as each research question is addressed. Figure 3.1 provides an overview of the methodology.

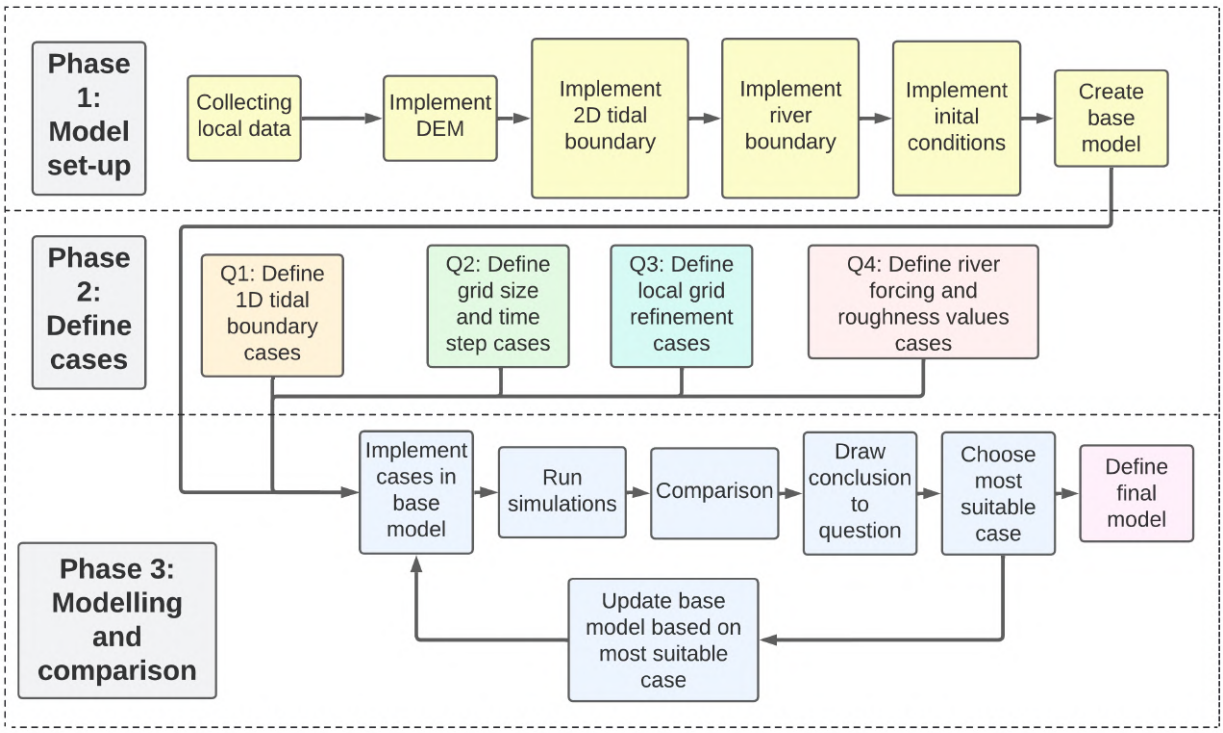

Figure 3.1: Research methodology

3.1 Phase 1: Model setup

The BAW has provided several data sets to facilitate the model setup, including a bathymetry raster and river and tidal boundary conditions.

3.1.1 Subgrid

For a subgrid model, bathymetry is a crucial input, as the model uses the high-accuracy bathymetry for its subgrid. Due to its significance, considerable effort was dedicated to preparing the bathymetry. The BAW has provided a bathymetry raster of the Elbe. Unfortunately, this raster cannot be directly applied as a digital elevation map (DEM) in 3Di. Several notable issues have been identified in this raster, such as an area with inverted values and missing data points. The explanations of how these issues have been addressed and improved can be found in Appendix A.1. The final DEM is visualized in Figure 3.2. The subgrid will use this DEM in all simulations, which has a high-accuracy of 5 m x 5 m, regardless of the computational grid width. Since both the subgrid and the computational grid are square, the term 'grid width' will be used instead of 'grid size'. Thus, the subgrid has a grid width of 5 m rather than a size of 5 m x 5 m.

Additionally, roughness values must be defined for the subgrid. In this research, a uniform roughness was applied to the model, using a Manning value of 0.0245 $s/m^{1/3}$, as recommended by the BAW.

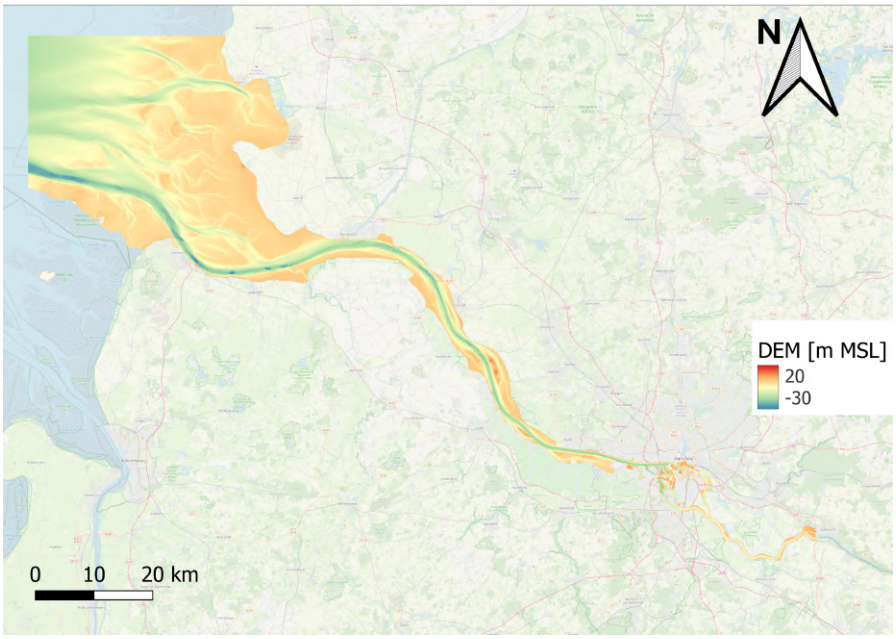

Figure 3.2: Final DEM to be used as subgrid in all simulations

3.1.2 River boundary

A discharge boundary will be established in the model near Geesthacht. For this location the BAW has provided river discharge data for a 15-day period from 05-07-2006 00:00 to 20-07-2006 00:00 (Figure 3.4). This period was chosen by the BAW due to its relatively calm weather conditions, which minimized wind influence, and its capture of a spring-neap cycle. These factors are crucial for an accurate comparison of water levels between the model, which does not account for wind influence, and actual measurements.

To ensure natural water flow near the boundary, a "tub" with a bed level of -10 m MSL, based on the lowest bed level at the boundary, is added upstream of the existing DEM. A 2D discharge boundary condition is defined on the lower river branch with temporally changing discharge values. Due to the presence of a lock at the upper branch, no significant amount of water flows in this area. Therefore, it functions as a closed boundary.

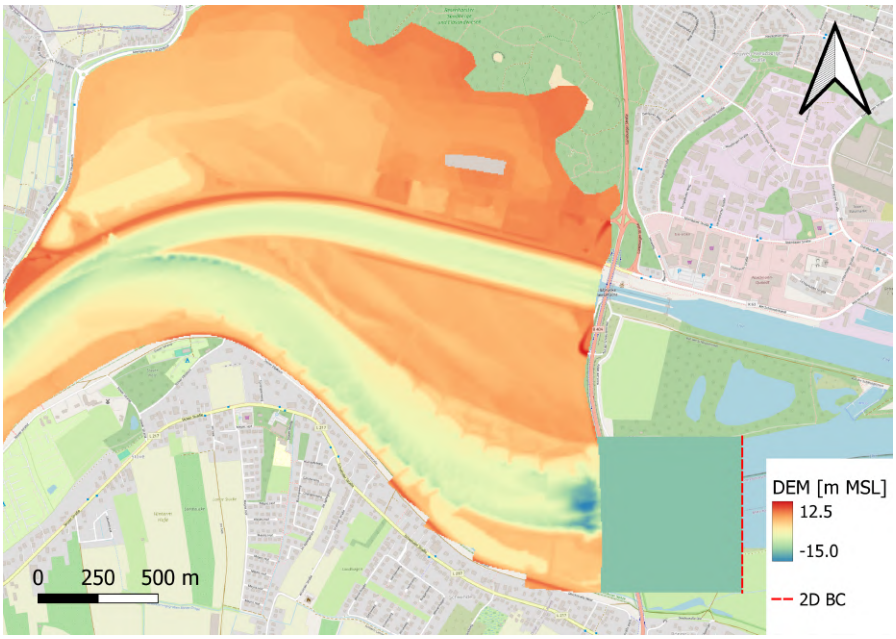

Figure 3.3: 2D river boundary with "tub"

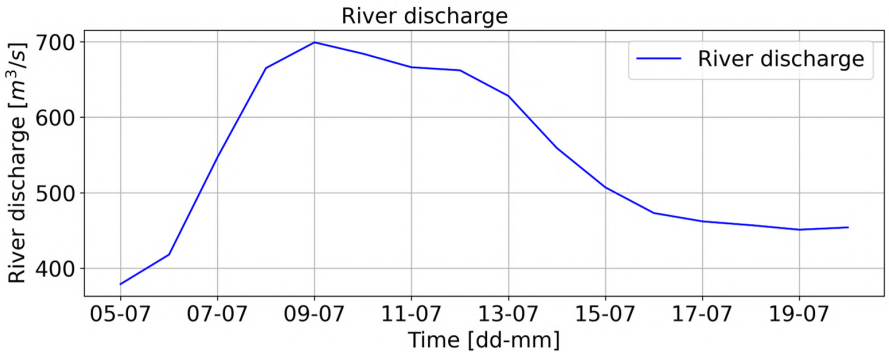

Figure 3.4: River discharge applied to the river boundary for the two weeks simulation period, with a maximum discharge of 699 m^3/s, mean discharge of 553 m^3/s and a minimum discharge of 379 m^3/s.

3.1.3 Tidal boundary

On the west side of the model domain, a water level boundary condition is defined using the water levels provided by the BAW. Water levels are known at three locations along the boundary over a 15-day period, from 5 July 2006 00:00 to 20 July 2006 00:00. The water levels between these locations are linearly interpolated, to create spatially varying water levels.

However, 3Di cannot accommodate a single 2D boundary with spatially varying water levels. For an initial assessment, two separate 2D boundaries were applied (one horizontal and one vertical) as shown in Figure 3.5. The water levels for these boundaries were determined by averaging the water levels at the boundary's endpoint locations. While the water levels fluctuate over time, they remain spatially uniform, making them less realistic compared to a spatially varying boundary. Nonetheless, an initial assessment of the model using 2D boundary conditions produced quite accurate results despite this spatial uniformity.

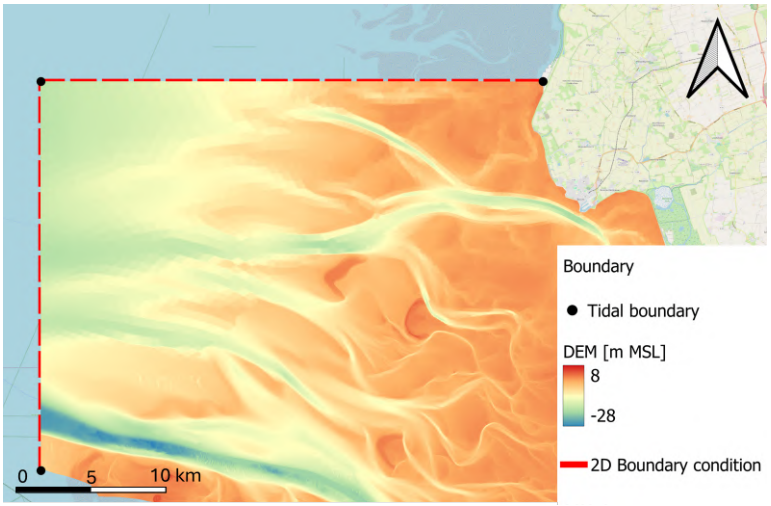

Figure 3.5: 2D tidal boundary where the black dots are the locations of the known water levels

3.1.4 Initial conditions

Setting initial conditions is crucial for initializing a simulation (Merwade et al., 2008). Initially, a water level of 0 m MSL is applied. Subsequently, a preliminary run is conducted with a grid width of 200 meters and a time step of 10 seconds. From this run, the water level raster at 19-07-2006 12:10 is extracted, as it aligns with the water levels at the first time step and is also after the high water peak just as the first time step. This extracted raster is then employed as the initial water level for the model. At the initial state, flow velocities are set to zero across the domain, meaning there is no water flow. A warm-up period of one full tidal cycle is used in this research to allow the system to stabilize.

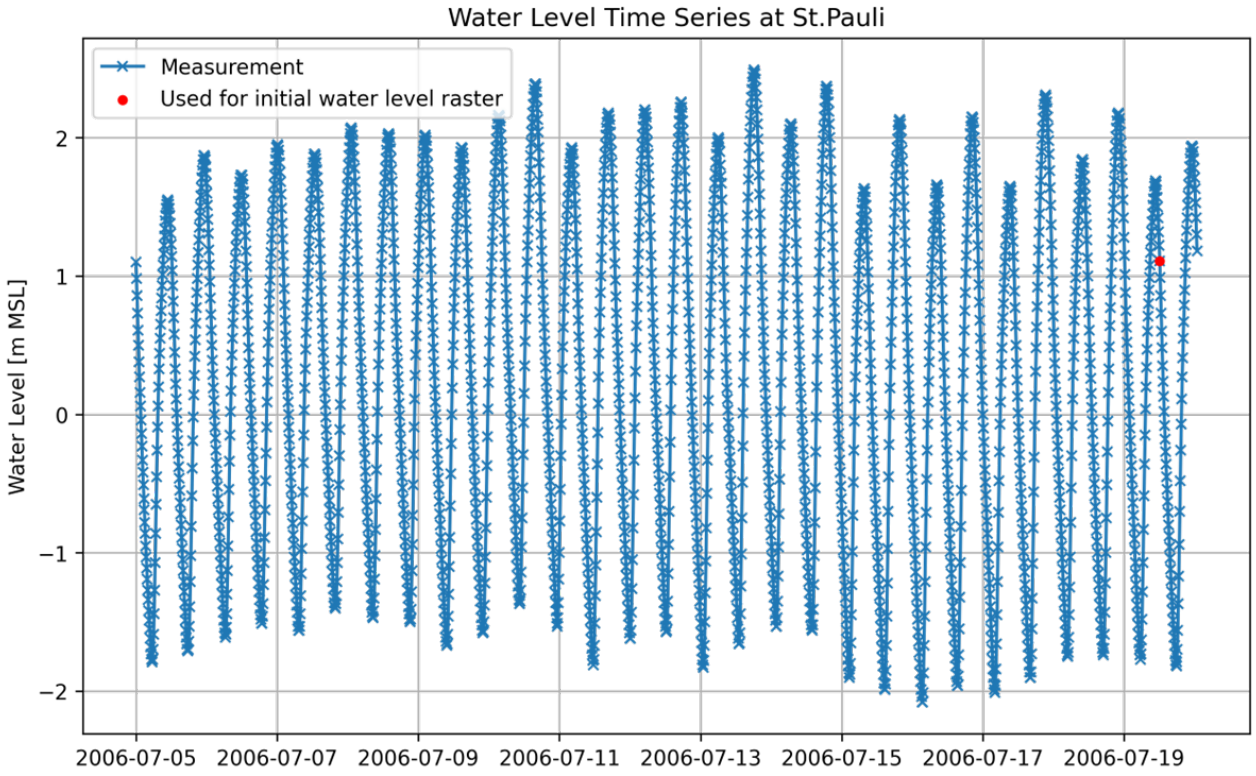

Figure 3.6: Water level measurements at St.Pauli where the moment marked with a red dot is used to extract the initial water levels

3.2 Phase 2: Defining cases

In this section, various model cases will be introduced. This will be done for each question separately. An overview of all cases is provided in Table 3.1. Specific settings not included in the table can be found in Appendix A.2. For each topic, the case that best balances accuracy and computational time, based on expert judgment, will be used in the subsequent steps of the research.

Table 3.1: Overview cases

Question:	**Topic:**	**Cases:**
Q1 - Tidal boundary	Connection node storage areas [m^2]	0, 5000, 10000, 20000, 30000, 40000
	Boundary channel length [m]	20, 60, 90
	Validation tidal boundary	2D tidal boundary, 1D spatially varying, 1D non-spatially varying
Q2 - Grid width and Time step	Grid width [m]	200, 300, 400, 500, 750, 1000, 1500
	Time step [s]	10, 40, 75, 120, 200
	Combinations	Combinations different grid widths and time steps
Q3 - Local grid refinements	Port Hamburg [m outside refinement area - m inside refinement area]	400-50, 400-100, 400-200, 400-400, 800-200, 800-400
	River widening [m outside refinement area - m inside refinement area]	400-100, 400-200, 400-400, 800-100, 800-200, 800-400, 1600-200, 1600-400
	River - Sea [m outside refinement area - m inside refinement area]	400-100, 400-200, 400-400, 800-100, 800-200, 800-400, 1600-200, 1600-400
	Navigation channel [m outside refinement area - m inside refinement area]	400-100, 400-200, 400-400, 800-100, 800-200, 800-400, 1600-200, 1600-400
	Combinations	Combinations from the topics discussed for this question
Q4 - Roughness values and River discharge	Manning values [$s/m^{1/3}$]	0.0235, 0.024, 0.0245, 0.0250 0.0255
	Steady river discharge [m^3/s]	0, 126.3, 184.3, 223

3.2.1 Q1: Tidal boundary

For Question 1 the influence of the tidal boundary will be researched. Boundary conditions are crucial inputs that significantly affect hydrodynamics throughout the estuary, making it essential to establish a realistic boundary that varies both temporally and spatially. Since 3Di cannot implement a 2D boundary with a temporally and spatially varying signal, multiple 1D boundaries will be used to create this boundary. In this report, when referring to a 1D boundary, the combination of multiple elements is meant. A 1D boundary consists of a 1D boundary element, two connection nodes, an isolated channel, a cross-section, and an embedded manhole used as an outlet (Figure 3.7a). An isolated channels means that there is no interaction of water between the 1D channel and the 2D cell. An embedded manhole ensures that the water level of the 1D element matches the water level of the 2D cell (3Di Documentation, n.d.). The water level of the 1D element is controlled by a boundary condition, causing the 2D cell to adopt the same water level.

A 1D boundary will be placed at each computational cell along the tidal boundary (Figure 3.7b), with each boundary assigned its own water level time series based on interpolated values from known water level locations. The simulation period for this specific question is 2.5 days, this since the focus is on what the effect of the boundary is on the hydrodynamics.

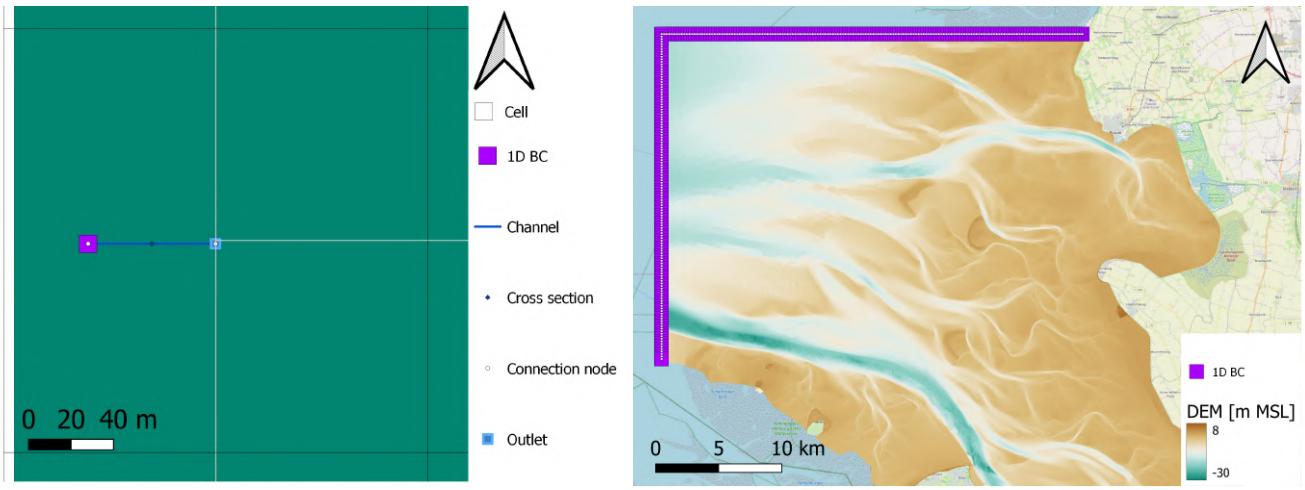

(a) One single 1D boundary

(b) 1D boundaries over complete boundary

Figure 3.7: 1D tidal boundaries

To the elements in the 1D boundary certain parameter values need to be assigned. During this research, the influence of the connection node storage area and boundary channel length values will be investigated on the tidal signal introduced in the model. The storage area of a connection node is additional to the water storage defined by the dimensions of the channel. If the storage area is too large compared to the channel's area, it can lead to a reduction in flow velocities and advective force (3Di Documentation, n.d.). The range of connection node storage cases, mentioned in Table 3.1, is selected to study the effects of different storage capacities,

with 40000 m^2 representing the cell area, making it impractical to use larger values. Following this, the recommended storage from the initial study will be used to investigate the influence of channel length. The channel length cases, as mentioned in Table 3.1, are chosen to be shorter than the cell width (200 m) to avoid lag caused by setting boundaries at a different location.

If unexpected flow velocities or water levels are observed near the tidal boundary a "tub" will be established, similar to the one at the river boundary (section 3.1.2). The irregularities can occur since water levels are forcefully imposed on a specific cell, disrupting natural flow patterns. To ensure natural flow, a tidal "tub" system is established, with a width matching the largest grid width used in this research and a bed level according to the lowest point at the tidal boundary. If a tidal "tub" is added the manhole of the 1D boundary will be positioned at the center of the cell nearest to the original DEM. The connection node storage area and the channel length will be based on the results found in the analysis of these settings. Due to time constraints, no additional sensitivity analyses will be conducted regarding settings in conjunction with this tidal "tub".

After analyzing the previous topics, a validation will be conducted to assess the simulated hydrodynamics at the tidal boundary. Three cases will be compared: (i) a 1D spatially and temporally varying boundary, (ii) a 1D temporally varying boundary without spatial variation, and (iii) a 2D non-spatially varying boundary. The 1D non-spatially varying case will use the same averaged time series as the 2D boundary. To compare the effects of spatial variation, the two 1D cases will be analyzed, and the difference between 1D and 2D boundaries will be assessed by comparing the 1D non-spatially varying case with the 2D case.

3.2.2 Q2: Grid width and time step

Question 2 will investigate the influence of grid width and time step on the model results. The boundary settings derived from the first research question will be implemented in the model. The range of grid width cases, presented in Table 3.1, offers insights into model behaviour across both small and large grid widths. Smaller grid widths are not considered due to the excessive computational time and memory limitations of 3Di. Larger grid widths are excluded, as they are likely to inadequately capture hydrodynamics due to inadequate resolution.

These time step cases (Table 3.1) are chosen to investigate a wide range of time steps and to comply with the Courant-Friedrichs-Lewy (CFL) condition. The grid width used for these simulations will be the one recommended from the previous grid width analysis. The time step that has the best balance between accuracy and computational time, based on expert judgement, will be used for all subsequent simulations.

Since both hydrodynamics and computational times are influenced by grid width and time step, combinations of different time steps and grid widths will be tested to assess the differences in hydrodynamics. Only combinations deemed suitable based on the individual analysis of grid width and time step will be evaluated. All combinations of time step and grid width used in this research comply with the CFL condition.

3.2.3 Q3: Local grid refinement

For Question 3, the focus is on implementing local grid refinement to evaluate its impact across various locations and extents. The grid width identified as most suitable for the Elbe estuary in Question 2 will serve as the base case for exploring these refinements. The refinement areas are illustrated in Figure 3.8. Comparing results across the different refinement areas will help identify where local grid refinement most effectively captures the physical processes throughout the estuary. The cases are denoted in Table 3.1, where the first number represents the grid width [m] outside the refinement area, and the second number represents the grid width [m] inside the refinement area. Due to the quad-tree method, grid widths differ by a factor of 2 or its multiples, ensuring that neighboring cells that differ in size vary exclusively by a factor of 2 (Stelling, 2012).

The Port refinement is selected because of the complex flow dynamics introduced by the docks and piers, which act as obstacles influencing flow patterns. Given the small size of the Port, the primary focus is on decreasing the grid resolution in this area to better capture physical processes. Additionally, the grid width outside the Port will be increased to 800 m to assess how a larger grid affects hydrodynamics within the Port. No grid widths larger than 800 m will be tested, as this would result in only one grid cell capturing the entire river width, which is inadequate for accurately representing flow dynamics.

The river widening section is chosen due to the narrower width of the river in the refinement area compared to the outside, which may lead to tidal amplification that a finer grid can better capture. Additionally, the grid analyses (Q2) indicated this area as important, since distinct patterns were found there. The river/sea division is selected for similar reasons. The navigation channel is included primarily due to depth variations. The water depth within the channel is greater than outside, potentially impacting flow velocities in the estuary, which can be more accurately represented with a finer grid.

The selected cases for these topics are comparable, with combinations of finer and coarser grids than the base case chosen to provide a broad spectrum of simulations. This will facilitate an investigation into the effects of varying grid widths, both finer and coarser, within and outside the refined areas. This makes it possible to get insight in both the effect on hydrodynamics as computational times. The cases chosen for these topics are similar to each other. The combinations of finer and coarser grids than the base case are selected to provide a broad spectrum of simulations, allowing to investigate the impact of varying grid widths both finer and coarser grids within and outside the refined areas. This allows for insights into both the effects of the refinements on hydrodynamics and computational times.

The results from the various local grid refinements will be evaluated to identify the most effective areas and extents. These findings will be used to create new simulations incorporating multiple refined areas. The outcomes of these combined simulations will then be compared to those from individual refinements to determine the most effective grid refinement strategy.

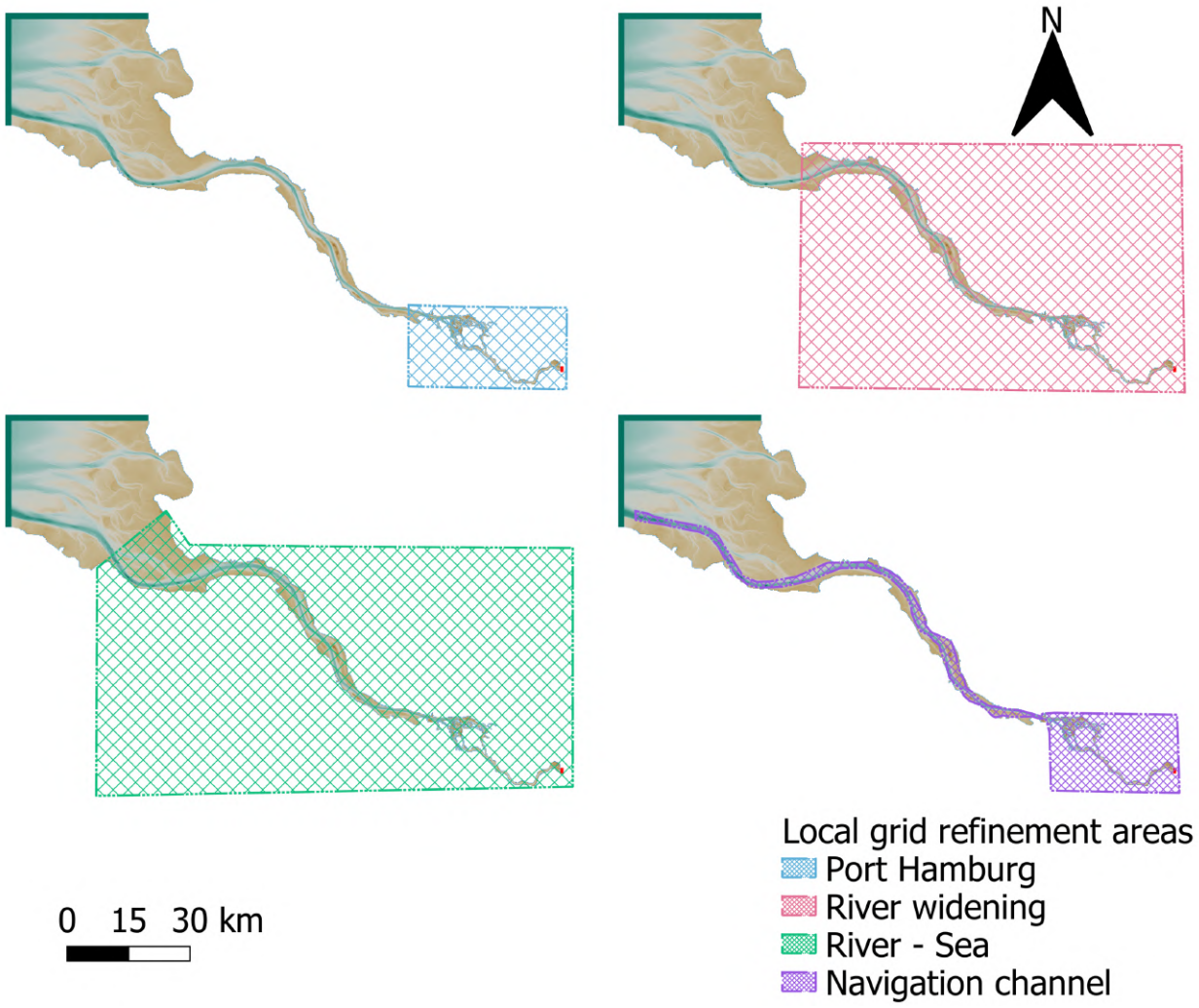

Figure 3.8: Local grid refinement areas

3.2.4 Q4: Roughness values and River discharge

Question 4 focuses on the influence of physical parameters, specifically roughness values and river discharge, on the simulated hydrodynamics. The range of roughness cases used for this question (Table 3.1), includes both higher and lower variations around the suggested value by the BAW (0.0245 $s/m^{1/3}$) to assess the effects of changes in both directions. Additionally, these values still represent the physical properties of the bed material, while values outside this range correspond to other materials.

River discharge at the estuary's upstream boundary can significantly impact hydrodynamics across the entire model domain. To assess this influence four simulations will be conducted using steady river discharges, with zero, minimum, average and maximum discharge (values provided in Table 3.1). The discharge values are derived from the time series introduced in section 3.1.2. This selection allows for an evaluation of the model results under various river discharge conditions.

3.3 Phase 3: Comparison strategy

3.3.1 Qualitative comparison

For the qualitative comparison of the simuations the water levels and flow velocities will be compared to measurements. The BAW has provided water level measurements at five locations and velocity measurements at three locations. The water level and velocity measurement locations are shown in Figure 3.9.

Water levels

The water level results will be qualitatively compared, for all questions, at Cuxhaven, Schulau, and St.Pauli, focusing on the differences in timing and magnitude of high and low water levels, as well as tidal amplitude, between simulations and to measurements. These locations are selected as they are spread throughout the estuary, allowing for a comprehensive assessment of water level differences across different areas. Differences within 1 cm are considered negligible, since such small differences would not have an impact in reality and this uncertainty margin is also incorporated in the input data.

Flow velocities

Flow velocities will be compared qualitatively between simulations and measured data at LZ1 and LZ3, this will be done for all research questions. Comparisons will focus on timing and peak velocities, differences within 0.01 m/s are considered not significant. Since the measured data is provided as absolute velocities, the cell-averaged and depth-averaged velocities from 3Di will be converted to absolute values for consistency. Consequently, only the magnitude of the 2D flow velocity vector (u, v) will be considered, while the direction of the flow will be excluded from the analysis. Direct comparisons to measurement values will not be made, as 3Di's velocities are depth-averaged.

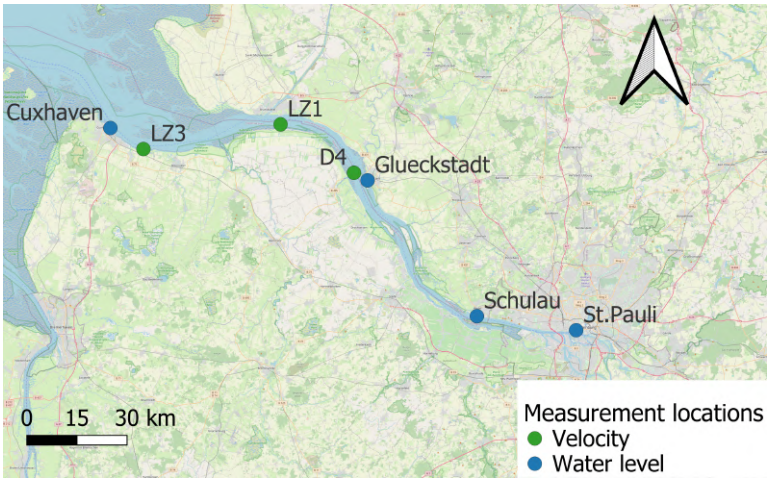

Figure 3.9: Measurement locations along the Elbe estuary: three for velocity (LZ3, LZ1 and D4) and five for water levels (Bake A, Cuxhaven, Glueckstadt, Schulau and St.Pauli)

3.3.2 Quantitative comparison

Boundary in- and outflow volumes

The boundary in- and outflow volumes represent the total water entering and leaving the system, influenced by both tidal and river boundaries. As river discharge is fixed, variations in these volumes are due to changes at the tidal boundary. Adjustments to the tidal boundary settings can impact these volumes and, consequently, the model's hydrodynamics. Therefore, this comparison will only be executed for Q1. Monitoring these values is essential for a thorough comparison.

Computational time

The computational time for each simulation will be recorded upon completion. Since modelling involves balancing accuracy with computational efficiency, both factors must be considered in assessment of results. Modifications to the grid width (Q2 and Q3) or the time step (Q2) directly impact computational time. In contrast, changes to tidal boundary conditions (Q1), river discharge, and roughness values (Q4) do not affect computational time, so computational time will only be considered in the result comparisons for questions 2 and 3. The computational time required for a simulation is independent of the device type, as the simulation is executed in the cloud (3Di Documentation, n.d.).

RMSE values

To measure agreement between simulations and measurements, the root mean square error (RMSE) will be calculated for water levels. RMSE assesses simulation accuracy and will be used for Q3 and Q4 to evaluate how well simulations match to the measurements and how different settings affect accuracy.

RMSE values will be computed for Cuxhaven, Schulau, and St.Pauli, where a lower RMSE indicates better agreement. Differences within 0.5 cm are considered insignificant, since water level differences of 0.5cm would not have an impact in reality. Each simulation will have three RMSE values: total, for high water peaks, and for low water peaks. The total RMSE considers the differences in water level at each time step. For the peak RMSE's, the values of the simulated peak are compared to the corresponding measured peak, so timing differences are not considered here. The RMSE are calculated by Equation 3.1 (Toth et al., 2021):

$$RMSE = \sqrt{\frac{1}{N}\sum_{i=1}^{N}(S_i - O_i)^2} \tag{3.1}$$

The differences in RMSE between cases and the base case will be analyzed using Equation 3.2. A negative difference indicates an improvement in accuracy. The base cases are derived from the results of previous questions.

$$\Delta\text{RMSE} = \text{RMSE}_{\text{Case}} - \text{RMSE}_{\text{Base case}} \tag{3.2}$$

Chapter 4

Results Q1: Spatially and temporally varying tidal boundary condition

How do the settings of a spatially and temporally varying tidal boundary condition affect the simulated estuarine hydrodynamics throughout the model domain?

4.1 Connection node storage area and boundary channel length

A spatially and temporally varying tidal boundary is created using multiple 1D boundaries. The behaviour of the estuarine hydrodynamics is closely linked to the settings at this boundary. The cases used in this section are stated in Table 3.1.

4.1.1 Boundary in- and outflow volumes

Both the connection node storage area and the boundary channel length directly impact the volumes of water flowing in and out of the model. Larger storage areas (Table 4.1) or shorter channel lengths (Table 4.2) lead to greater inflow and outflow volumes.

For the storage area this is the case since the 1D boundary imposes a specific water level, and as the connection node storage area adopts this water level, it results in a greater volume (product of depth and area) when the storage area increases. Therefore, more water is pushed into the system during rising tide, resulting in more momentum. Conversely, during falling tide, the larger volume in the connection node means that more water needs to exit the system to maintain the water level. This happens since the model tries to equalize the water levels for the 1D and 2D nodes.

For the boundary channel this occurs because the gradient between the 1D boundary's water level and the adjacent cell decreases with increasing channel length, leading to less momentum and thus lower flow velocities. Consequently, with lower flow velocities, the computational cell fills more gradually. This slower rate of inflow reduces the pressure to push large volumes of water rapidly into the cell, preventing the immediate outflow that can occur with higher

velocities. As a result, the system requires less water to achieve and maintain the desired water level in the cell, as the gradual filling process allows for a more efficient and stable adjustment of the water level.

In summary, the total inflow at the boundary depends on both the connection node storage area and the boundary channel length. The former primarily affects water storage, while the latter influences the flow dynamics through the changing gradient. The absolute values for these comparisons are provided in Appendix B.

Table 4.1: Relative inflow and outflow boundary volumes for different connection node storage areas compared to the inflow and outflow volumes of the 0 m^2 storage area case. All cases have a boundary length of 60 m.

Connection node storage area [m^2]	0	5000	10000	20000	30000	40000
Boundary inflow [%]	-	+0.8	+2.0	+4.3	+7.8	+11.5
Boundary outflow [%]	-	+0.8	+2.0	+4.3	+7.8	+11.5

Table 4.2: Relative inflow and outflow boundary volumes for different boundary channel lengths compared to the inflow and outflow volumes of the channel length case of 20 m. All cases have a connection node storage area of 0 m^2.

Boundary channel length [m]	20	60	90
Boundary inflow [%]	-	-5.1	-6.2
Boundary outflow [%]	-	-5.1	-6.2

4.1.2 Water level results

The water levels are examined for both settings near the boundary and further in the estuary. The effects of the settings are the same for increasing connection node storage areas or decreasing channel lengths. This is because both scenarios lead to higher inflow and outflow volumes and more momentum, which influence the hydrodynamics throughout the estuary. Directly, near the boundary, no significant differences (less than 0.1 cm) could be identified between simulations with different settings.

When examining water levels upstream, for example at Schulau (Figures 4.1 and 4.2), cases which have higher inflow and outflow volumes and more momentum have increased water levels during both high and low peaks. However, the difference is more pronounced during high water, indicating that the cases with larger in and outflow volumes have an expanded tidal range, as more water and momentum are introduced into the system. The differences between simulations grow with increasing volumes, but they are more significant at high water than at low water, where roughness plays a larger role and the impact of the 1D boundary is reduced. This pattern is consistent across all locations and the connection node storage area

and boundary channel length settings have more influence far upstream in the model domain. Additional figures are provided in Appendix B.

In simulations with larger connection node areas or smaller channel lengths (which result in larger in- and outflow volumes and more momentum), the high and low water peaks occur slightly later compared to simulations with less in and outflow volumes. This delay (between different simulations), up to 10 minutes at all locations, reflects the additional time needed for the system to reach high water levels due to the increased water volume. Furthermore, it suggest that the tide penetrates further into the system due to the extra momentum. However, the exact delay is uncertain due to the 10-minute output interval.

When comparing simulations to measurements, the smallest connection node area (0 m^2) and the largest channel length (90 m) align best with observed water levels. Timing differences with measurements show a delay of 20 minutes at Cuxhaven and 10 minutes at Schulau and St.Pauli (locations are stated in Figure 3.9).

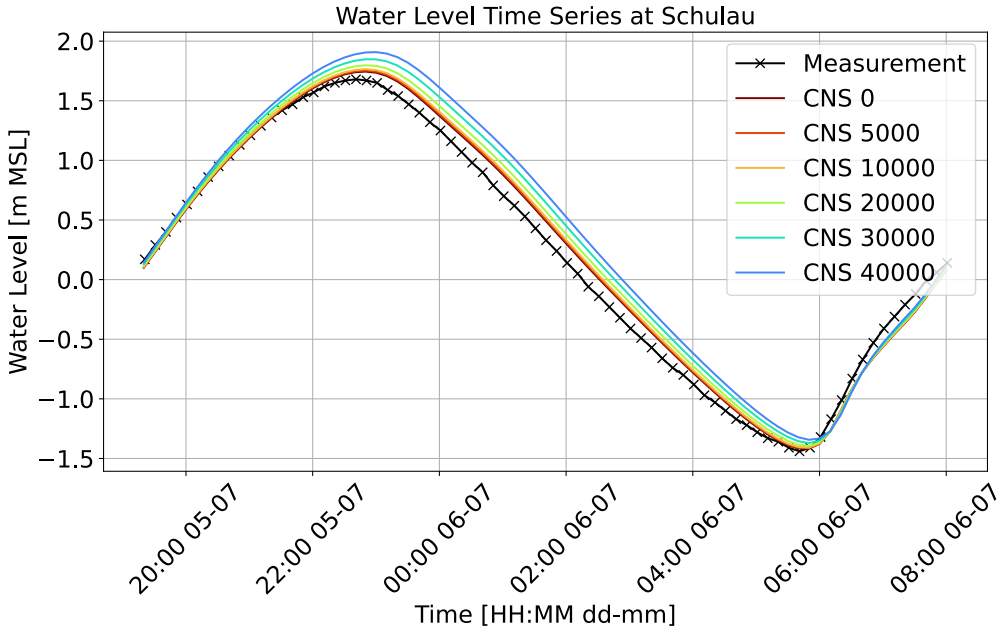

Figure 4.1: Water levels for different connection node storage areas (CNS) at Schulau [m^2]

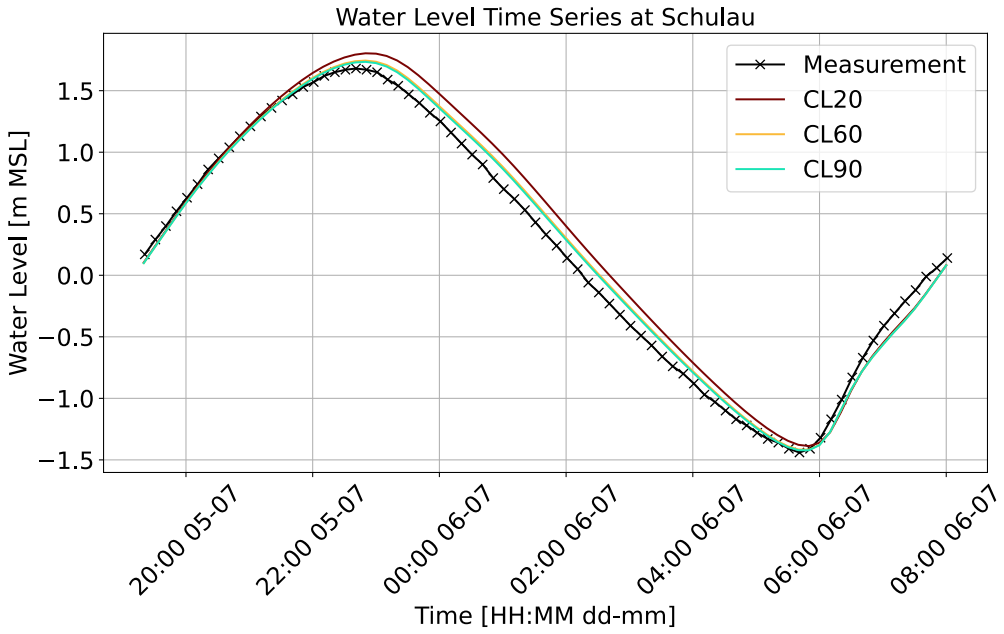

Figure 4.2: Water level results for different boundary channel lengths (CL) at Schulau [m]

4.1.3 Flow velocity results

Just as for the water levels the effects on the flow velocities are dependent on the in and outflow boundary volumes and momentum. Near the boundary, water levels remain consistent across simulations, but higher flow velocities are observed with larger connection node storage areas or shorter channel lengths, with differences up to 0.1 m/s. As more water and thus momentum enters the system without a change in water levels, velocities must increase.

Further in the model domain at LZ1 and LZ3 higher velocity peaks occur during both rising and falling tides for simulations with larger in and outflow volumes (LZ1 shown in Figures 4.3 and 4.4 and LZ3 in Appendix B). Simulations with larger in and outflow volumes and more momentum at the boundary, allow for larger water movements through the estuary, which resulted in the increased tidal ranges. However, to reach these enlarged tidal ranges higher flow velocities are needed. Also here if the difference increases in volumes the differences in flow velocities increase, this is also the case at the water level results (section 4.1.2). When looking at timing differences, the simulations with larger in and outflow volumes reach their highest velocities at a later moment in time, so they have the largest tidal delay, as already explained in the water level results.

Timing differences compared to the measurements are evident in the velocity results at LZ3, whereas no timing differences were observed at LZ1. This aligns with the trend found in the water level results (section 4.1.2) where the tidal delay was most pronounced near Cuxhaven. Since LZ3 is located close to Cuxhaven, it exhibits a larger tidal delay than LZ1, which is situated further upstream, similar to Schulau and St.Pauli. However, a key factor in these differences is in how LZ1 and LZ3 are measured. The measurements at these locations capture

velocities at a specific point and depth, whereas the 3Di model calculates cell- and depth-averaged velocities. Additionally, LZ3 is positioned within a cell where the bed slope varies significantly, while LZ1 is located in a relatively flat area. These differences in bed topography contribute to timing and amplitude mismatches when comparing the model results to point measurements.

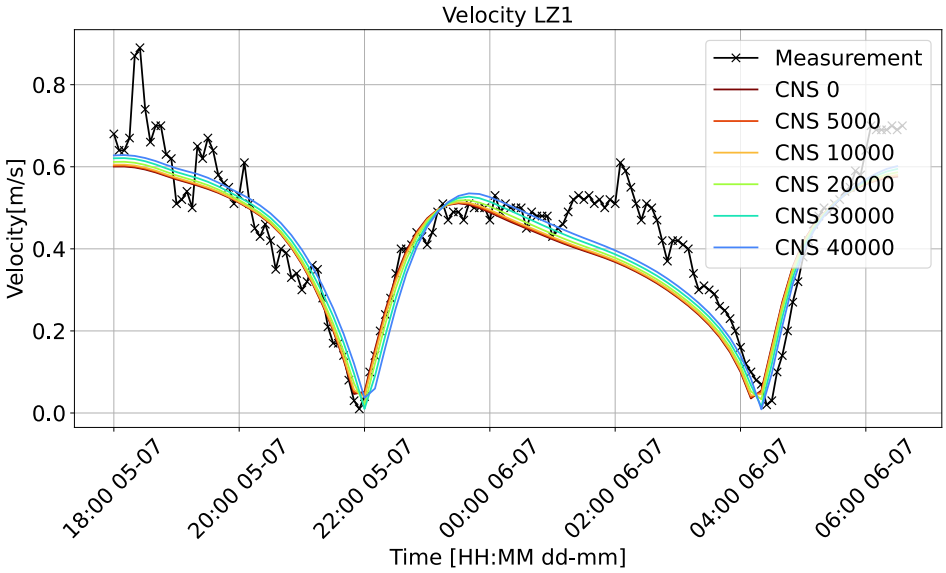

Figure 4.3: Flow velocity results for different connection node storage areas (CNS) at LZ1 [m^2]

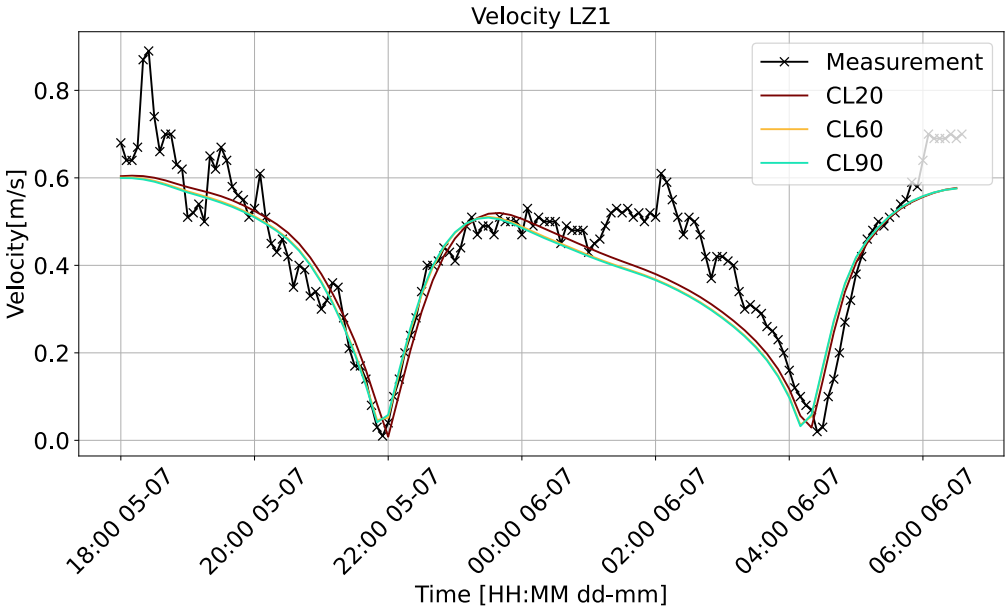

Figure 4.4: Flow velocity results for different channel lengths (CL) at LZ1 [m]

4.2 Tidal "tub"

At the boundary near the main navigation channel, unexpected locally higher flow velocities and water levels have been observed compared to other locations near the boundary. Therefore, as explained in section 3.2.1, a tidal "tub" will be artificially added into the DEM (shown in Figure 4.5). The 1D boundaries will have a channel length and width equivalent to the grid width, thus the tidal boundary will vary per grid width. The connection node area is set to zero. The outcomes of this 1D boundary setup will be discussed in the next section.

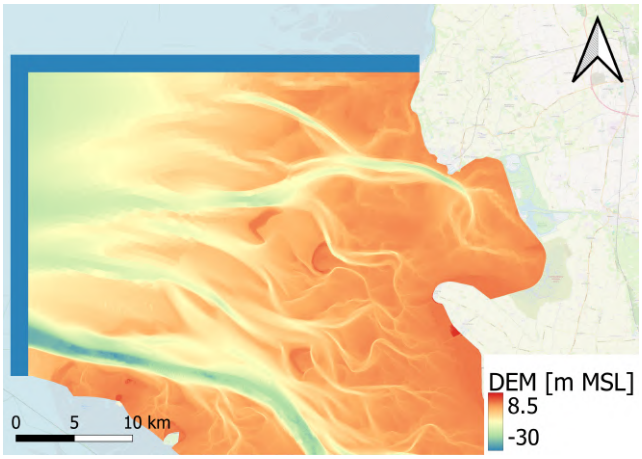

Figure 4.5: Updated DEM with tidal "tub"

4.3 Validation of applied boundary conditions

The performance of different boundary setups—1D spatially varying, 1D non-spatially varying, and 2D—was evaluated to assess their effects on the hydrodynamics of the study area. Near the boundary at Bake A, simulations with spatially varying 1D boundaries were able to better match the measured low water levels (Figure 4.8), while both the spatially varying and non-spatially varying 1D setups captured high water levels similarly well (Figure 4.7). However, the spatially varying boundaries provided more realistic representations of the smaller fluctuations in water levels. Since there is only one measurement location in the sea part of the estuary, it cannot be verified if hydrodynamics in other parts of the sea are also better captured, but it is presumed to be the case due to the more realistic water level definitions at the boundary.

In contrast, the 2D boundary simulation exhibited slightly higher high water levels (+1 cm) compared to the 1D non-spatially varying boundary (Figure 4.7), while low water levels between the two were closely aligned (Figure 4.8). This difference in high water levels likely arises from the additional storage capacity in the "tub" region, which allows for more water to flow during outflow periods—a dynamic absent in the 1D simulations. This storage effect impacts high water levels more significantly, leading to the observed discrepancy.

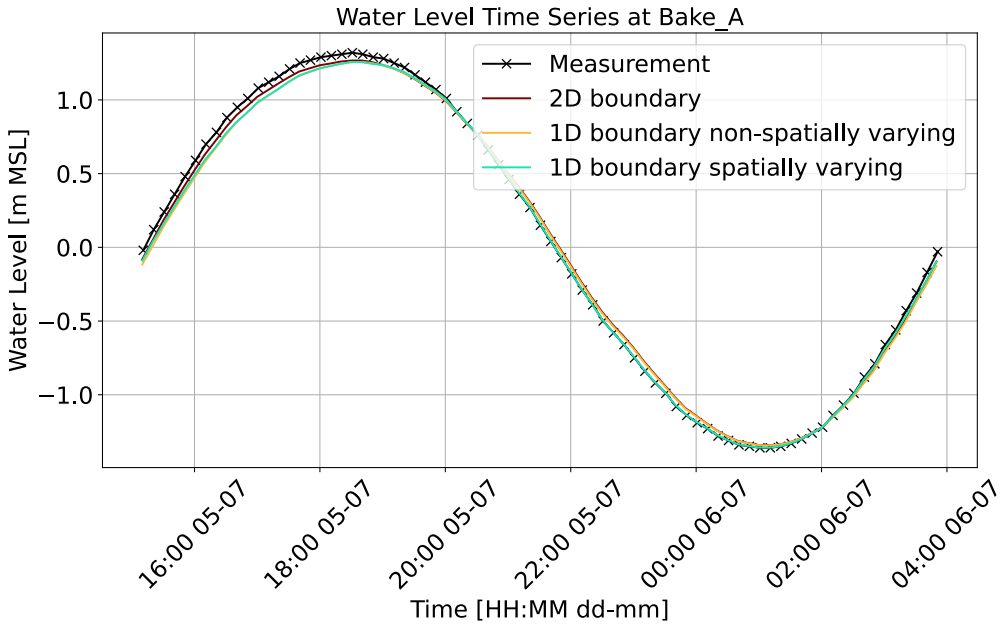

Figure 4.6: Water level results for different boundary types at Bake A

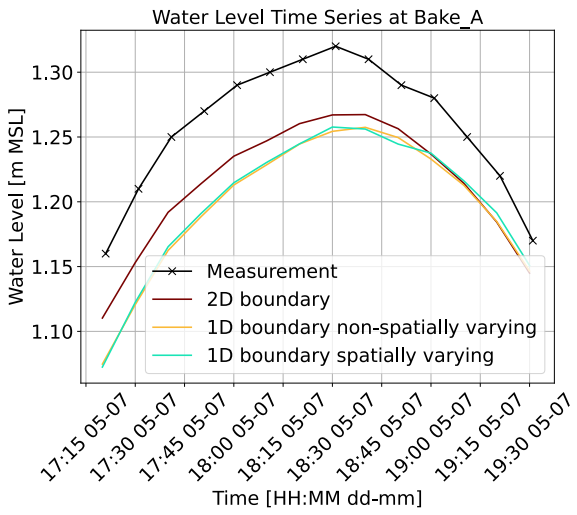

Figure 4.7: High water level results for different boundary conditions at Bake A

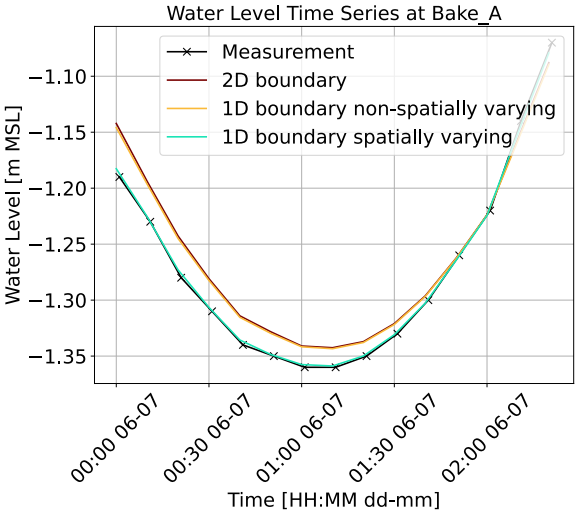

Figure 4.8: Low water level results for different boundary conditions at Bake A

Further upstream at Schulau and St.Pauli, the differences between the boundary setups, whether 1D or 2D, became less pronounced. The influence of the boundary types diminished with distance, as tidal and river boundary conditions together determine the water levels in these locations. The spatially varying boundary matched slightly better to the measurements, but overall, the differences between all boundary setups remained small, typically less than 0.5 cm. This suggests that while boundary configuration impacts near-boundary conditions, its influence on upstream hydrodynamics is minimal due to the dampening effects over distance. The figures are shown in Appendix B.3.

When assessing flow velocities, the results followed a similar pattern. At LZ1 (Figure 4.9) and LZ3 (Appendix B.3), no difference between the 1D non-spatially varying and spatially varying simulations could be identified. The 2D boundary simulation, however, exhibited slightly higher flow velocities compared to the 1D setups. These differences are not significant, but can explained by the difference in set-up of the boundary. Ultimately, while spatially varying boundaries capture finer details near the boundary, the impact of these boundary setups on upstream conditions remains limited.

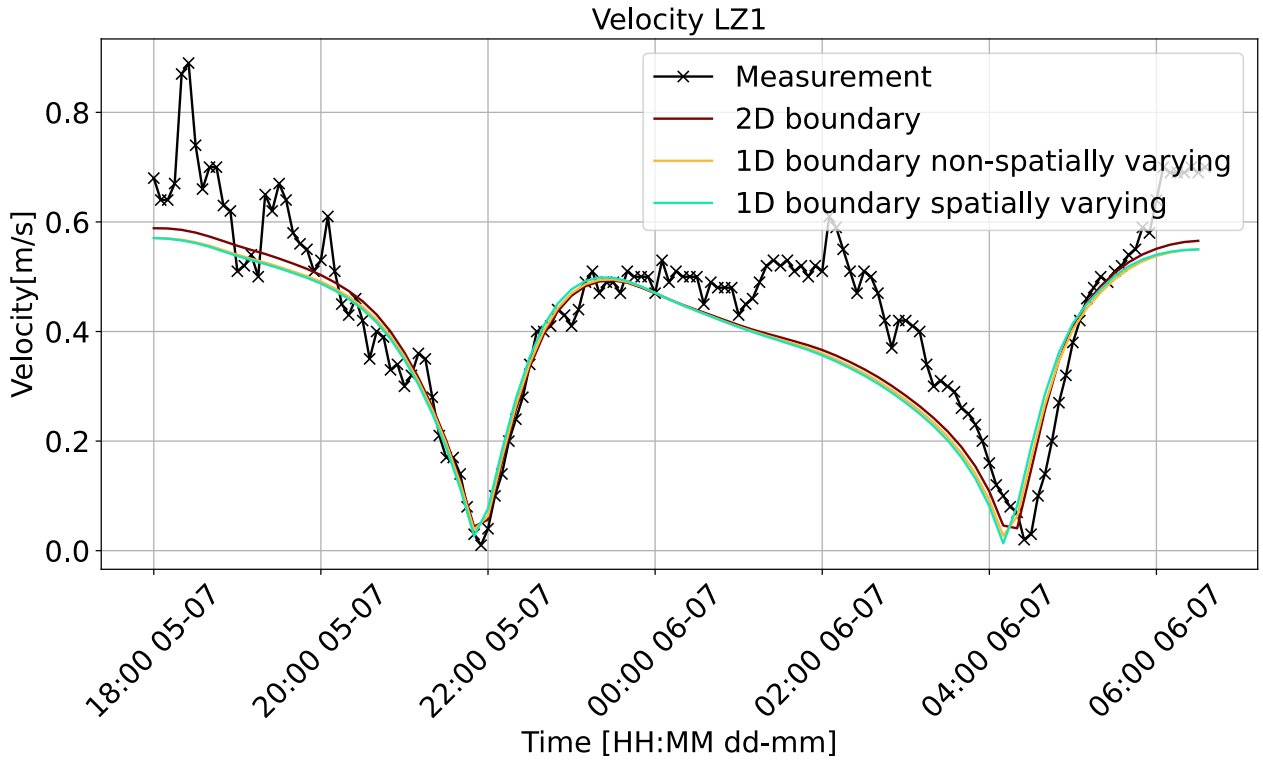

Figure 4.9: Flow velocity results for different boundary conditions at LZ1

Chapter 5

Results Q2: Grid width and Time step

How do grid width and time step settings affect the simulated estuarine hydrodynamics throughout the model domain and the computational time required for a simulation?

First, the effects of various computational grid widths will be examined while keeping the time step constant and the subgrid width fixed at 5 m. Next, the influence of different time steps will be analyzed using a fixed grid width. Finally, the combined effects of computational grid width and time step will be explored, highlighting the interrelationship between these two factors.

5.1 Grid width

5.1.1 Water level results

The water level results are analyzed for grid widths ranging from 200 to 1500 meters. The simulations generally align well with the measurements, showing differences of less than 10 cm to the measurements for all grid sizes, likely due to the subgrid method. The simulations are so close to each other and to the measurements that it is necessary to zoom in on specific high and low water peaks to clearly observe differences. In general, the model tend to underestimate the tidal ranges, the underestimation increases during larger tidal events, such as during spring tide.

At Cuxhaven, the simulations show that for high water levels (Figure 5.2), larger grid widths result in higher water levels, with a maximum difference of 2 cm between simulation cases. For low water levels (Figure 5.3), no clear pattern emerges, the maximum differences between the cases is 6 cm.

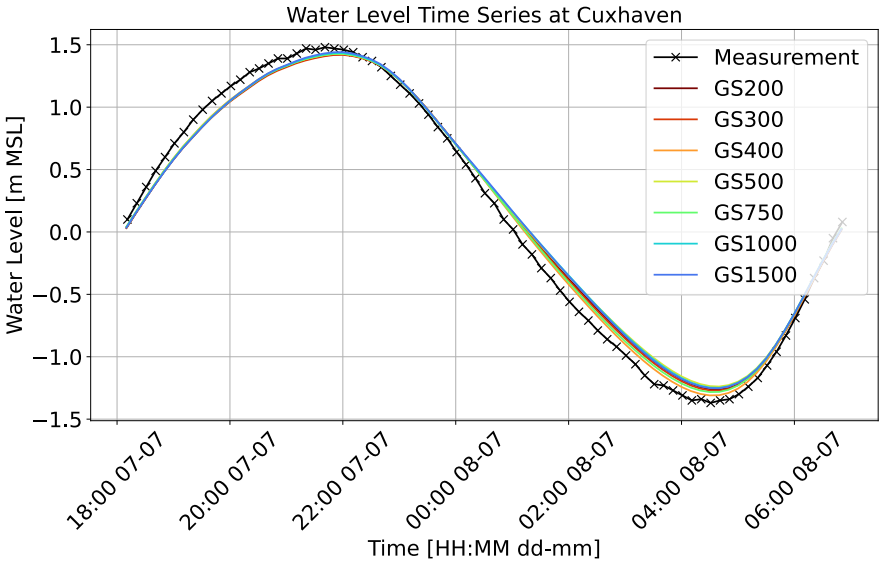

Figure 5.1: Water level results for different grid widths at Cuxhaven [m]

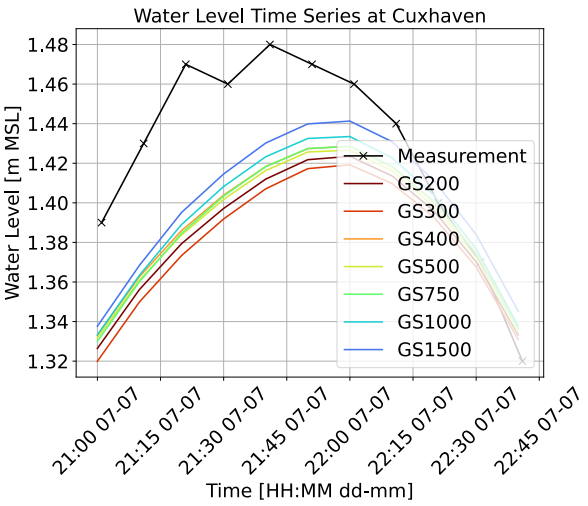

Figure 5.2: High water level results for different grid widths at Cuxhaven [m]

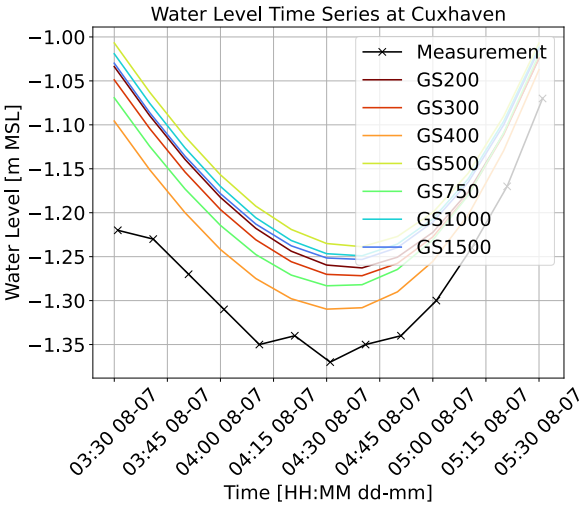

Figure 5.3: Low water level results for different grid widths at Cuxhaven [m]

At Schulau (Figure 5.4) and St.Pauli, like at Cuxhaven the tidal ranges tend to be underestimated. The water level results show that smaller grid widths produce the highest water levels at high tide (Figure 5.5) and the lowest at low tide (Figure 5.6), leading to a increase in tidal range. The order of high water levels and tidal ranges is reversed compared to Cuxhaven (Figure 5.2), where the largest grid widths produced the largest high water levels and tidal ranges. Further analysis of water levels at various locations showed that this reversal occurs where the river meets the sea and the channel widens significantly. In this region, the flow patterns change, and other physical processes, such as flow dispersion and tidal amplification, may become more dominant due to changes in river width. This region is depicted in Figure 5.7. The figures of St.Pauli are presented in Appendix C.1.2.

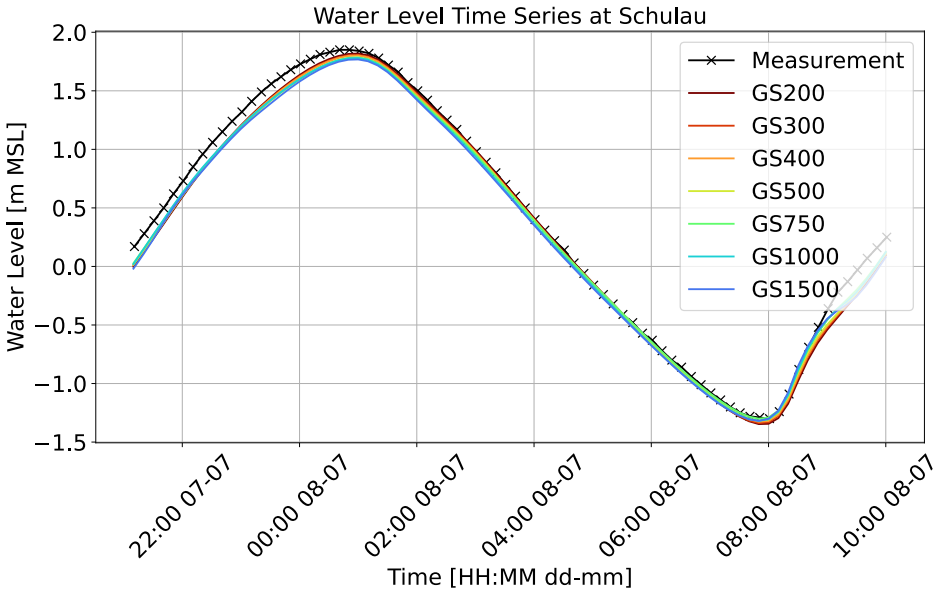

Figure 5.4: Water level results for different grid widths at Schulau [m]

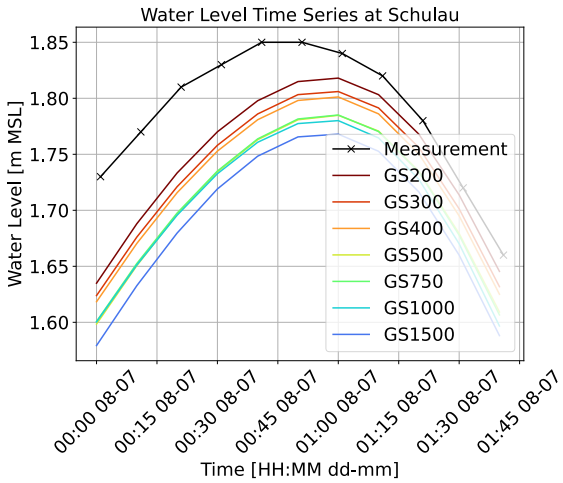

Figure 5.5: High water level results for different grid widths at Schulau [m]

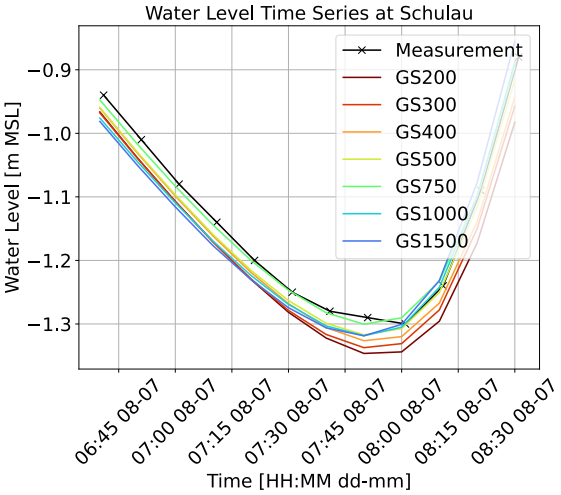

Figure 5.6: Low water level results for different grid widths at Cuxhaven [m]

Comparing the results to the measurement, show that at Cuxhaven, for high water levels, the simulations with larger grid widths are closer to the measurements. For low water the simulation that matches the best to the measurements is the simulation with a 400 m grid width. At Schulau and St.Pauli, during high water, the simulations with smaller grid widths show the closest alignment with the measured data. For low water levels, the runs with the smallest grid width are the least closest. The timing difference between the simulations and the measurements was around 15 minutes at Cuxhaven for both high and low water levels, while at Schulau, it was less than 10 minutes. This indicates that the modelled tidal wave propagates faster through the model domain than in reality.

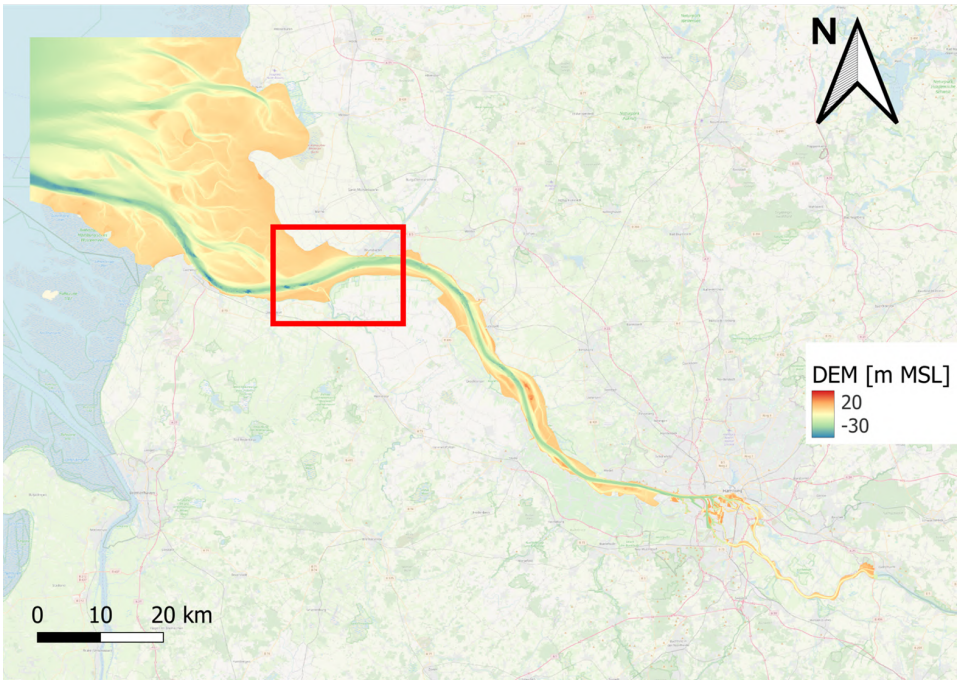

Figure 5.7: Reversal area of grid width order in water level results, area indicated with red box

5.1.2 Flow velocity results

Figure 5.8 shows the absolute flow velocity results at LZ1, with the 1500 m grid simulation (dark blue line) displaying significantly higher velocities and a tidal delay compared to other simulations. The differences among the other simulations are minimal. The lack of a clear trend is due to the dependence of flow velocities on the specific placement of LZ1 within the computational cell, as 3Di uses cell-averaged velocities (as explained in section 3.3.1). The timing of the cases matches to those of the measurements.

The simulation with a grid width of 1500 m has higher depth-averaged velocities, which can be explained by its cell capturing a deeper part of the main channel, unlike the others. This pattern is also observed in other simulations, where those with slightly higher velocities correspond to deeper cells. Figure 5.9 shows the 1500 m computational cell, and Figure 5.10 provides an example of a computational cell that does not include the navigation channel. The figures showing the placement of measurement point LZ1 within the computational cell and the cell's position relative to the bed level.

5.1.3 Computational time

Analyzing the computational time required for these simulations (Table 5.1), it is evident that larger grid widths result in reduced computational time. The amount of time reduction when increasing the grid width decrease, for example when increasing the grid width from 300 m to 400 m the time reduction is 33 minutes while the time reduction from 400 m to 500 m is 16 minutes.

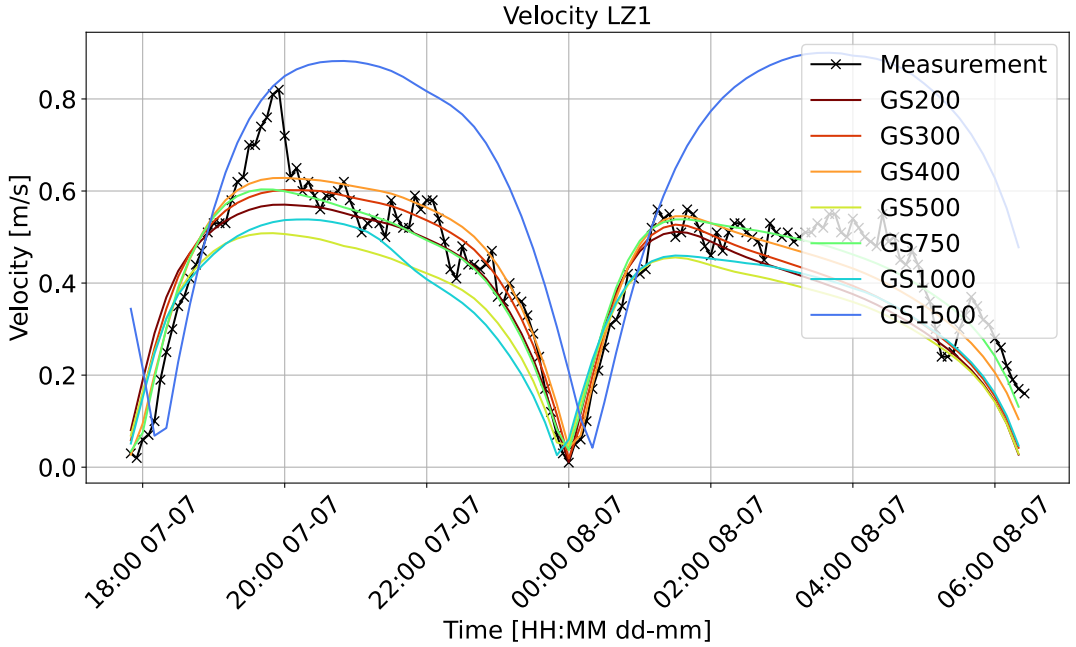

Figure 5.8: Flow velocity results for different grid widths at LZ1 [m]

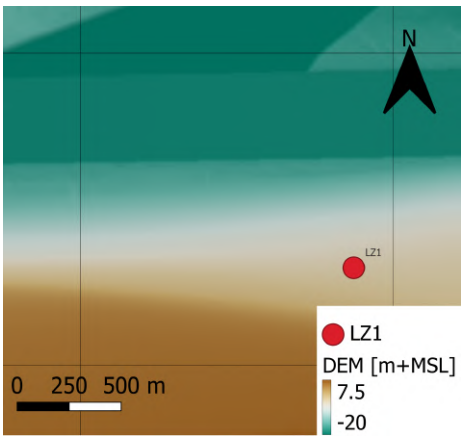

Figure 5.9: LZ1 located in a cell with a width of 1500 m, the navigation channel (dark green) is located in the cell

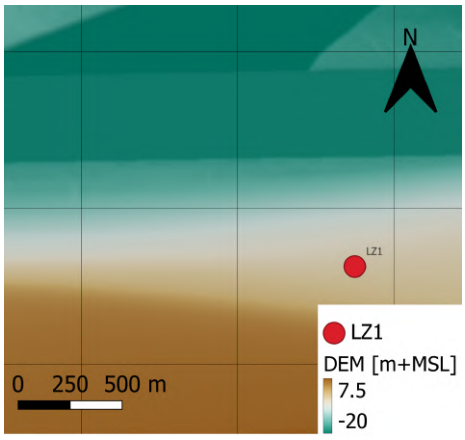

Figure 5.10: LZ1 located in a cell with a width of 750 m, the navigation channel (dark green) is not located in the cell

Table 5.1: Grid width and computational time, when using a time step of 10 s

Grid width [m]	200	300	400	500	750	1000	1500
Computational time for a simulation of 15 days [min]	164	78	45	29	14	8	4

5.2 Time step

Balancing the accuracy with the computational time needed, the 400 m grid emerges as the most suitable for further use. The simulation with this grid had acceptable hydrodynamic results while maintaining a reasonable computational load of 45 minutes for a 15-day simulation. Therefore, the 400 m grid width will be used in the time step cases (Table 3.1).

5.2.1 Water level results

The impact of changing time steps is the same across the measurements locations. The tidal cycle at Cuxhaven is shown in Figure 5.11, where it can be seen that increasing the time step results in an increased tidal range. This can also be seen in Figures 5.12 and 5.13, which shows the high and low water levels of a tidal cycle. The difference between the simulations during both high and low water is 3 cm. At Schulau and St.Pauli, the differences between simulations are larger. During high water the differences between the simulations have a maximum of 12 cm at both Schulau and St.Pauli, during low water this difference is 5 cm. The differences between the simulations increase further upstream. The differences between Schulau and St.Pauli are not notable, as these locations are close to each other. The figures of the water level results at Schulau and St.Pauli are provided in Appendix C.2.1.

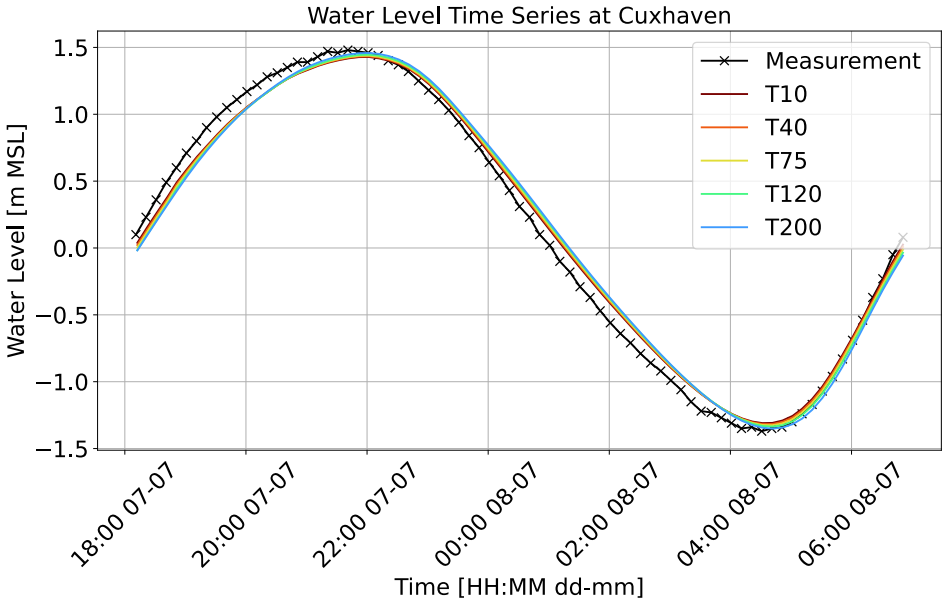

Figure 5.11: Water level results for different time steps at Cuxhaven with a grid width of 400 m

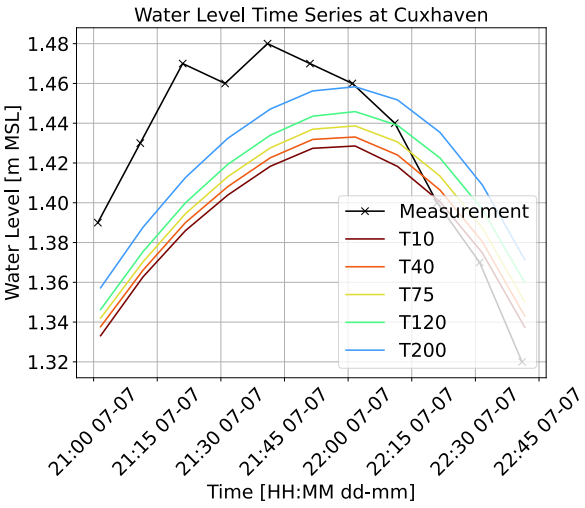

Figure 5.12: High water level results for different time steps [s] at Cuxhaven with a grid width of 400 m

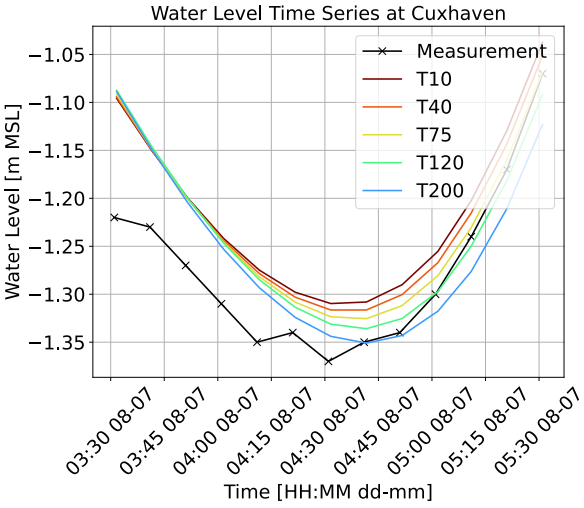

Figure 5.13: Low level results for different time steps [s] at Cuxhaven with a grid width of 400 m

Not only the tidal ranges differ, also the timing of the peaks differs between simulations. Where the tidal delay at Cuxhaven was 5 minutes, it reaches up to 15 minutes at Schulau and St.Pauli when comparing the cases T10 and T120. These differences between simulations in water levels and tidal range can be attributed to the model's ability to capture small-scale processes which is less when using larger time step leading to discrepancies.

Comparing the simulations to the measurements, it is evident that the simulations with the largest time steps align best with the measured peak values in both high and low water, although when looking at timing the worst.

5.2.2 Flow velocity results

Flow velocity simulations (Figure 5.14) also display variations tied to time step size, with larger time steps resulting in higher velocities and tidal delays. The higher velocities are inline with the larger tidal ranges, discussed in Section 5.2.1. A comparable pattern is observed at location LZ3 (Appendix C.1.3).The simulations with the shortest time steps matches the best to the measurements.

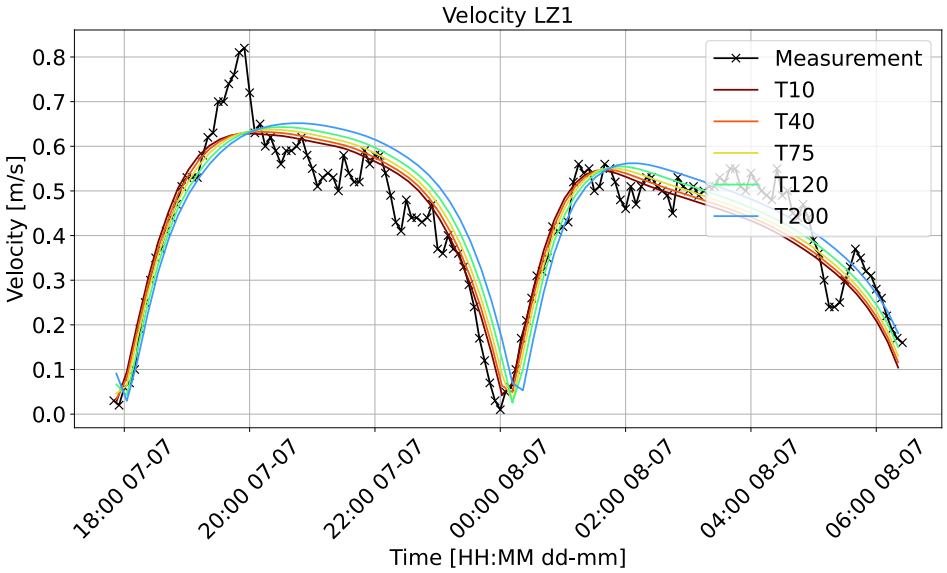

Figure 5.14: Flow velocity results for different time steps [s] at LZ1 with a grid width of 400 m

5.2.3 Computational time

In terms of computational efficiency, larger time steps drastically reduce the time required for simulation. As shown in Table 5.2, simulations with time steps of 120 s and 200 s are the fastest, but they exhibit the largest lag times. For the remaining time steps of 10 s, 40 s, and 75 s, the simulation with a 10 s time step demonstrates the best match to measurements, but with marginal differences compared to simulations with 40 s and 75 s time steps. The most substantial reduction in computational time is achieved when transitioning from a 10 s time step to a 40 s time step. The reduction in computational time between the 40 s and 75 s simulations is less, with the 40 s time step simulation providing a slightly better match to the measurements.

Table 5.2: Time step and computational time when using a grid width of 400 m

Time step [s]	10	40	75	120	200
Computational time for a simulation of 15 days [min]	45	16	12	9	8

5.3 Combination time step and grid width

The relationship between time step and grid width significantly impacts model results, so it's essential to explore the combined effect across different grid widths and time steps. Since time steps of 120 s and 200 s caused an extra timing shift of 15 minutes compared to the 10 s case, when using a grid width of 400 m, they will not be applied to other grid widths. The focus will be on time steps of 10, 40, and 75 s for grid widths of 200, 300, 500, and 750 m, excluding 1000 m and 1500 m grids due to their inaccuracy in the river section.

5.3.1 Water level results

A consistent trend is observed across all measurement locations for simulations with varying grid widths: when the time step increases, both the tidal range and lag time increase. The extent of this increase depends on the grid width, with larger grids better able to accommodate longer time steps due to greater numerical stability, thereby reducing the influence of larger time steps. In contrast, the smaller grids capture smaller-scale processes, making them more sensitive to changes in time steps. This pattern is illustrated in Figure 5.15, where simulations with a 200 m grid show greater variation in both tidal range and lag time compared to those with a 750 m grid.

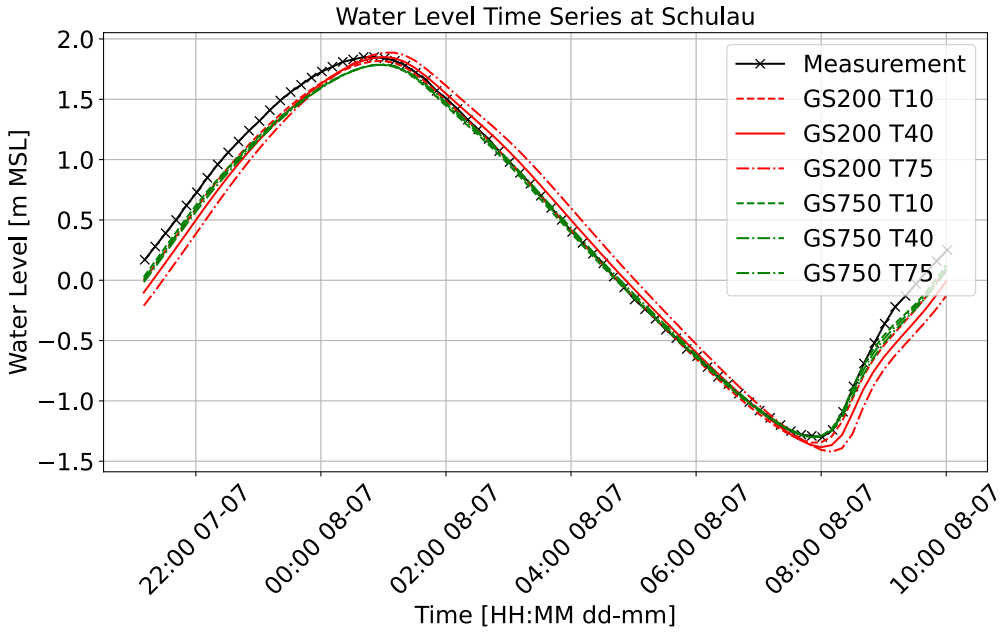

Figure 5.15: Water level results for different time steps at Schulau with a grid width of 200 m or 750 m

5.3.2 Flow velocity results

For all grid widths, velocity values increase with larger time steps, and lag times also increase across the different grid widths. However, the impact of time step variations is more pronounced for smaller grid widths (Figure 5.16), similar to the water level trends. The explanation for this increased sensitivity in smaller grids is discussed in the previous section.

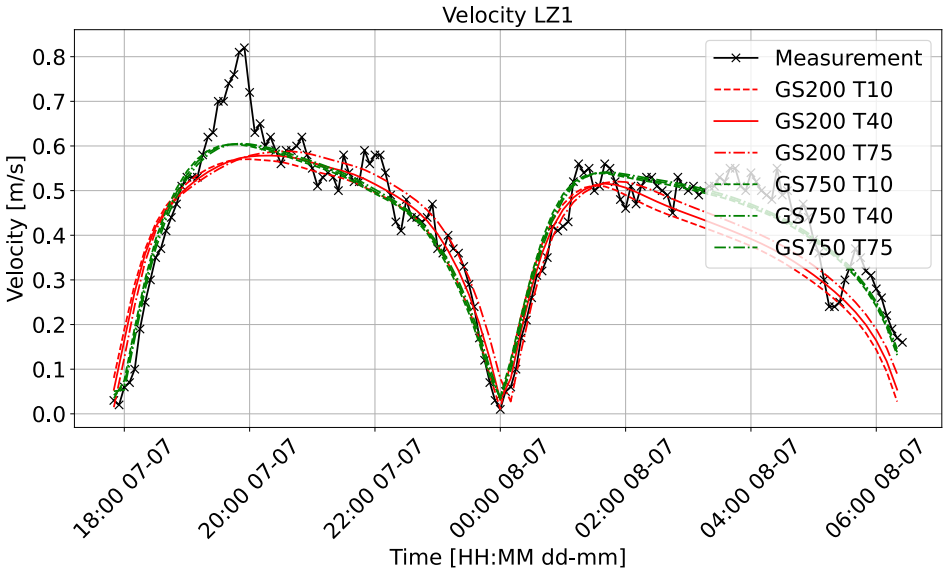

Figure 5.16: Flow velocity results for different time steps at LZ1 with a grid width of 200 m or 750 m

5.3.3 Computational time

Table 5.3 presents the computational times for various grid widths and time steps. The data show that increasing either the grid width or the time step leads to a reduction in computational time. As already observed for the 400 m simulations, the most substantial decrease in computational time across all grid widths occurs when transitioning from a 10 s to a 40 s time step.

Table 5.3: Computational time for different grid widths [m] and time steps [s]

Time step [s]/Grid width [m]	**10**	**40**	**75**
200	164	67	58
300	78	27	22
400	45	16	12
500	29	10	7
750	14	5	3

Chapter 6

Results Q3: Local grid refinements

How do the location and extent of local grid refinements affect the simulated estuarine hydrodynamics throughout the model domain and the computational time required for a simulation?

The previous chapter has shown the effect of different grid widths on the hydrodynamics in the estuary. In this chapter, the results of simulations with various types and extents of local grid refinements will be analyzed, where the effect on the hydrodynamics will be researched throughout the model domain. Based on the results of the previous question, a base case with a grid width of 400 m together with a time step of 40 s is recommended to use, this combination gives the most promising combination for accuracy and computational time. The refinement cases are stated in Table 3.1 and the locations are shown in Figure 3.8. These cases will be referred to using the format [outside grid width]-[inside grid width], with the grid width expressed in meters. Nevertheless, this unit will not be mentioned when referring to specific cases. For clarity the base case is shown as 400-400 in the results of this chapter.

6.1 Port of Hamburg

6.1.1 Water level results

The local grid refinement has been implemented just downstream and in the port of Hamburg. The St.Pauli measurement location is within the refined grid area, while Schulau is just outside, and Cuxhaven is further downstream.

At St.Pauli, high water levels increase as the inside grid width decreases (same color different line style), while low water levels decrease, indicating a larger tidal range with finer grids (Figures 6.2 and 6.3). The differences are more pronounced during high tide (up to 6 cm) than low tide (up to 4 cm). No timing differences are observed. Comparing simulations with the same grid width in the port but different grid widths outside (e.g., 800-200 to 400-200), a smaller grid width outside results in a larger tidal range. This aligns with previous findings at St.Pauli (section 5.1.1).

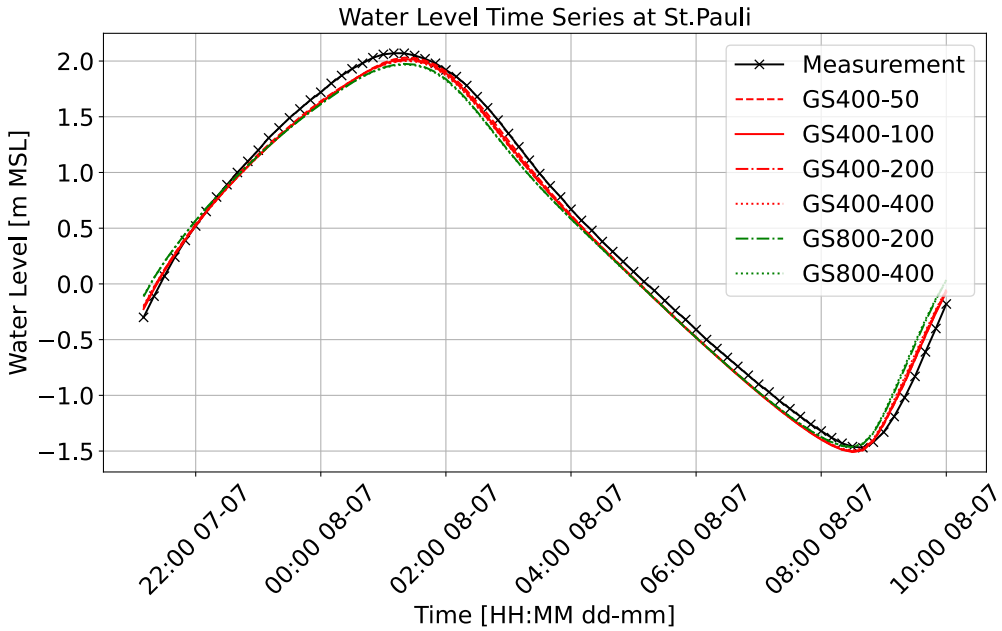

Figure 6.1: Water level results at St.Pauli for different local grid refinements [m] in the Port area

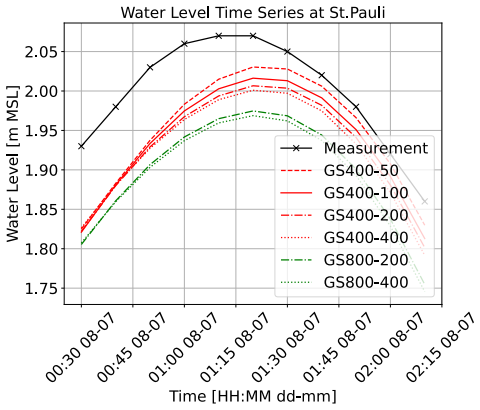

Figure 6.2: High water level results at St.Pauli for different local grid refinements [m] in the Port area

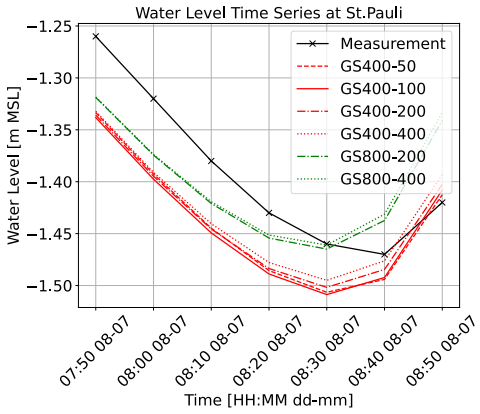

Figure 6.3: Low water level results at St.Pauli for different local grid refinements [m] in the Port area

At Schulau, smaller grids in the port leads to a decrease in high water levels (Figure 6.5) and an increase in low water levels (Figure 6.6), reducing the tidal range. Increasing the grid width outside the port decreases the tidal range.

The effects of grid width reduction differ between St.Pauli and Schulau. At St.Pauli, smaller grid widths in the port lead to an increased tidal range, likely due to reduced numerical diffusion. In contrast, at Schulau, a smaller grid width in the port slightly decreases the tidal range, though the differences are minimal and cannot be attributed to a single process. Water level results at Cuxhaven (Appendix D.1.1) show no significant differences between simulations

with different grid widths in the port, with variations under 0.5 cm. Cuxhaven's distance from the refinement area likely makes the effects of the refinement in the port negligible.

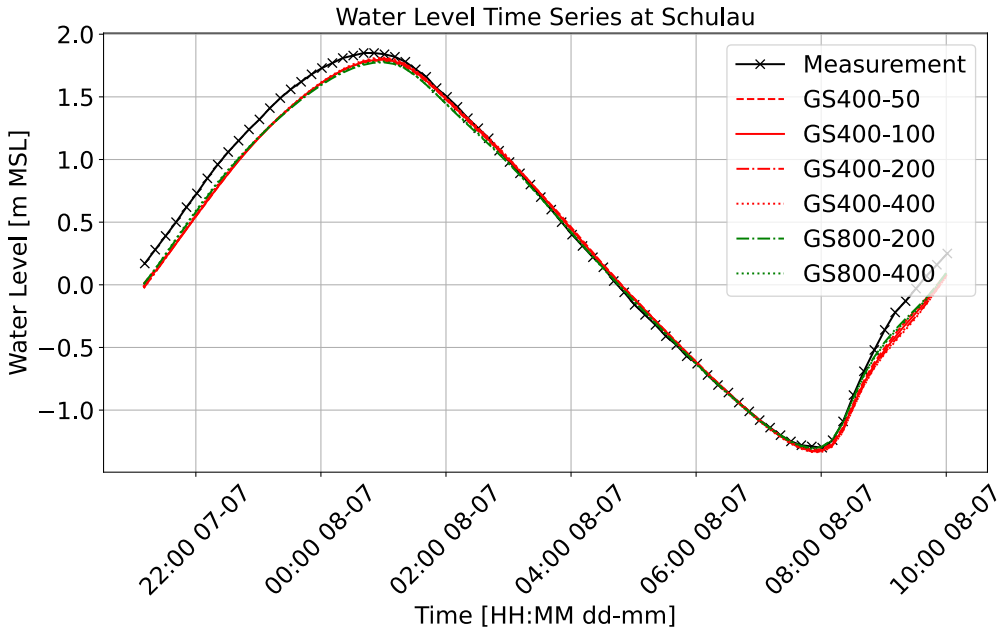

Figure 6.4: Water level results at Schulau for different local grid refinements [m] in the Port area

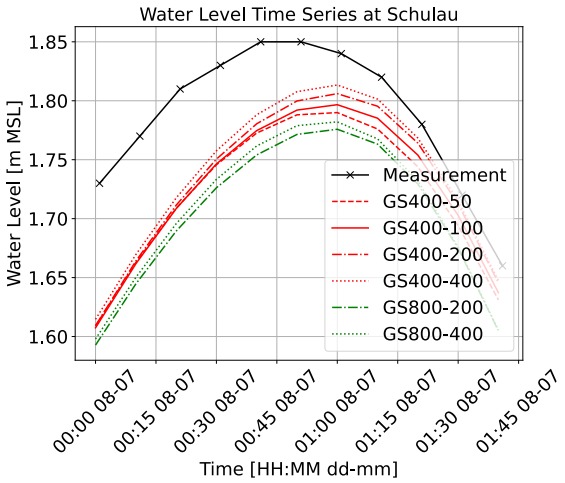

Figure 6.5: Water level results at Schulau for different local grid refinements [m] in the Port area

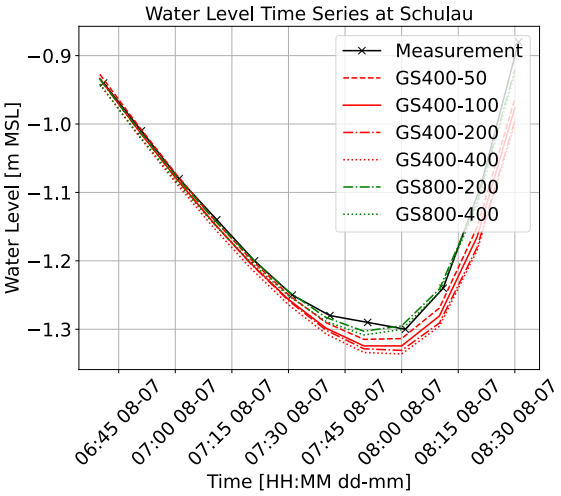

Figure 6.6: Water level results at Schulau for different local grid refinements [m] in the Port area

The Port refinement cases will be evaluated against the measurements using RMSE values and the previously provided figures. Table 6.1 presents the differences in RMSE values and computational time, using the 400 m grid simulation as the reference case. The comparison with the base case aims to evaluate whether the refinement cases enhance the model's results compared to the measurements, relative to the current base configuration.

Reducing the grid width in the port area to 200 m has minimal impact on water levels, but further reductions to 100 m or 50 m significantly improve the match to the measurements at St.Pauli, especially when a 400 m grid is used outside the port. Conversely, increasing the grid width outside the port from 400 m to 800 m leads to results that deviate more from the measurements, particularly at Schulau and St.Pauli during high water, and at Cuxhaven during low water.

In summary, the most significant differences are observed at St.Pauli and Schulau, near the local grid refinement area, while locations farther away, like Cuxhaven, show no notable effects.

Table 6.1: Comparison of RMSE values for the Port area's local grid refinement cases against the base case [cm]. Green indicates significant improvement, yellow represents an insignificant difference, and red shows a significant worsening. (T: total water levels including timing differences, H: high water levels excluding timing differences, L: low water levels excluding timing differences)

Grid width [m]	Computational time [min]	Cuxhaven [cm]			Schulau [cm]			St.Pauli [cm]		
		T	H	L	T	H	L	T	H	L
Base case: 400-400	16	12.5	5.1	4.7	14.7	7.2	5.2	9.4	8.9	4.5
400-50	+92	-0.6	+0.3	+0.0	-0.7	+1.7	-1.0	-1.0	-1.7	+0.8
400-100	+17	-0.7	+0.0	-0.2	-0.3	+1.3	-0.7	-0.6	-1.0	+0.7
400-200	+2	-0.1	+0.0	-0.1	+0.1	+0.6	-0.4	-0.2	-0.3	+0.3
800-200	-10	+3.7	-0.1	+8.1	-1.6	+3.7	-1.4	+2.2	+3.0	-0.2
800-400	-12	+3.8	-0.1	+8.2	-1.8	+3.0	-1.4	+2.6	+3.4	-0.2

6.1.2 Flow velocity results

The flow velocity results at location LZ1 are visualized in Figure 6.7. Simulations with the same grid width outside but different widths inside the refinement area show no significant velocity differences. Comparing the cases with the same inside grid width but different outside grid width shows a large difference in flow velocities, caused by the alignment of the grid at the measurement location, as explained in 5.1.2. Location LZ3 shows the same pattern and is located in Appendix D.1.2. Since LZ1 and LZ3 are located far from the refinement area, no velocity comparisons have been made within the refinement zone, and therefore no conclusions can be drawn about velocity differences in that region between the cases.

6.1.3 Computational time

Table 6.1 details the computational time required for each simulation compared to the 400 m base case, which took 16 minutes. Refining the grid in the port area increases computational time, while increasing the grid width outside the port reduces it. The 400-50 grid refinement case adds 92 minutes, making it impractical. The 400-100 case doubles the computational time, which is not justified by the slight improvement in results. The 400-200 case only adds 2

minutes, but it is only worth considering if the model results significantly improve. Given that increasing the grid width outside the port to 800 m worsens the results, along with the other findings, grid refinement in the port area will not be implemented in this model.

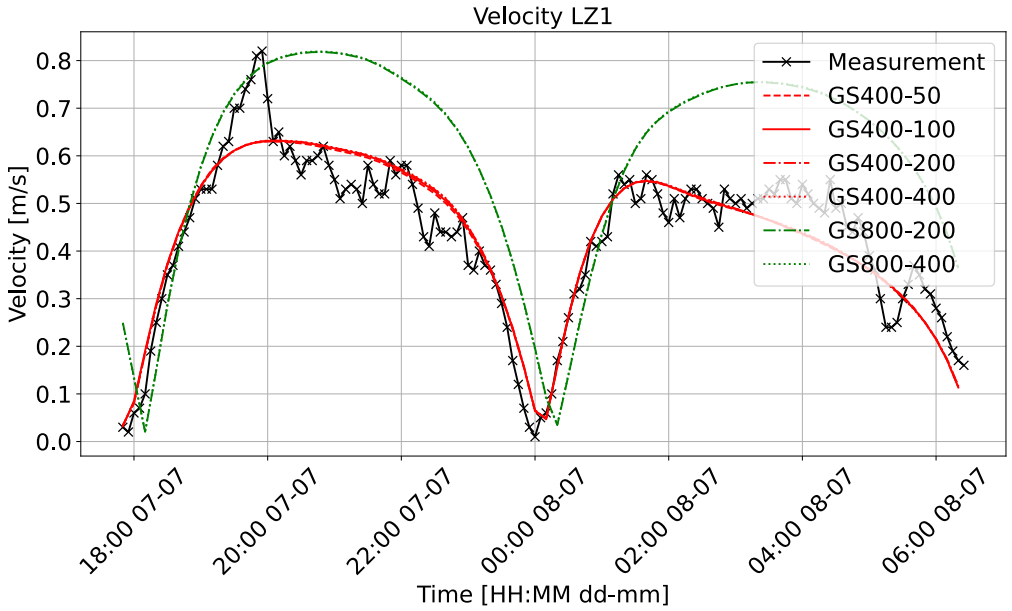

Figure 6.7: Flow velocity results at LZ1 for different local grid refinements at the Port area

6.2 River widening, river/sea division and navigation channel

In the previous section the impact of the grid refinement in the Port area is discussed. In this section the impact of the other three areas will be discussed. These refinement areas had the same trend in the results both for water levels as for flow velocity values. Only the amount of impact differs. Therefore, the areas will be discussed together. Since the areas have similar patterns, there has been chosen to only show the figures of the navigation channel, the figures of the two other refinement areas are shown in Appendix D.2 and D.3.

6.2.1 Water level results

At Cuxhaven, during high water (Figure 6.9), an increase in grid width outside the refinement area results in higher water levels. In contrast, the grid width inside the refinement area has minimal influence (>1cm) on high water levels. During low water (Figure 6.10), the grid width in the refinement area primarily determines water levels. Cases with a grid width of 400 m inside the refined area show the lowest low water levels, consistent with the results from Question 2. Additionally,increasing the grid width outside the refined area leads to even lower low water levels, resulting in larger tidal ranges.

The explanation from the previous paragraph generally applies to all three refinement areas: river widening, river/sea division, and the navigation channel. However, there are some differences in the results for the various refinement area. In the river widening case, where Cuxhaven is not located in the refined area, the inner grid had less influence during low water. In contrast, for both the river/sea division and navigation channel refinements, the grid width inside and outside the refinement area influenced water levels during low water.

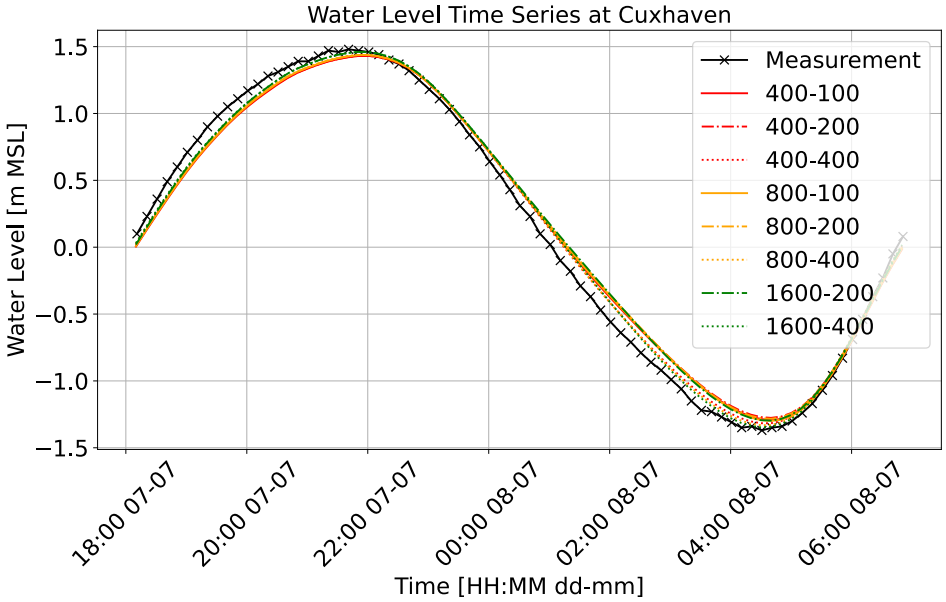

Figure 6.8: Water level results at Cuxhaven for different local grid refinements [m] in the navigation channel

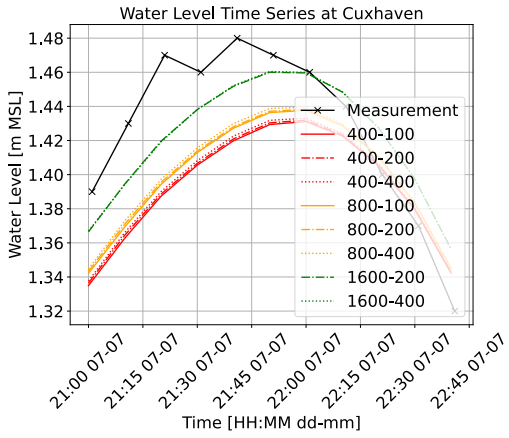

Figure 6.9: High water level results at Cuxhaven for different local grid refinements [m] in the navigation channel

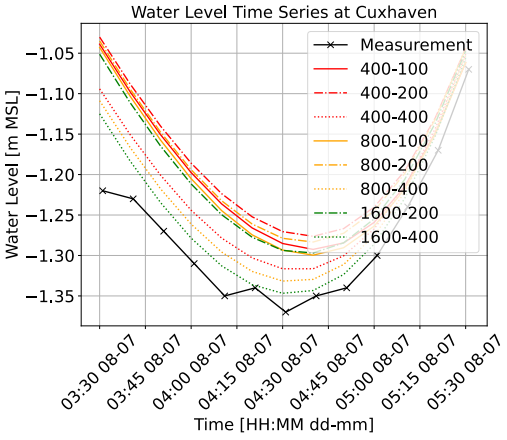

Figure 6.10: Low water level results at Cuxhaven for different local grid refinements [m] in the navigation channel

At Schulau and St.Pauli, both located within the refinement area, tidal ranges vary due to differences in both the grid widths inside and outside the refinement area. However, the grid inside the refinement area has a much greater impact, as the measurement locations are far from the area with the outside grid and key flow dynamics are captured locally. Smaller grid widths in the refinement area lead to larger tidal ranges (as discussed in Section 5.1.1), while larger outside grid widths reduce tidal ranges. Additionally, tidal delays increase with smaller grid widths inside the refined area. These trends apply to all three refinement areas: river widening, river/sea division and the navigation channel. The main difference between Schulau and St.Pauli is that the variations between cases are slightly larger at St.Pauli.

Comparing the results of the river widening, river/sea division, and navigation channel refinement cases against the measurements reveals distinct patterns. In the river widening case (Table 6.2), only the 400-100 and 400-200 cases improved the total RMSE at Cuxhaven. However, at Schulau and St.Pauli, none of the cases yield better results than the base case during low and high water levels, indicating that the base case remains the best match to the measurements overall. Therefore, grid refinement solely in the river widening area is not recommended.

In contrast, the river/sea division and navigation channel refinements show better results (Table 6.3). The 1600-400 case achieves the greatest improvement at Cuxhaven, closely followed by the 800-400 case. These cases also perform the best at Schulau and St.Pauli, outperforming the other cases in RMSE values. While some other cases show slight improvements at Schulau and St.Pauli during high water, they do not enhance RMSE at Cuxhaven. Ultimately, the 1600-400 case consistently provides the most significant overall improvement across all nine RMSE criteria for both the river/sea division and navigation channel refinements. The RMSE table of the river/sea division can be found in Appendix D.3.3.

Table 6.2: Same as Table 6.1, but now the river widening refinement cases are compared to the base case.

Grid width [m]	Computational time [min]	Cuxhaven [cm]			Schulau [cm]			St.Pauli [cm]		
		T	H	L	T	H	L	T	H	L
Base case: 400-400	16	12.5	5.1	4.7	14.7	7.2	5.2	9.4	8.9	4.5
400-100	+64	-2.4	+0.0	+0.9	+6.1	-2.7	+7.3	+2.5	-3.5	+9.7
400-200	+14	-0.7	+0.1	+0.4	+1.8	-2.0	+2.1	-1.5	-3.6	+3.1
800-100	+48	+1.3	+0.1	+9.8	+5.1	-2.9	+7.1	+1.6	-4.2	+9.7
800-200	+2	+2.7	+0.3	+9.3	+0.6	-1.5	+2.0	-1.4	-2.9	+2.9
800-400	-9	+3.4	+0.1	+8.8	-1.1	+0.7	-0.1	+0.8	+0.9	+0.0
1600-200	-3	+2.6	-1.3	+11.2	-0.4	-0.4	-0.2	-0.8	-1.7	+0.6
1600-400	-12	+3.2	-1.4	+10.7	-1.7	+2.0	-1.4	+1.9	+2.3	-0.3

Table 6.3: Same as Table 6.1, but now the navigation channel refinement cases are compared to the base case.

Grid width [m]	Computational time [min]	Cuxhaven [cm]			Schulau [cm]			St.Pauli [cm]		
		T	H	L	T	H	L	T	H	L
Base case: 400-400	16	12.5	5.1	4.7	14.7	7.2	5.2	9.4	8.9	4.5
400-100	+65	+2.1	-0.4	+2.6	+12.9	-1.7	+10.2	+9.6	-1.5	+13.1
400-200	+11	+2.2	-0.1	+4.5	+4.0	-2.4	+3.5	-0.5	-4.1	+4.6
800-100	+11	+2.1	-1.1	+1.8	+12.9	-1.4	+10.4	+9.5	-1.0	+13.4
800-200	+0	+2.2	-0.8	+3.6	+3.8	-2.5	+3.6	-0.8	-4.3	+4.8
800-400	-10	-0.4	-0.7	-1.5	-0.3	-0.2	+0.2	-0.1	-0.2	+0.2
1600-200	-2	+1.9	-2.6	+2.3	+3.7	-2.8	+4.1	-1.0	-4.7	+5.5
1600-400	-12	-0.6	-2.5	-2.4	-0.5	-1.3	+0.5	-0.6	-1.8	+0.5

6.2.2 Flow velocity results

Measurement locations LZ1 and LZ3 exhibit similar trends for the river widening and river/sea division area. The highest flow velocities are observed in the 400 m inside grid cases, followed by the 200 m and 100 m cases, with no significant tidal delays between these cases. Interestingly, the velocity values do not appear to be influenced by the grid width outside of the river at these locations.

However, the velocity results for the navigation channel refinement cases present a different pattern. At LZ3 (Figure 6.11), simulations with the 100 m inside grid capture the timing of the measured flow velocities to a better extent, showing an earlier response than the other grid widths. In contrast, at LZ1 (Figure 6.12), the 100 m inside grid simulations exhibit delayed flow velocities compared to the others. This suggests that some processes influencing peak timing are being captured by the smaller inside grid, where the tidal wave propagates faster at LZ3, but later at LZ1, indicating a localized influence of the grid placement on tidal propagation in this region.

6.2.3 Computational time

As previously mentioned, computational time depends on both grid width and time step. The computational times are noted in Tables 6.2, 6.3 and Appendix D.1. For all three refinement areas, the 400-100 case results in an excessive increase in computational time, while the extra time needed for the 400-200 and 800-100 cases may be acceptable if the results significantly improve. The 800-400 and 1600-400 cases, however, show reduced computational times across all refinement areas. Additionally, the 1600-200 case in the river widening area also requires less time. However, cases can only be chosen in consideration of the computational time together with the accuracy.

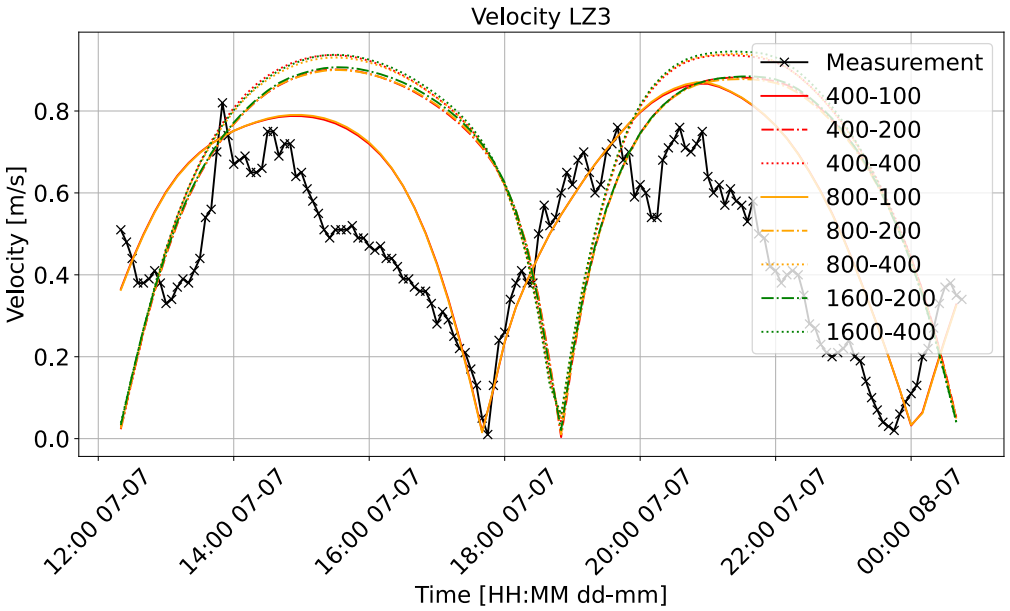

Figure 6.11: Flow velocity results at LZ3 for different local grid refinements [m] in the navigation channel, LZ3 is located in the refined area

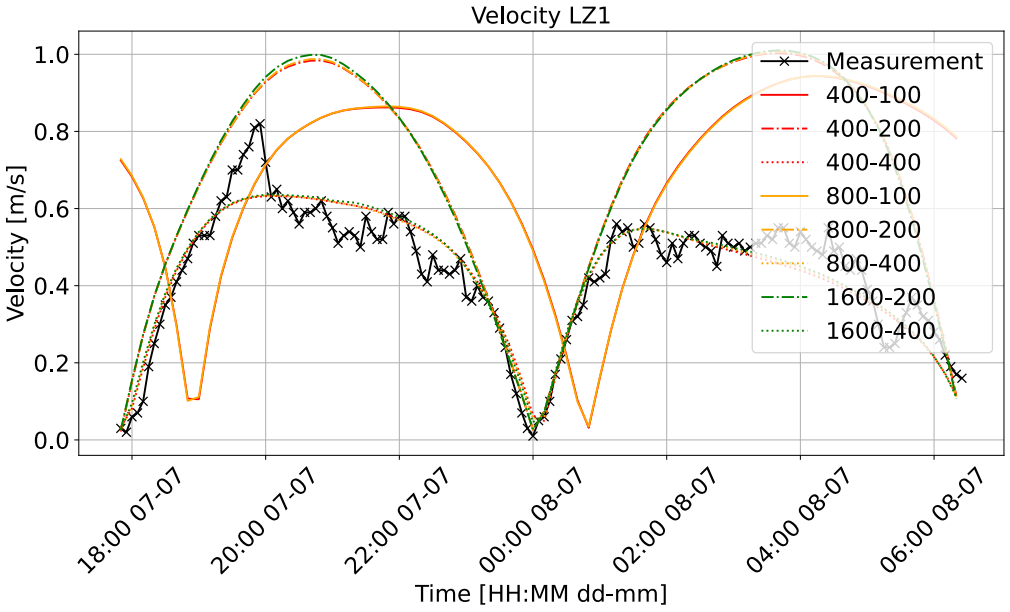

Figure 6.12: Flow velocity results at LZ1 for different local grid refinements [m] in the navigation channel, LZ1 is located in the refined area

6.3 Combining findings

In previous sections, the results highlighted the effects of local grid refinement at individual locations, focusing on areas like the port, river widening, river/sea division, and navigation channel. These analyses revealed that refining only certain parts, such as the port or until the river widening, had limited impact on improving model accuracy together with computational time. However, refinements including the navigation channel or the transition area between the sea and river demonstrated a positive influence on model results and computational time, especially using the 1600-400 grid. This finding underlines the importance of selective grid refinement in areas where hydrodynamic processes are more sensitive to grid resolution.

Building on these insights, grid refinements are applied to multiple locations simultaneously. By comparing various combinations of refinement zones, particularly focusing on the successful 1600-400 extent and refinement in the area where the river widens, this section aims to extent the understanding of how grid resolution influences model results. The combinations selected are based on previously defined areas (Figure 3.8) and are shown in Appendix D.5. The following refinement areas are chosen for comparison, with their corresponding names as shown in the figures used throughout this section:

- 1600 outside - 400 in Navigation channel (NC)
- 1600 outside - 400 in navigation channel and River/sea line (NC + R/S)
- 1600 outside - 400 Sea/river division (R/S)
- 1600 outside - 400 Navigation channel + river widening (NC + RW)
- 1600 outside - 400 Navigation channel only between river widening and sea/river line + river widening (NC partly + RW)

6.3.1 Water level results

For all cases, Cuxhaven, Schulau, and St.Pauli are within the refinement area. In Cuxhaven, the base case shows the smallest tidal range. The tidal ranges (Figures 6.14 and 6.15) are the highest for the NC + RW and NC cases, which have almost similar grid refinement, followed by NC + R/S, NC partly, and R/S. Refining the navigation channel in the sea increases the tidal ranges compared to cases without refinement there. There are no timing differences between the simulations. Comparing the simulations to the measurements, show that the NC + RW and the NC cases perform the best.

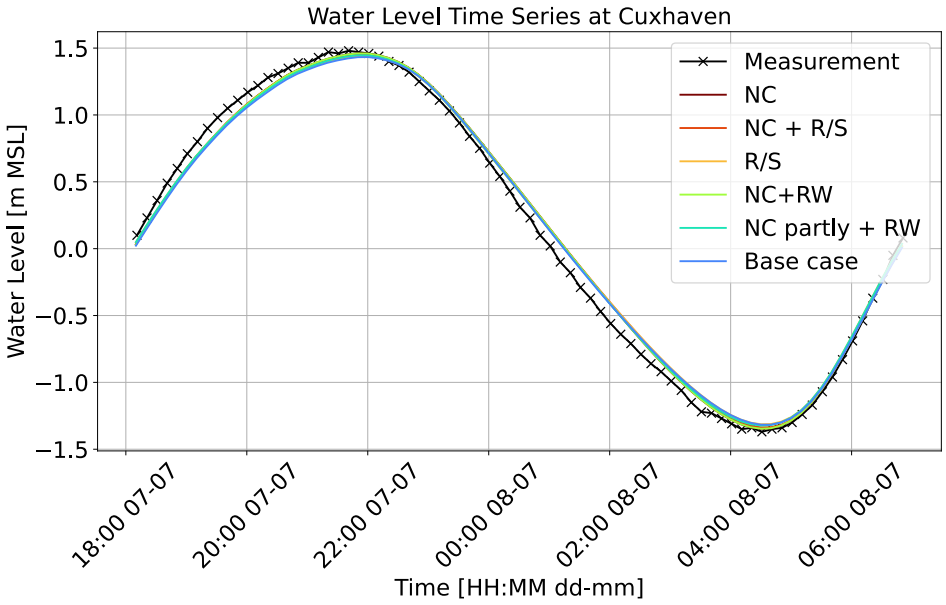

Figure 6.13: Water level results at Cuxhaven for different local grid refinements combinations

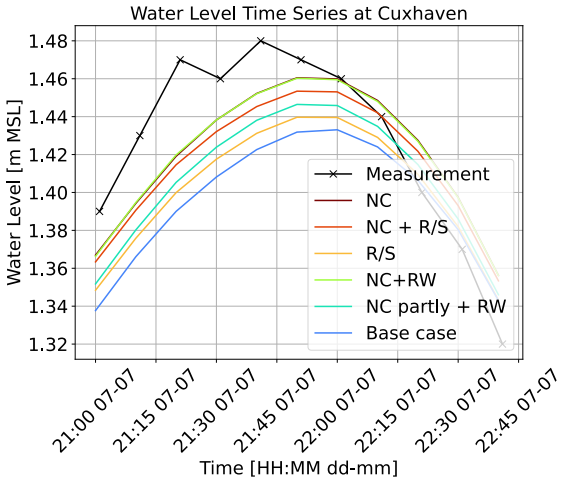

Figure 6.14: High water level results at Cuxhaven for different local grid refinements combinations [m]

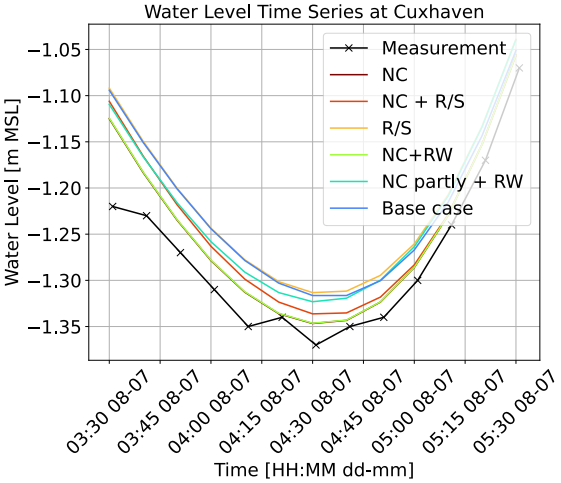

Figure 6.15: Low water level results at Cuxhaven for different local grid refinements combinations [m]

At Schulau and St.Pauli, the tidal ranges show only minor differences between cases (less than 1 cm), making them all similarly close to the measurements. This may be because these locations are far from the areas where the refinement differences occur. Detailed results for Schulau and St.Pauli can be found in Appendix D.5.1.

Overall, at all locations, NC, NC + R/S, and NC + RW cases have the largest tidal ranges and best match to the measurements (Table 6.4). Local grid refinement in the navigation channel at sea is crucial, next to some refinements in the river widening area. For low water, NC and NC + RW cases perform best at Cuxhaven, with no significant differences at other locations during low tide.

Table 6.4 shows the RMSE values of the discussed runs. All cases perform better or equally on the RMSE's compared to the base case, except for a slight worsening in low water levels at Schulau in the NC + RW case. The R/S and NC partly + RW cases perform the worst among the refined grid cases, likely due to the lack of extra refinement in the sea navigation channel. The NC and NC + RW cases show the most significant improvements, but due to the NC + RW case's minor setback, the NC case is considered to have the best match in simulated hydrodynamics compared to the measurements.

Table 6.4: Same as Table 6.1, but now the local grid refinement combinations are compared to the base case.

Grid width	Computational time [min]	Cuxhaven [cm]			Schulau [cm]			St.Pauli [cm]		
		T	H	L	T	H	L	T	H	L
Base case: 400-400	16	12.5	5.1	4.7	14.7	7.2	5.2	9.4	8.9	4.5
NC	-12	-0.6	-2.5	-2.4	-0.5	-1.3	+0.5	-0.6	-1.8	+0.5
NC + R/S	-10	-0.4	-2.0	-1.8	-0.6	-1.3	+0.2	-0.8	-1.7	+0.2
R/S	-11	-0.6	-0.8	+0.3	-1.3	-0.7	-0.3	-0.1	-0.7	-0.1
NC + RW	-11	-0.6	-2.5	-2.3	-0.6	-1.5	+0.6	-0.7	-2.0	+0.5
NC partly + RW	-11	-0.9	-1.4	-0.6	-1.4	-0.9	+0.0	+0.0	-1.1	+0.1

6.3.2 Flow velocity results

The flow velocity measurement locations LZ1 and LZ3 are both located in the refinement areas. The results of location LZ3 are shown in Figure 6.16. No significant differences in flow velocities can be found between the different simulations. This is also the case for LZ1, which is located in Appendix D.5.2.

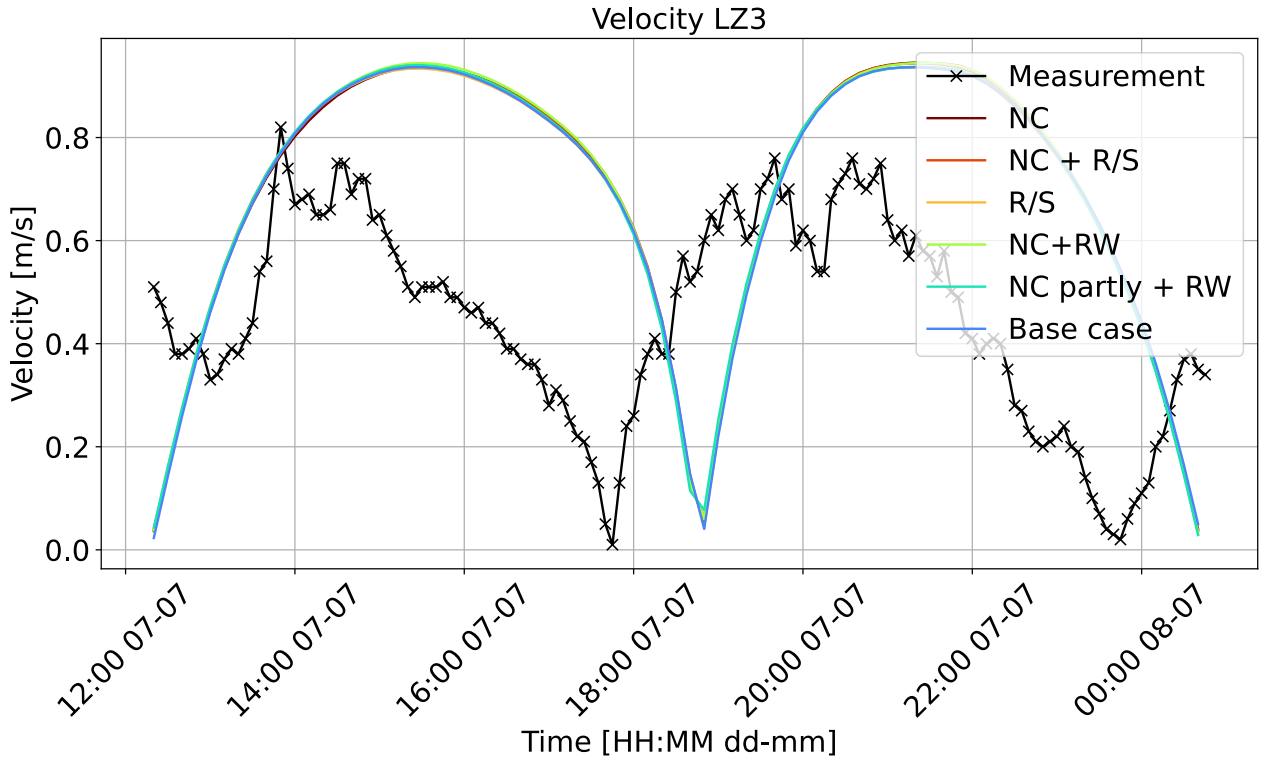

Figure 6.16: Flow velocity results at LZ3 for different local grid refinements combinations [m]

6.3.3 Computational time

The computational times are stated in Table 6.4. All the cases need less computational time than the base case. There is a small difference in computational times between the cases, where the cases with the most refinement area need the most computational time. The NC case is the most computational efficient.

Chapter 7

Results Q4: Roughness values and River discharge

How do the variations in uniform roughness values, as well as the inclusion/exclusion of upstream river discharge, influence the simulated estuarine hydrodynamics throughout the model domain?

This chapter, will focus on physical parameters, specifically roughness values and river discharge. In the previous chapter, various local grid refinements were considered. Based on the results, the case with a grid width of 1600 m outside the navigation channel and 400 m within the navigation channel provides the best match to the measurements and is the most computational efficient. Therefore, this case will be used as base case in this chapter.

7.1 Roughness values

7.1.1 Water level results

The influence of varying roughness values is similar across all measurement locations. The water level results indicate that smaller roughness values increase the tidal range. Differences between simulations are more pronounced during low water (Figure 7.3) than high water (Figure 7.2), particularly before the tide turns. The differences between the cases increase for locations upstream, indicating that the applied roughness value has a greater influence upstream.

Based on the figures and the RMSE values in Table 7.1, it can be observed that at Cuxhaven, simulations with lower roughness generally align more closely with the measurements. At Schulau, lower roughness also shows a better match overall and during high tide. However, during low water, higher roughness match better to the measurements, with the 0.0250 $s/m^{1/3}$ case showing a closer fit than the 0.0255 $s/m^{1/3}$ case. In St.Pauli, increasing roughness worsens the overall match to the measurements, while reducing roughness has little impact. During high tide, lower roughness improves the match, but only the 0.0250 $s/m^{1/3}$ case provides better results during low tide compared to the base case.

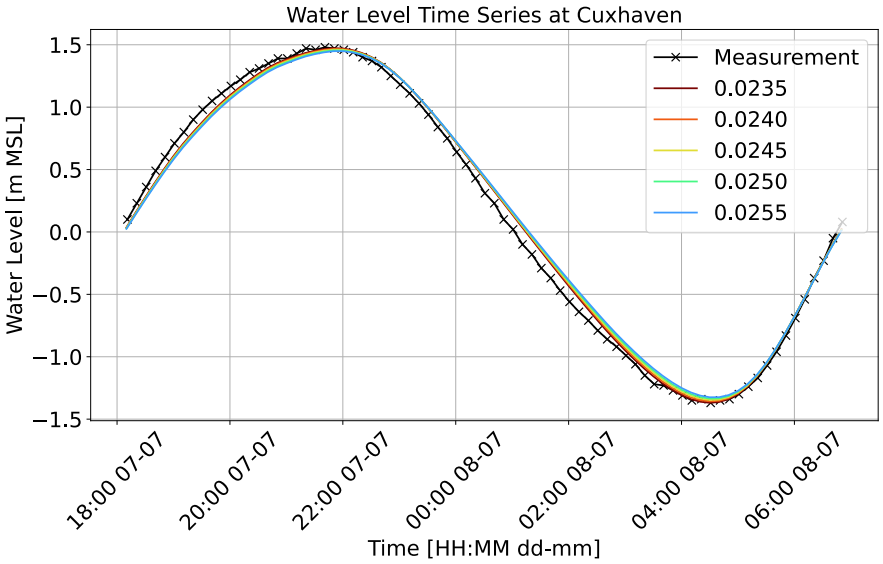

Figure 7.1: Water level results for different roughness values at Cuxhaven [s/m$^{1/3}$]

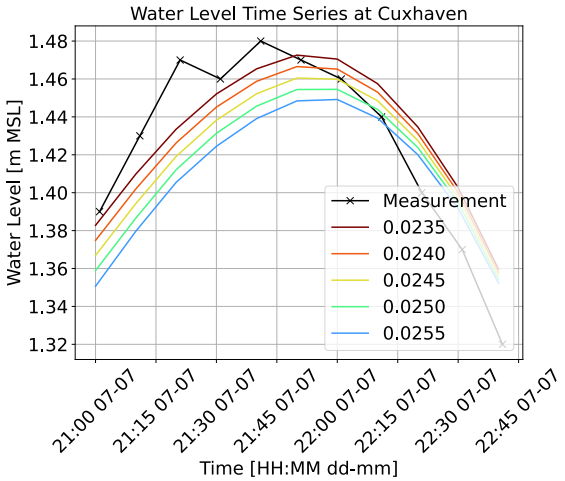

Figure 7.2: High water level results for different roughness values at Cuxhaven s/m$^{1/3}$

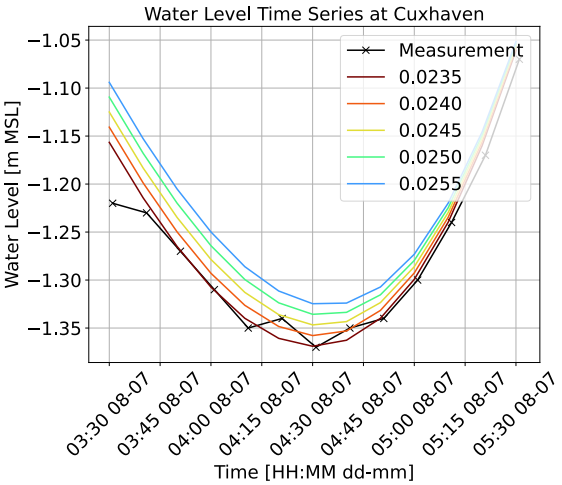

Figure 7.3: Low water level results for different roughness values at Cuxhaven [s/m$^{1/3}$]

Table 7.1: Same as Table 6.1, but now the cases with different roughness values are compared to the base case.

Roughness values	Computational time	Cuxhaven			Schulau			St.Pauli		
	[min]	T	H	L	T	H	L	T	H	L
Base case: 0.0245	4	11.9	2.6	2.3	14.2	5.8	5.7	8.8	7.1	5.0
0.0235	+0	-1.4	-0.4	+0.2	-1.1	-0.9	+6.8	+0.5	-2.8	+7.2
0.0240	+0	-0.7	-0.3	-0.2	-0.8	-1.3	+3.2	-0.3	-2.1	+3.2
0.0250	+0	+0.8	+0.4	+0.7	+1.1	+2.1	-1.9	+1.2	+2.6	-0.9
0.0255	0	+1.5	+1.0	+1.6	+2.5	+4.4	-0.9	+3.0	+5.3	+1.4

7.1.2 Flow velocity results

The flow velocity results of the simulations with different roughness values at location LZ1 are shown in Figure 7.4. It can be seen that if a higher roughness value is implemented in the model the flow velocities decrease, this is both for rising and falling tide the case. The difference in maximum flow velocities between two simulations with a difference of 0.0005 $s/m^{1/3}$ in roughness values is the same when comparing different pairs of simulations. The patterns identified at location LZ1 also hold for measurement location LZ3, these results are provided in Appendix E.1.2.

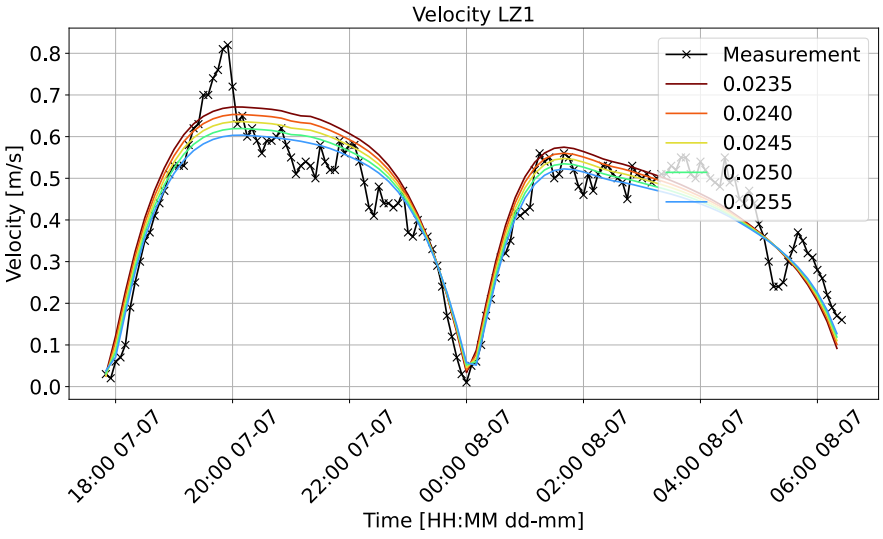

Figure 7.4: Flow velocity results for different roughness values at LZ1 [$s/m^{1/3}$]

7.1.3 Computational time

The applied roughness values do not affect the computational time for the simulations. Therefore, the selection of an appropriate roughness value is based solely on its effects on water levels and flow velocities. While reducing roughness improves conditions for total and high water levels, it worsens the match at low water. Consequently, the base case with a Manning roughness value of 0.0245 $s/m^{1/3}$ remains the most suitable choice for the Elbe estuary.

7.2 River discharge

7.2.1 Water level results

Different river discharge time series (Table 3.1) were applied to the river boundary of the base case. At Cuxhaven, the furthest from the river boundary, no significant differences between simulations are observed, since the tidal impact here is larger compared to locations upstream. During high water the differences between cases are smaller than during low water, likely due to the greater influence of river discharge during low tide when tidal effects are weaker.

At Schulau and St.Pauli, more noticeable differences in water levels are observed, where the differences at St.Pauli are larger, since this one is more closely located to the boundary. Within a single tidal cycle, simulations with higher river discharge consistently result in higher water levels (Figure 7.5). The applied time series has more influence on the water levels during low water than during high water, this was also the case at Cuxhaven. Also shown in table 7.2, which illustrates the impact of river discharge on both high and low water levels at 7 locations throughout the model domain, comparing the cases with the highest and lowest discharge. Downstream of the point where the river widens, the discharge has no significant effect on water levels anymore. The figures of Cuxhaven and St.Pauli are located in Appendix E.2.1.

Table 7.2: Average differences in water levels between the maximum discharge case and the zero discharge case, Elbe-km shown in Figure 2.2

Elbe-km	Difference during high water [cm]	Difference during low water [cm]
600	43	108
625	10	11
650	6	7
675	3	4
700	1	3
720	<1	2
740	<1	<1

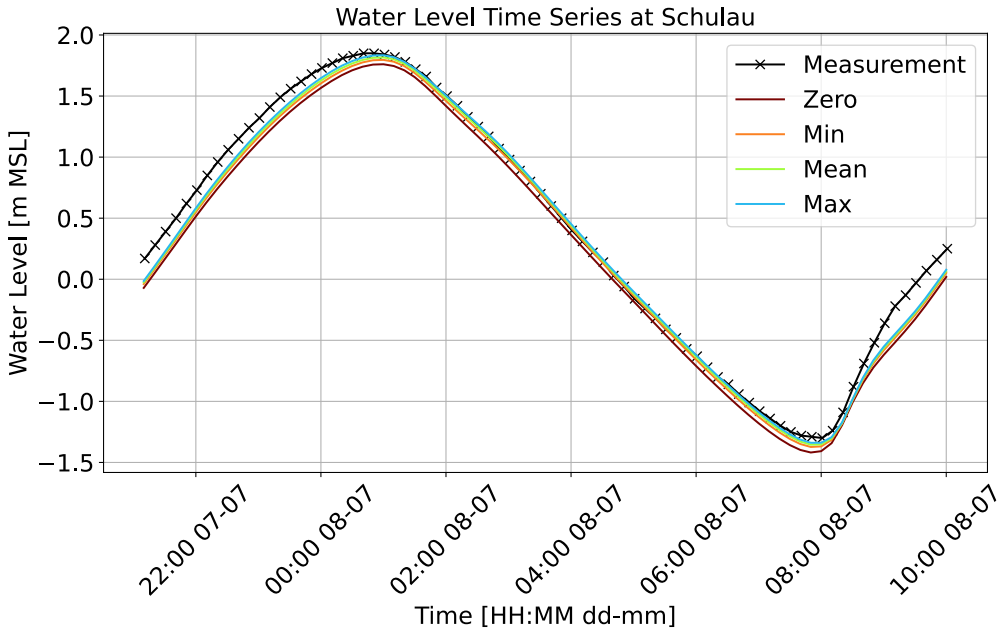

Figure 7.5: Water level results for different river discharge cases at Schulau [m^3/s]

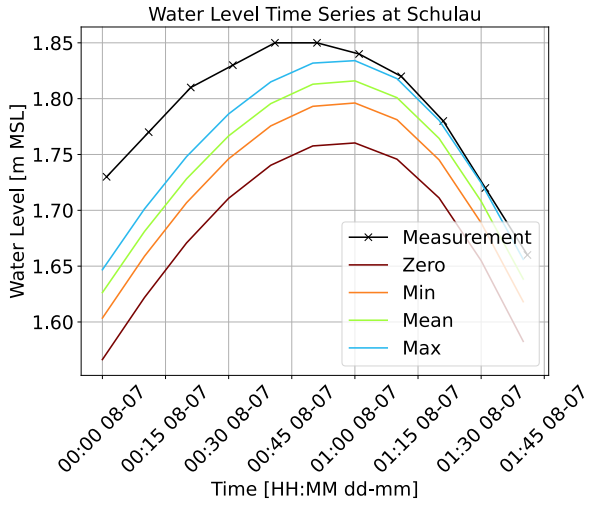

Figure 7.6: High water level results for different river discharge cases at Schulau [m^3/s]

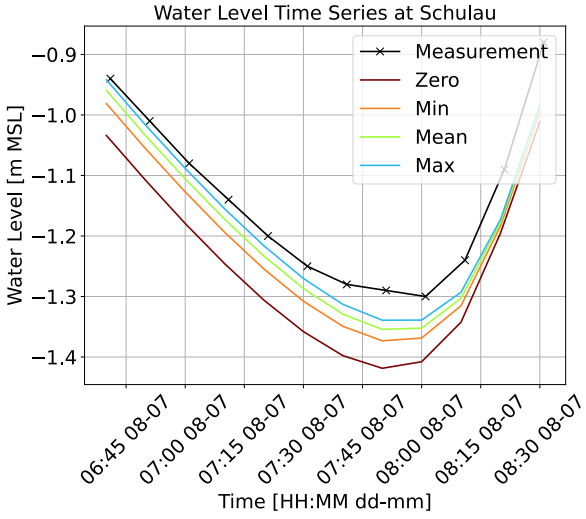

Figure 7.7: Low water level results for different river discharge cases at Schulau [m^3/s]

7.2.2 Flow velocity results

Flow velocity results at location LZ1, shown in Figure 7.8, highlight key trends. During rising tide, simulations with lower river discharge exhibit the highest flow velocities, whereas during falling tide, higher river discharge leads to increased velocities. This pattern arises because during rising tide, the tidal flow pushes toward the river, while river discharge opposes this force, resulting in higher velocities with lower discharge. Conversely, during falling tide, both tidal and river flows move seaward, so higher discharge amplifies this effect, resulting in increased flow velocities seaward. Additionally, a slight delay in the timing of minimum velocities is observed in the simulations with the highest discharge. This is likely due to the longer time required for the larger water volume to drain. Similar trends are observed at location LZ3, the results of this location are provided in Appendix E.2.2.

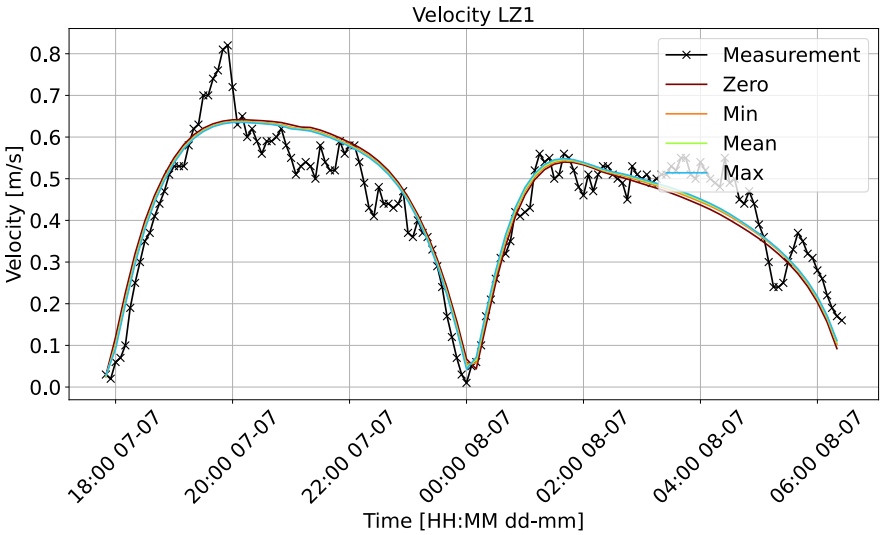

Figure 7.8: Flow velocity results for different river discharge cases at LZ1, rising tide falling tide [m^3/s]

7.2.3 Computational time

The applied time series to the river boundary do not influence the computational time needed for simulation.

Chapter 8

Discussion

8.1 Impact of subgrid

In this research, a hydrodynamic model was developed, which uses a structured grid with a subgrid. To demonstrate the impact of the subgrid, a comparison has been made between two models: one with the subgrid and one without. The final settings of the subgrid model, based on the findings from each research question, include a DEM with a resolution of 5m x 5m (matching the subgrid resolution), a spatially varying tidal boundary, a simulation time step of 40 seconds, grid widths of 1600 m outside and 400 m inside the navigation channel, a Manning coefficient of 0.0240 $s/m^{1/3}$, and a discharge time series applied at the river boundary. The model without subgrid has similar settings, but without the use of the subgrid. The models have the same computational grid resolution.

Figures 8.1 and 8.2 illustrate that the subgrid model significantly outperforms the non-subgrid model in capturing estuarine hydrodynamics, particularly in terms of timing, tidal asymmetry, and tidal range. This aligns with the findings of Casulli (2009) and Volp et al. (2013), who also demonstrated that subgrid models, by incorporating high-resolution bathymetric data, can capture hydrodynamics more accurately then a model without subgrid for the same computational grid. However, some small discrepancies remain between the measurements and the subgrid model, which can be partly due to inaccuracies in the DEM, despite efforts to improve it.

As mentioned before, the BAW currently employs an unstructured grid in their model of the Elbe estuary, because it can handle complex geometries and flow patterns, which structured grid cannot (Bomers et al., 2019; Zhang et al., 2012). However, this study demonstrated that a structured grid combined with a subgrid can accurately and efficiently capture these complexities. Additionally, the orthogonality of structured grids reduces computational time and enhances model accuracy by minimizing numerical diffusion compared to unstructured grid models (Bomers et al., 2019; Kernkamp et al., 2011). This indicates the potential for improved performance in models like the Elbe estuary by using structured grids with subgrids,

instead of unstructured grids. However, this research did not compare results with existing Elbe models for validation.

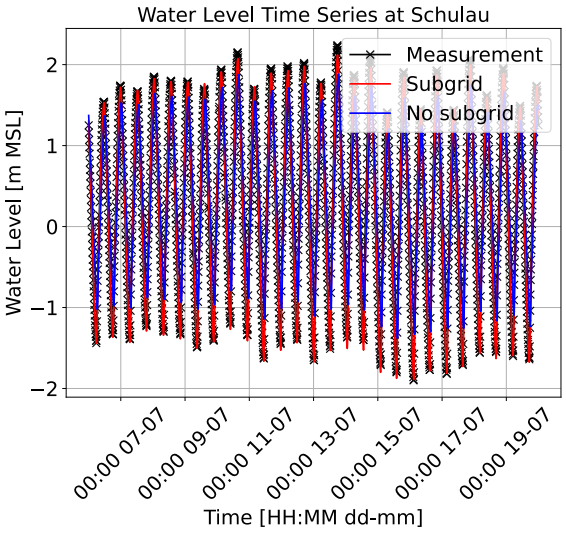

Figure 8.1: Water level results at Schulau for final model with and without subgrid (Grid width of 1600 m outside navigation channel and 400 m in the navigation channel)

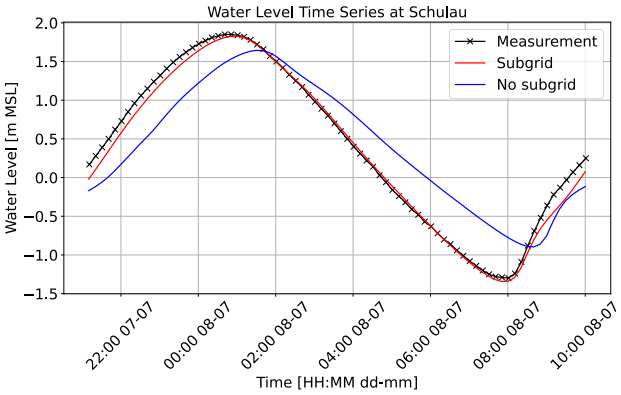

Figure 8.2: Water level results for one cycle at Schulau for final model with and without subgrid (Grid width of 1600 m outside navigation channel and 400 m in the navigation channel)

8.2 Impact of boundary settings

Boundary conditions for both tidal and river boundaries are crucial in hydrodynamic modelling and can influence the hydrodynamics across the model domain, as supported by Carter and Merrifield (2007) and Walters and Cheng (1979). Tidal boundaries can be modeled with a simple non-spatially varying boundary, or a more detailed spatially varying boundary for greater realism, where the latter better captures small water level variations. However, these differences diminish upstream. Therefore, boundary settings should align with research objectives: spatially varying boundaries are ideal for studying the sea part of the estuary, while non-spatially varying boundaries are sufficient for upstream studies.

The key to setting up a boundary is ensuring natural water flow without introducing artificial forcing from the boundary conditions, which would affect the hydrodynamics throughout the whole model domain. To achieve this natural flow, in addition to careful selection of boundary settings, an extra set of cells near the boundary was incorporated to allow natural flow through the DEM. Nash and Hartnett (2010) also used extra cells to maintain natural conditions in their model. For 3Di models, when implementing a spatially varying boundary using multiple 1D boundaries, it is recommended to match the channel width and length of the 1D boundary to the grid width. This prevents extra forcing from wider or narrower flow channels. However,

no research has been conducted on the impact of the boundary settings combined with the extra cells due to time constraints.

The spatially varying time series used in this research is based on linear interpolation between three water level data points located in the sea, provided by the BAW. Chen et al. (2014) and Young et al. (2001) also applied interpolation methods, with the latter also applying linear interpolation to create a spatially varying boundary. Linear interpolation of water levels may introduce minor errors, as actual water level variation is more complex. Extra measurement locations along the tidal boundary could improve the interpolation of the water levels. Additionally, adding another measurement location in the sea, would be useful for comparison purposes, as currently only one sea-based measurement point is available for validation.

8.3 Impact of grid width, grid refinements and time step setting

This research examined the impact of various grid widths and refinements on hydrodynamic modelling, utilizing a subgrid resolution of 5 m x 5 m independently of the computational grid resolution.

In the river section, until the part where the river widens, increasing grid width reduced tidal ranges due to enhanced numerical diffusion. However, in the sea region, larger grid widths resulted in higher tidal ranges. This could be due to small-scale physical processes that a coarse grid fails to capture, which otherwise should have lead to energy dissipation, for example turbulence. Another reason could be that in deeper water, which is the sea compared to the river, where the influence of friction is reduced, the tidal range is more amplified rather than diminishing them through numerical diffusion. A minimum grid width of 200 m was used due to 3Di's memory constraints, though finer grids may be feasible in smaller study areas. The relationship between grid width and flow velocity remains unclear. However, reliable flow velocity results were obtained across all grid widths, with accurate timing. While it is possible to compute velocities at subgrid level, this was not implemented in this research, due to time constraints.

In this research, larger time steps increased tidal ranges, since small scale processes are oversimplified. In regions with complex or rapidly changing flow patterns, processes like eddies, turbulence, and high-frequency oscillations play a significant role in dissipating energy. When these processes are not accurately captured due to coarser time steps, the lack of energy dissipation can lead to exaggerated tidal ranges, as seen in this research. However, this effect of time steps is highly location-specific and depends on the flow conditions of the study area. In study areas with for example simpler, more uniform flow, the impact of varying time steps may differ. The grid width also impacts the time step's effect on hydrodynamics. In the end, increasing grid width or time step reduces computational time, which aligns with the findings of Bomers et al. (2019).

Local grid refinements were applied in areas like the river widening, river-sea transition, and navigation channel. Minimal impacts were observed in the port area, despite its complex bathymetry, likely due to the subgrid technique which incorporates complex bathymetry. Significant improvements occurred when refinement was applied to the river widening area and navigation channel. Refinements here better captured physical processes, such as flow dispersion, tidal amplification and other complex flow patterns. The suitable refinement location are consistent with other studies, models with unstructured grids often use smaller computational cells in navigation channels or at river mouths compared to surrounding areas (Bomers et al., 2019; Fringer, 2023; Zhang et al., 2012; Zhu et al., 2021). For other study areas, it is crucial to strategically place local refinements in regions where small-scale processes, such as flow dispersion and tidal amplification, are important. These processes can be found particularly in regions with substantial river widening or steep bathymetric gradients, such as near navigation channels. If a fine grid is used in such regions, a coarser grid can be used in the sea.

8.4 Impact of roughness value and river discharge

In this research the roughness affects how the tidal wave moves through the whole estuary, consistent with the findings of Bao et al. (2009) and Cheng et al. (2022). Reducing roughness simulates a smoother bed, which lowers water resistance and reduces energy dissipation. This results in increased flow velocities and larger tidal ranges, as supported by Ibrahim and Abdel-Mageed (2014). Differences in water levels between simulations are more pronounced at low tide than at high tide due to the shallower depths amplifying the effects of roughness. The effects described above apply to other estuarine areas as well. Using spatially varying roughness instead of uniform roughness would better represent the bed's varying physical characteristics, improving both timing and magnitude of hydrodynamic results. Spatially varying roughness can be defined based on different soil types across regions or in specific areas, such as the navigation channel, which is dredged and features a smoother bed compared to the surroundings.

Next to the other topics discussed, river discharge also play a significant role, particularly during falling tides or neap tides when tidal forces are weaker. Increased discharge raises water levels near the river boundary, also noted by Cai et al. (2014), though this effect decreases further downstream where tidal forces dominate (Whitfield & Elliott, 2011). This effect will apply to other estuarine models as well. Using a discharge time series provides realistic fluctuations of predicted flow velocities, however if this is unavailable the choice of discharge boundary settings should depend on whether the focus is on flood safety (maximum discharge) or low water levels important for navigation (minimum discharge) (Boehlich & Strotmann, 2008; Jiang et al., 2012).

Chapter 9

Conclusion and Recommendations

9.1 Conclusion

The aim of this study was to explore whether a structured model together with the subgrid method can capture the estuarine hydrodynamics accurately and computationally efficient, together with how various model settings and schematizations impact the simulated estuarine hydrodynamics and computational time. Four questions have been used to help achieving this research aim.

Q1 How do the settings of a spatially and temporally varying tidal boundary condition affect the simulated estuarine hydrodynamics throughout the model domain?

A tidal boundary determines the tidal forcing into the model domain, impacting the hydrodynamics throughout the whole model domain. This research used a spatially varying boundary, existing out of multiple 1D boundaries, which captures small local variations in sea water levels better than a non-spatially boundary. However, these variations are dampened upstream, diminishing the advantages of using a spatially varying boundary.

This research examined the influence of the connection node storage area and boundary channel length, both elements of the 1D boundary. Increasing the connection node storage area allows for more water storage, requiring greater inflow volume and more momentum, while decreasing the channel length steepens the water level gradient, increasing momentum and inflow volume. Both adjustments result in higher water levels and flow velocities across the model, particularly at high tide. To enhance accuracy, an extra set of cells was added to the DEM, ensuring natural flow along the boundary. Ensuring natural water flow without artificial forcing is key for tidal boundaries. If 1D boundaries are used, this can be achieved by avoiding extra connection node storage areas, setting the channel length and width equal to the grid width, and incorporating an extra set of cells at the DEM to further enhance natural flow. The 1D tidal boundary settings influence hydrodynamics across the entire model domain, while the applied time series primarily affects the lower estuary. This applies to other study areas as well, making it essential to choose boundary types and settings that align with research objectives.

Q2 How do grid width and time step settings affect the simulated estuarine hydrodynamics throughout the model domain and the computational time required for a simulation?

Grid width and time step settings both significantly influence simulated hydrodynamics and computational time. When the grid width is changed, the subgrid resolution remains fixed at 5 m x 5 m. Smaller grid widths reduce numerical diffusion, resulting in larger tidal ranges (by a couple of centimeters) and higher accuracy, particularly in the river sections of the estuary. However, in the sea part of the estuary, larger grid widths can lead to larger tidal ranges. This unexpected result may be due to small-scale physical processes that a coarse grid fails to capture, which could otherwise lead to energy dissipation. Consequently, tidal ranges are now amplified, by a couple of centimeters, rather than diminished, contrary to what was expected based on numerical diffusion solely.

Time step settings also impact tidal ranges and flow velocities. Larger time steps tend to increase tidal ranges (by a couple of centimeters), flow velocities, and tidal delays. This is likely due to numerical dispersion, which distorts water movement by oversimplifying small-scale hydrodynamics that would otherwise lead to energy dissipation. As a result, tidal ranges are increased rather than decreased.

Larger grid widths and time steps reduce computational time by decreasing the number of computational cells and the frequency of hydrodynamic calculations. However, this reduction in computational load can affect accuracy. Therefore, it is important to choose a combination of grid width and time step that balances accuracy with computational efficiency. In this study, a grid width of 400 m was used in combination with a time step of 40 s based on the results of this question.

Q3 How do the location and extent of local grid refinements affect the simulated estuarine hydrodynamics throughout the model domain and the computational time required for a simulation?

Strategically applied local grid refinements, without affecting the subgrid resolution, have a noticeable impact on both hydrodynamics and computational efficiency in estuarine simulations. Refinements near the port resulted in minimal changes, primarily due to the advantages of the subgrid model. This study highlighted the importance of applying grid refinements in areas where the river widens and in the navigation channel, as these regions exhibit complex flow patterns that are better captured with finer grids. Notably, a coarse grid can be used in open sea areas without compromising accuracy, as long as critical regions such as the river and navigation channel are properly refined. In line with question 2, computational time is largely influenced by the number of grid cells, making it essential to balance resolution across different regions to optimize both accuracy and efficiency. In this study, refinements (400 m) are placed in the navigation channel while having a coarse grid outside the navigation channel (1600 m), resulting in a decrease in computational time of 12 minutes compared to the model of Q2.

Q4 How do the variations in uniform roughness values, as well as the inclusion/exclusion of upstream river discharge, influence the simulated estuarine hydrodynamics throughout the model domain?

While previous questions focused on the set-up of the tidal boundary and numerical settings, this question addresses physical parameters such as roughness values and river discharge. Variations in uniform roughness values impact estuarine hydrodynamics significantly, with water level differences between cases reaching up to 15 cm. Lower roughness values result in increased tidal ranges and higher flow velocities due to reduced energy dissipation. The differences in water levels between simulations are more pronounced during low tide, as roughness has a greater relative effect when water levels are lower. Roughness values do not significantly affect the timing of the tide.

Upstream river discharge has a notable impact on water levels, particularly during falling or neap tides, when tidal forces are weaker and river discharge plays a larger role. Increased river discharge raises water levels, though its influence decreases with distance from the river boundary. River discharge also affects flow velocities: during rising tides, lower river discharge leads to higher flow velocities, while during falling tides, higher river discharge results in increased flow velocities. Consequently, the impact of river discharge varies by location and time, a pattern that is likely consistent across all estuaries. In the Elbe estuary, river discharge has a significant impact on water levels up to the point where the river widens substantially.

In conclusion, tidal boundary settings, grid width, time step settings, local grid refinements, roughness values, and river discharge all significantly influence estuarine hydrodynamics in various ways. Additionally, grid width, time step, and grid refinements affect computational time. The structured model combined with the subgrid method used in this research effectively captured the estuarine hydrodynamics of the Elbe, with differences of less than 10 cm compared to the measurements, while maintaining computational efficiency. For a 15-day simulation only 5 minutes of computational time was required. It is anticipated that a structured model combined with a subgrid will also be capable of accurately and efficiently capturing hydrodynamics in other study areas.

9.2 Recommendations for future research

This study demonstrated that the structured model with the subgrid method in 3Di effectively captures estuarine hydrodynamics in a computationally efficient way, while also revealing the impact of various model settings and schematizations on the simulated hydrodynamics and computational time. Based on the findings, five recommendations for future research and model enhancement can be made.

Firstly, while this research effectively simulated estuarine hydrodynamics, a comparative analysis with other models of the Elbe estuary was not conducted. Conducting such a comparison is recommended, as it would provide insight into the model's relative strengths and areas for improvement, helping validate its accuracy and computational efficiency compared to alternatives.

Secondly, spatially varying roughness values should be explored. This study used a uniform roughness, but varying bed characteristics, such as soil types and smoother dredged areas like the navigation channel, significantly impact hydrodynamics.Therefore, implementing spatially varying roughness based on these soil types or areas could improve model accuracy.

Thirdly, the grid width analysis revealed unexpected results in the tidal regions, where coarser grids amplified tidal ranges instead of reducing them through numerical diffusion. This suggests that small-scale physical processes are not fully captured. Further research is necessary to identify the cause of this effect and to develop a strategy for addressing it in future model applications.

Fourthly, setting the channel dimensions of the 1D boundary equal to the grid size was assumed to enhance natural flow without external forcing. However, this assumption has not been validated. In future studies, if multiple 1D boundaries are employed to define spatially varying boundaries, it is essential to establish clear guidelines for the settings of the 1D boundaries.

Finally, obtaining more measurement data would benefit future research on the Elbe estuary. The spatially varying boundary currently relies on only three data points; increasing the number of measurements would provide a more detailed representation of water level variations along the boundary. Additionally, an extra measurement location in the sea could facilitate better result comparisons in the sea.

References

3Di Documentation. (n.d.). 3Di Documentation. https://docs.3di.live/

Alakashi, A. M., & Basuno, I. B. (2014). Comparison between structured and unstructured grid generation on two dimensional flows based on finite volume method (FVM). *Int. J. Min., Metall. Mech. Eng*, *2*(2), 97–103. https://www.academia.edu/download/90198391/1_2014101J3_20paper_20formatted.pdf

Bao, W.-m., Zhang, X.-q., & Qu, S.-m. (2009). Dynamic Correction of Roughness in the Hydrodynamic Model. *Journal of Hydrodynamics*, *21*(2), 255–263. https://doi.org/10.1016/S1001-6058(08)60143-2

Barbier, E. B., Hacker, S. D., Kennedy, C., Koch, E. W., Stier, A. C., & Silliman, B. R. (2011). The value of estuarine and coastal ecosystem services. *Ecological Monographs*, *81*(2), 169–193. https://doi.org/10.1890/10-1510.1

Bartl, S., Schümberg, S., & Deutsch, M. (2009). Revising time series of the Elbe river discharge for flood frequency determination at gauge Dresden. *Natural hazards and earth system sciences*, *9*(6), 1805–1814.

Boehlich, M. J., & Strotmann, T. (2008). The Elbe Estuary. *Die Küste*, *74*(1), 288–306. https://hdl.handle.net/20.500.11970/101612

Bomers, A., Schielen, R. M. J., & Hulscher, S. J. M. H. (2019). The influence of grid shape and grid size on hydraulic river modelling performance. *Environmental Fluid Mechanics*, *19*(5), 1273–1294. https://doi.org/10.1007/s10652-019-09670-4

Bounagui, A., Benichou, N., McCartney, C., & Kashef, A. (2003). Optimizing the grid size used in CFD simulations to evaluate fire safety in houses. *3rd NRC Symposium on Computational Fluid Dynamics, High Performance Computing and Virtual Reality*, *4*. https://www.researchgate.net/profile/Noureddine-Benichou/publication/44077621_Optimizing_the_grid_size_used_in_CFD_simulation_to_evaluate_fire_safety_in_houses/links/004635321f2bb6e8d1000000/Optimizing-the-grid-size-used-in-CFD-simulation-to-evaluate-fire-safety-in-houses.pdf

Cai, H., Savenije, H. H. G., & Toffolon, M. (2014). Linking the river to the estuary: influence of river discharge on tidal damping. *Hydrology and Earth System Sciences*, *18*(1), 287–304. https://doi.org/10.5194/hess-18-287-2014

Carter, G. S., & Merrifield, M. A. (2007). Open boundary conditions for regional tidal simulations. *Ocean Modelling*, *18*(3-4), 194–209. https://doi.org/10.1016/j.ocemod.2007.04.003

Casulli, V. (2009). A high-resolution wetting and drying algorithm for free-surface hydrodynamics. *International Journal for Numerical Methods in Fluids*, *60*(4), 391–408. https://doi.org/10.1002/fld.1896

Chen, H., Cao, A., Zhang, J., Miao, C., & Lv, X. (2014). Estimation of spatially varying open boundary conditions for a numerical internal tidal model with adjoint method. *Mathematics and Computers in Simulation*, *97*, 14–38. https://doi.org/10.1016/j.matcom.2013.08.005

Cheng, Y., Li, Y., Wang, Y., Tang, C., Shi, Y., Sarpong, L., Li, R., Acharya, K., & Li, J. (2022). Uncertainty and sensitivity analysis of spatial distributed roughness to a hydrodynamic water quality model: a case study on Lake Taihu, China. *Environmental Science and Pollution Research*, *29*(9), 13688–13699. https://doi.org/10.1007/s11356-021-16623-2

Dahm, R., Hsu, C., Lien, H. C., Chang, C. H., & Prinsen, G. (2014). Next Generation Flood Modelling using 3Di: A Case Study in Taiwan. *DSD international conference*. https://3diwatermanagement.com/uploads/sites/5/3Di-Taiwan-case-study.pdf

Elliott, M., & McLusky, D. (2002). The Need for Definitions in Understanding Estuaries. *Estuarine, Coastal and Shelf Science*, *55*(6), 815–827. https://doi.org/10.1006/ecss.2002.1031

Elliott, M., & Whitfield, A. (2011). Challenging paradigms in estuarine ecology and management. *Estuarine, Coastal and Shelf Science*, *94*(4), 306–314. https://doi.org/10.1016/j.ecss.2011.06.016

Elliott, M., Whitfield, A. K., Potter, I. C., Blaber, S. J. M., Cyrus, D. P., Nordlie, F. G., & Harrison, T. D. (2007). The guild approach to categorizing estuarine fish assemblages: a global review. *Fish and Fisheries*, *8*(3), 241–268. https://doi.org/10.1111/j.1467-2679.2007.00253.x

Fringer, O. (2023). Research: Estuarine flow physics and modeling. https://web.stanford.edu/~fringer/research_estuaries.html

GEODUS. (n.d.). Hamburgse kaart. https://www.geodus.com/fr/carte-hambourg-planet-observer_PORHA.htm

Gong, W., Schuttelaars, H., & Zhang, H. (2016). Tidal asymmetry in a funnel-shaped estuary with mixed semidiurnal tides. *Ocean Dynamics*, *66*(5), 637–658. https://doi.org/10.1007/s10236-016-0943-1

Google Maps. (2024). Google Maps. https://www.google.nl/maps/@53.8309422,9.607055,7.87z?entry=ttu

He, X., Luo, L.-S., & Dembo, M. (1996). Some Progress in Lattice Boltzmann Method. Part I. Nonuniform Mesh Grids. *Journal of Computational Physics*, *129*(2), 357–363. https://doi.org/10.1006/jcph.1996.0255

Hein, H., Mai, S., & Barjenbruch, U. (2014). Long-term Changes of the Tidal Amplitudes and Phases in the Elbe Estuary. *Proc. of the ICHE, Hamburg*, *11*, 783–790. https://hdl.handle.net/20.500.11970/99502

Hein, S., Sohrt, V., Nehlsen, E., Strotmann, T., & Fröhle, P. (2021). Tidal Oscillation and Resonance in Semi-Closed Estuaries—Empirical Analyses from the Elbe Estuary, North Sea. *Water*, *13*(6), 848. https://doi.org/10.3390/w13060848

Herrling, G., Becker, M., Lefebvre, A., Zorndt, A., Krämer, K., & Winter, C. (2021). The effect of asymmetric dune roughness on tidal asymmetry in the Weser estuary. *Earth Surface Processes and Landforms*, *46*(11), 2211–2228. https://doi.org/10.1002/esp.5170

Ibrahim, M., & Abdel-Mageed, N. (2014). EFFECT OF BED ROUGHNESS ON FLOW CHARACTERISTICS. *International Journal of Academic Research*, *6*(5).

ICPER. (2016). The Elbe. https://www.ikse-mkol.org/en/themen/die-elbe

Jiang, C., Li, J., & de Swart, H. E. (2012). Effects of navigational works on morphological changes in the bar area of the Yangtze Estuary. *Geomorphology*, *139-140*, 205–219. https://doi.org/10.1016/j.geomorph.2011.10.020

Kernkamp, H. W. J., Van Dam, A., Stelling, G. S., & de Goede, E. D. (2011). Efficient scheme for the shallow water equations on unstructured grids with application to the Continental Shelf. *Ocean Dynamics*, *61*(8), 1175–1188. https://doi.org/10.1007/s10236-011-0423-6

Klingbeil, K., Lemarié, F., Debreu, L., & Burchard, H. (2018). The numerics of hydrostatic structured-grid coastal ocean models: State of the art and future perspectives. *Ocean Modelling*, *125*, 80–105. https://doi.org/10.1016/j.ocemod.2018.01.007

Lai, Y. G. (2010). Two-Dimensional Depth-Averaged Flow Modeling with an Unstructured Hybrid Mesh. *Journal of Hydraulic Engineering*, *136*(1), 12–23. https://doi.org/10.1061/(ASCE)HY.1943-7900.0000134

Lane, S., Bradbrook, K., Richards, K., Biron, P., & Roy, A. (1999). The application of computational fluid dynamics to natural river channels: three-dimensional versus two-dimensional approaches. *Geomorphology*, *29*(1-2), 1–20. https://doi.org/10.1016/S0169-555X(99)00003-3

Lee, R., & O'Sullivan, C. (2007). A Fast and Compact Solver for the Shallow Water Equations. https://doi.org/10.2312/PE/vriphys/vriphys07/051-057

Leonard, A., & Reed, D. (2002). Hydrodynamics and Sediment Transport Through Tidal Marsh Canopies. *Journal of Coastal Research*, *36*, 459–469. https://doi.org/10.2112/1551-5036-36.sp1.459

Levins, R. (1966). The strategy of model building in population biology. *American Scientist*, *54*(4), 421–431. https://www.jstor.org/stable/pdf/27836590.pdf

Li, M., Ge, J., Kappenberg, J., Much, D., Nino, O., & Chen, Z. (2014). Morphodynamic processes of the Elbe River estuary, Germany: the Coriolis effect, tidal asymmetry and human dredging. *Frontiers of Earth Science*, *8*(2), 181–189. https://doi.org/10.1007/s11707-013-0418-3

Merwade, V., Cook, A., & Coonrod, J. (2008). GIS techniques for creating river terrain models for hydrodynamic modeling and flood inundation mapping. *Environmental Modelling & Software*, *23*(10-11), 1300–1311. https://doi.org/10.1016/j.envsoft.2008.03.005

Morianou, G. G., Kourgialas, N. N., & Karatzas, G. P. (2016). Comparison between Curvilinear and Rectilinear Grid Based Hydraulic Models for River Flow Simulation. *Procedia Engineering*, *162*, 568–575. https://doi.org/10.1016/j.proeng.2016.11.102

Muller-Navarra, S., & Bork, I. (2011). Development of an operational Elbe tidal estuary model. *Coastal Engineering Proceedings*, *32*. https://icce-ojs-tamu.tdl.org/icce/article/view/1373/pdf_113

Nash, S., & Hartnett, M. (2010). Nested circulation modelling of inter-tidal zones: details of a nesting approach incorporating moving boundaries. *Ocean Dynamics*, *60*(6), 1479–1495. https://doi.org/10.1007/s10236-010-0345-8

Nelen & Schuurmans. (n.d.). 3Di Water Management. https://3diwatermanagement.com/

Ostroumov, S. (2006). Biomachinery for maintaining water quality and natural water self-purification in marine and estuarine systems: elements of a qualitative theory. *International Journal of Oceans and Oceanography*, *1*(1), 111–118. https://www.semanticscholar.org/paper/Biomachinery-for-maintaining-water-quality-and-in-a-Ostroumov/1e8e64994b030a0ce63f9bb827aab7292f128abe

Potter, I. C., Chuwen, B. M., Hoeksema, S. D., & Elliott, M. (2010). The concept of an estuary: A definition that incorporates systems which can become closed to the ocean and hypersaline. *Estuarine, Coastal and Shelf Science*, *87*(3), 497–500. https://doi.org/10.1016/j.ecss.2010.01.021

Potter, I. C., Tweedley, J. R., Elliott, M., & Whitfield, A. K. (2015). The ways in which fish use estuaries: a refinement and expansion of the guild approach. *Fish and Fisheries*, *16*(2), 230–239. https://doi.org/10.1111/faf.12050

Sang, W., & Li, F. (2007). An unstructured/structured multi-layer hybrid grid method and its application. *International Journal for Numerical Methods in Fluids*, *53*(7), 1107–1125. https://doi.org/10.1002/fld.1357

Sehili, A., & Lang, G. (2014). Use of the Subgrid Technique in Operational Models. *11th International Conference on Hydroscience & Engineering*.

Shipsgo. (2023, September). Top 10 European Ports by Size and Activity in 2023. https://blog.shipsgo.com/european-ports-ranking-list/

Short, A. D. (1991). Macro-meso tidal beach morphodynamics: an overview. *Journal of Coastal Research*, *7*(2), 417–436. https://www.jstor.org/stable/4297847

Sohrt, V., Hein, S., Nehlsen, E., Strotmann, T., & Fröhle, P. (2023). RefTide: The Reflection and Resonance Behaviour of Tide Dominated Estuaries. *Die Küste*, *93*. https://doi.org/https://doi.org/10.18171/1.093101

Stelling, G. S. (2012). Quadtree flood simulations with sub-grid digital elevation models. *Proceedings of the Institution of Civil Engineers - Water Management*, *165*(10), 567–580. https://doi.org/10.1680/wama.12.00018

Telesh, I. V., & Khlebovich, V. V. (2010). Principal processes within the estuarine salinity gradient: A review. *Marine Pollution Bulletin*, *61*(4-6), 149–155. https://doi.org/10.1016/j.marpolbul.2010.02.008

Thrush, S., Townsend, M., Hewitt, J. E., Davies, K. k., Lohrer, A. M., Lundquist, C., & Cartner, K. (2014). The many uses and values of estuarine ecosystems. *Ecosystem Services in New Zealand – Condition and Trends*, 226–237. https://www.researchgate.net/publication/281526181_The_many_uses_and_values_of_estuarine_ecosystems

Toth, L., Artur Găman, G., Pupăzan, D., Nicolescu, C., Kovacs, & Marius. (2021). Use of Performance Criteria in Calibrating Methods for Modeling and Simulating the Pollution Phenomena of Surface Waters. *E3S Web of Conferences*, *241*, 01003. https://doi.org/10.1051/e3sconf/202124101003

Tweedley, J. R., Warwick. R.M., & Potter, I. (2016). The Contrasting Ecology of Temperate Macrotidal and Microtidal Estuaries. *Oceanography and Marine Biology: An Annual Review*, 73–171. https://researchportal.murdoch.edu.au/esploro/outputs/bookChapter/The-Contrasting-Ecology-of-Temperate-Macrotidal/991005545253207891

Vasconcelos, R., Reis-Santos, P., Costa, M., & Cabral, H. (2011). Connectivity between estuaries and marine environment: Integrating metrics to assess estuarine nursery function. *Ecological Indicators*, *11*(5), 1123–1133. https://doi.org/10.1016/j.ecolind.2010.12.012

Volp, N. D., van Prooijen, B. C., & Stelling, G. S. (2013). A finite volume approach for shallow water flow accounting for high-resolution bathymetry and roughness data. *Water Resources Research*, *49*(7), 4126–4135. https://doi.org/10.1002/wrcr.20324

Walters, R. A., & Cheng, R. T. (1979). A two-dimensional hydrodynamic model of a tidal estuary. *Advances in Water Resources*, *2*, 177–184. https://doi.org/https://doi.org/10.1016/0309-1708(79)90033-2

Whitfield, A., & Elliott, M. (2011). Ecosystem and Biotic Classifications of Estuaries and Coasts. In *Treatise on estuarine and coastal science* (pp. 99–124). Elsevier. https://doi.org/10.1016/B978-0-12-374711-2.00108-X

Wijaya, O. T., Yang, T.-H., Hsu, H.-M., & Gourbesville, P. (2023). A rapid flood inundation model for urban flood analyses. *MethodsX*, *10*, 102202. https://doi.org/10.1016/j.mex.2023.102202

Winckler, P. (2015). Long Waves In Channels Of Non-Uniform Cross-Section. https://hdl.handle.net/1813/39462

Young, E., Brown, J., & Aldridge, J. (2001). Application of a large area curvilinear model to the study of the wind-forced dynamics of flows through the North Channel of the Irish Sea. *Continental Shelf Research*, *21*(13-14), 1403–1434. https://doi.org/10.1016/S0278-4343(01)00012-7

Zhang, W., Zhang, Z., & Chen, X. (2012). Three-dimensional elastic wave numerical modelling in the presence of surface topography by a collocated-grid finite-difference method on curvilinear grids. *Geophysical Journal International*, *190*(1), 358–378. https://doi.org/10.1111/j.1365-246X.2012.05472.x

Zhu, C., van Maren, D. S., Guo, L., Lin, J., He, Q., & Wang, Z. B. (2021). Effects of Sediment-Induced Density Gradients on the Estuarine Turbidity Maximum in the Yangtze Estuary. *Journal of Geophysical Research: Oceans*, *126*(5). https://doi.org/10.1029/2020JC016927

Zorndt, A. C., Wurpts, A., & Schlurmann, T. (2011). The influence of hydrodynamic boundary conditions on characteristics, migration, and associated sand transport of sand dunes in a tidal environment. *Ocean Dynamics*, *61*(10), 1629–1644. https://doi.org/10.1007/s10236-011-0452-1

Appendix A

Details of the methodology

A.1 Phase 1: Subgrid

The notable issues identified are listed below, along with their corresponding solutions.

A.1.1 Area with inverted values

An area with inverted values was identified (Figure A.1), and although the cause of this discrepancy was unclear, it was resolved by adjusting the signs of the values to align with those of the surrounding cells.

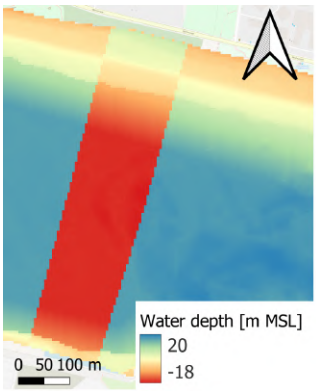

Figure A.1: Zoomed in part of water depth map, there is a rectangle area (red part + the orange/yellow part above) which has inverted values compared to the surrounding area

A.1.2 Missing data points

In the provided raster, some locations lacked values where data was expected. The area with the most missing data points was situated between the high accuracy section and the section with triangles. Using the nearest neighbour interpolation technique, these gaps were filled, ensuring that all locations now have appropriate values.

A.1.3 No data pixels

On the raster boundary, there was an extra line of pixels with a value of -10001, which is not a logical value for water depth. This was likely the no-data boundary of the system used to generate the map. The value of this line of pixels has been changed to a no-data pixel value of -9999, consistent with the 3Di system.

A.1.4 Interpolation of combined raster

The water depth raster is a combined raster with 5x5m cells. The river section of the raster is highly accurate (Figure A.2), but the sea section is less precise. In the sea section, a triangular raster with varying dimensions was converted to a 5x5m squared raster without interpolation (Figure A.3), resulting in a bed level with sharp gradients (Figure A.4), which negatively affects flow conditions. Addressing these sharp gradients will result in a smoother and more accurate raster. An improved water depth raster, which will be converted into a DEM, combined with the subgrid method, will enhance the capture of physical processes. For instance, since the influence of roughness is depth-dependent, a more accurate DEM will allow for a precise representation of water depth and, consequently, a more accurate assessment of roughness effects.

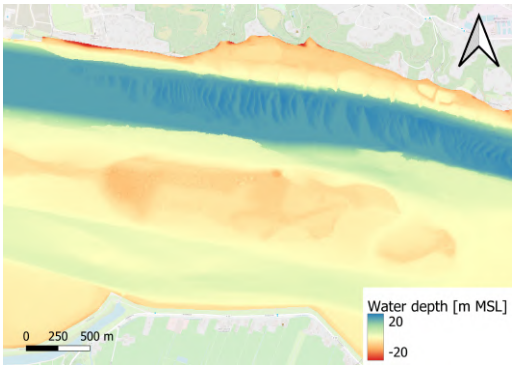

Figure A.2: Example of high resolution water depth map part

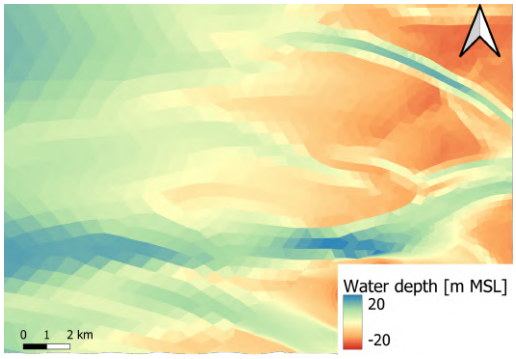

Figure A.3: Example of part of water depth raster with old triangular raster, red line shows cross-section location of Figure A.4 and Figure A.6

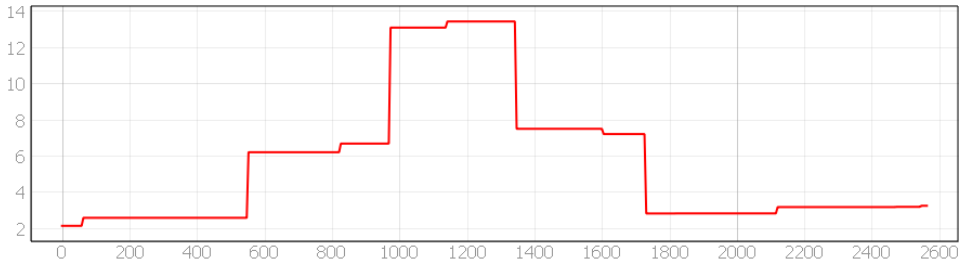

Figure A.4: Cross-section of water depth map, at location of red line in Figure A.3, unit of both axes: m

To address this issue, the raster was divided into three areas: area 1 with high accuracy, area 2 with small triangles, and area 3 with large triangles (Figure A.5). Areas 2 and 3 were resized to a larger grid width, which differs per area. These resized areas were then interpolated back to 5x5m dimensions and combined into a single raster. This process involved trial and error to determine the appropriate dimensions for the initial interpolation and the best interpolation method to use. The primary aim was to achieve a smoother bed level, while maintaining the channels' main form. In the end, areas 2 and 3 were resized to grid widths of 25 and 50 meters, respectively, using the spline interpolation method. These areas were then interpolated back to 5x5m dimensions and combined into a single raster.

Since the provided raster was a water depth raster based on mean sea level and 3Di requires a digital elevation map (DEM), the values for the entire raster were inverted. This adjustment means that negative values now indicate that the bed level is below mean sea level, while positive values indicate that it is above mean sea level.

Figure A.6 shows a cross-section of a channel, illustrating that the sharpest gradients were smoothed out without losing the channels' shape. Figure A.7 presents the difference map, highlighting that interpolation mainly occurred at the edges of the original triangles. The largest differences are found near the channels, where the gradient in bed level is the steepest and the error in the original DEM is most pronounced. Consequently, significant smoothing was required in these areas. The final DEM is shown in Figure 3.2.

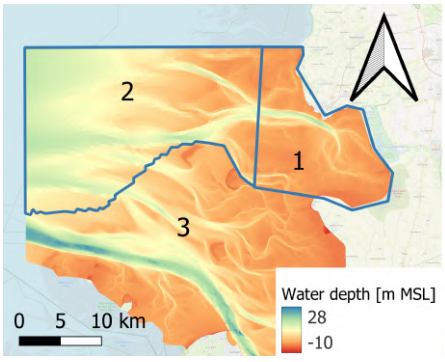

Figure A.5: Water depth raster divided into three areas

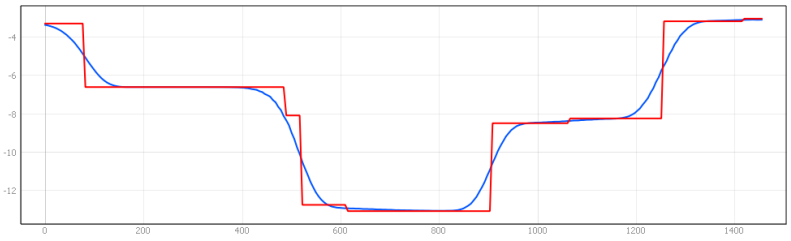

Figure A.6: Cross-section navigation channel, old DEM in red, improved DEM in blue, location shown in Figure A.3, unit of both axis: m

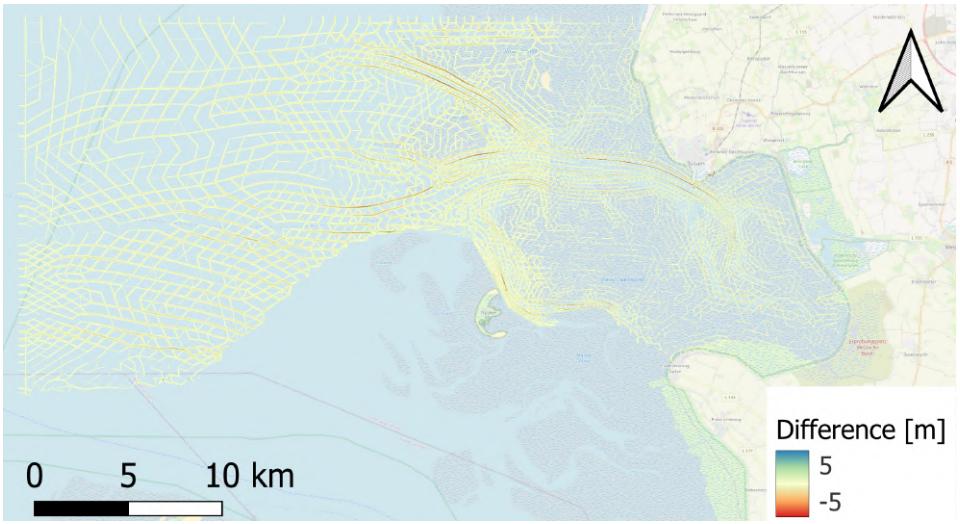

Figure A.7: Difference map between new and old DEM

A.2 Phase 2: Defining cases

In the main report an overview of cases is given. However, not all settings are mentioned in here, the rest of the settings are stated in Table A.1.

Table A.1: General settings of the different topics (- indicating setting depends on specific case)

	Q1		Q2		Q3	Q4	
Topics: Settings:	Connection node storage area	Boundary channel length	grid width	Time step	Local grid refinements	Roughness values	River discharge
Period [d]	2.5	2.5	15	15	15	15	15
Connection node storage area [m^2]	-	0	0	0	0	0	0
Boundary channel length [m]	60	-	Equal to grid width	400	Equal to outside grid width	1600	1600
Tidal "tub"	n/a	n/a	Yes	Yes	Yes	Yes	Yes
grid width [m]	200	200	-	400	1600 - 400 NC	1600 - 400 NC	
Time step [s]	10	10	10	-	40	40	40
Roughness values [$s/m^{1/3}$]	0.0245	0.0245	0.0245	0.0245	0.0245	-	0.0245
River discharge [m^3/s]	Time series	Time series	Time series	Time series	Time series	Time series	-

Appendix B

Q1: Spatially and temporally varying boundary condition

B.1 Connection node storage area

B.1.1 Boundary in- and outflow

Table B.1: Inflow and outflow boundary for different connection node storage areas

Connection node storage area $[m^2]$	Boundary inflow $[10^{10}m^3]$	Boundary outflow $[10^{10}m^3]$
0	2.37	2.24
5000	2.39	2.26
10000	2.42	2.28
20000	2.47	2.33
30000	2.55	2.41
40000	2.64	2.49

B.1.2 Water level results

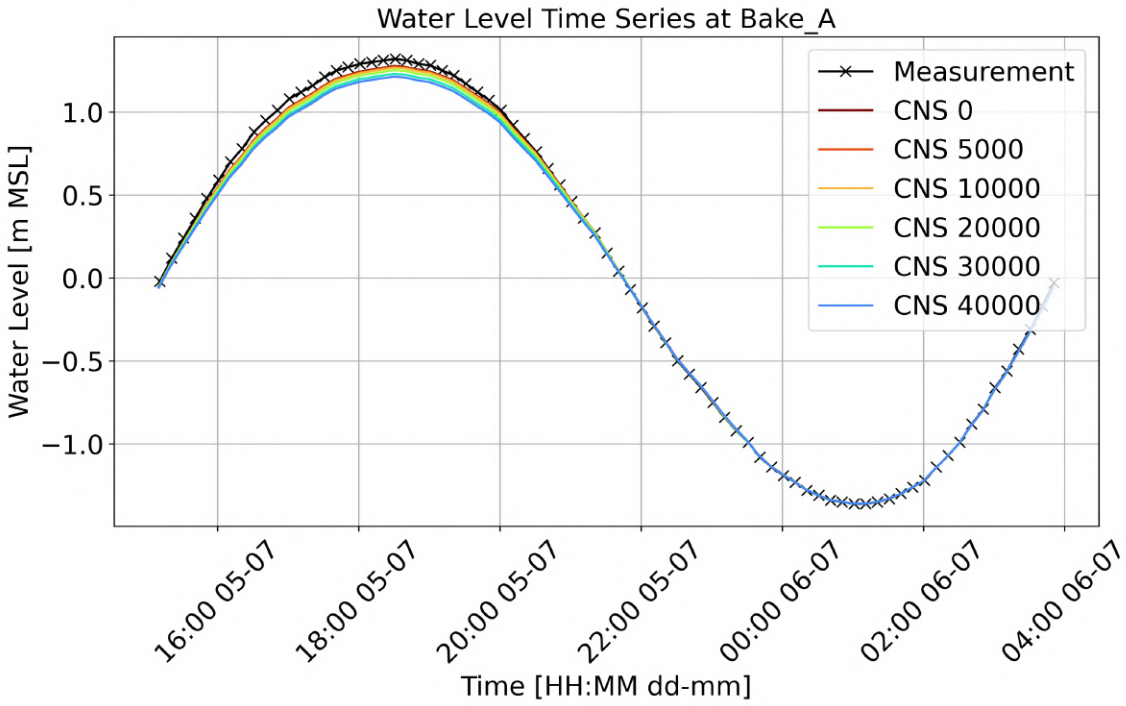

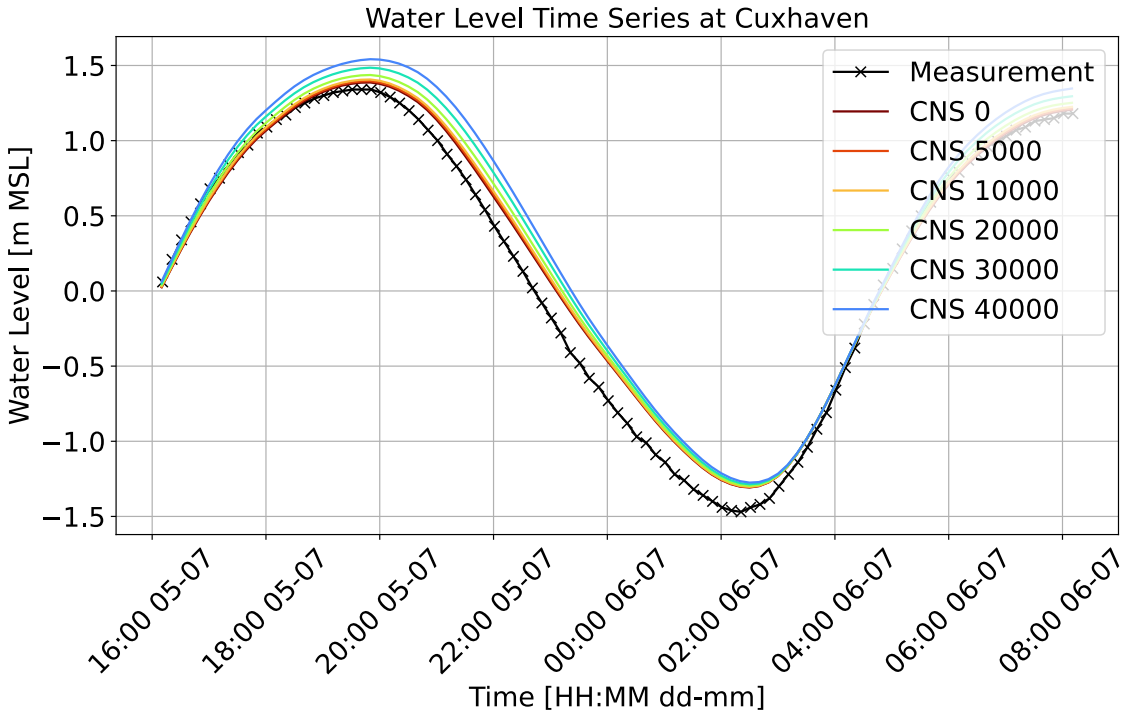

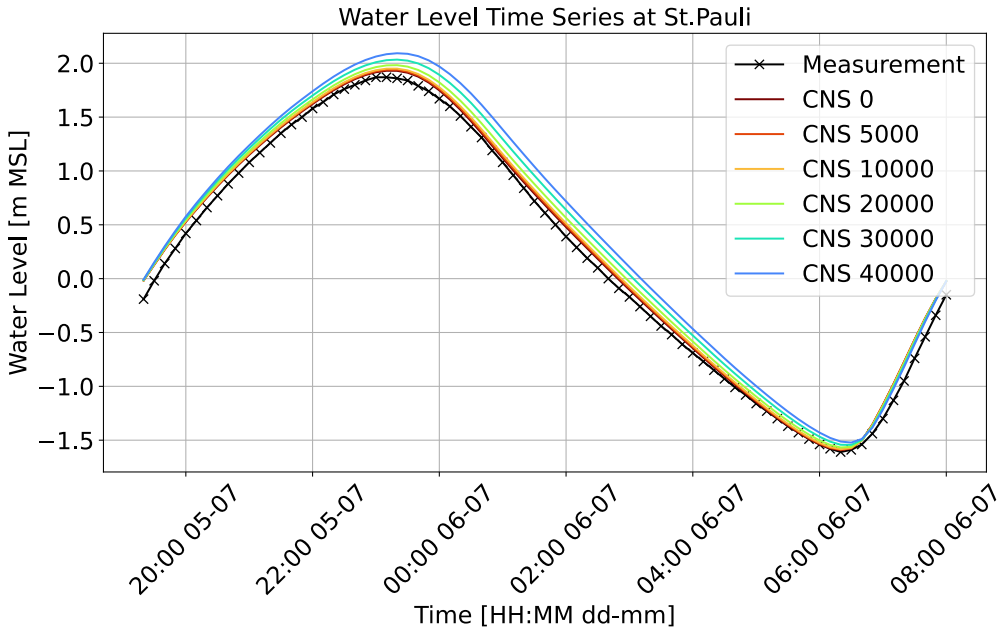

B.1.3 Flow velocity results

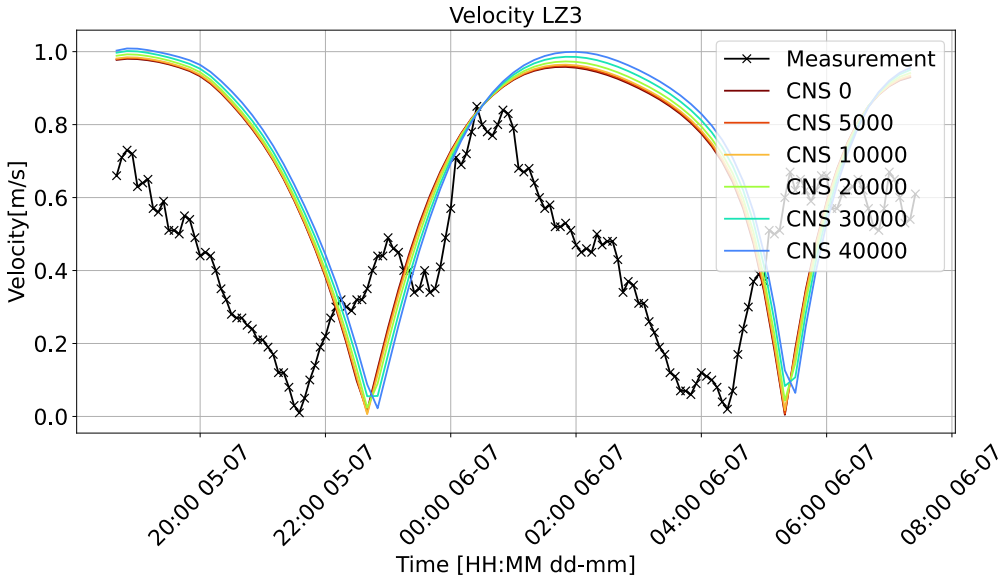

B.2 Boundary channel length

B.2.1 Boundary in- and outflow

Table B.2: Inflow and outflow boundary volume for different channel lengths

Channel length $[m]$	Boundary inflow $[10^{10}m^3]$	Boundary outflow $[10^{10}m^3]$
20	2.50	2.36
60	2.37	2.24
90	2.34	2.21

B.2.2 Water level results

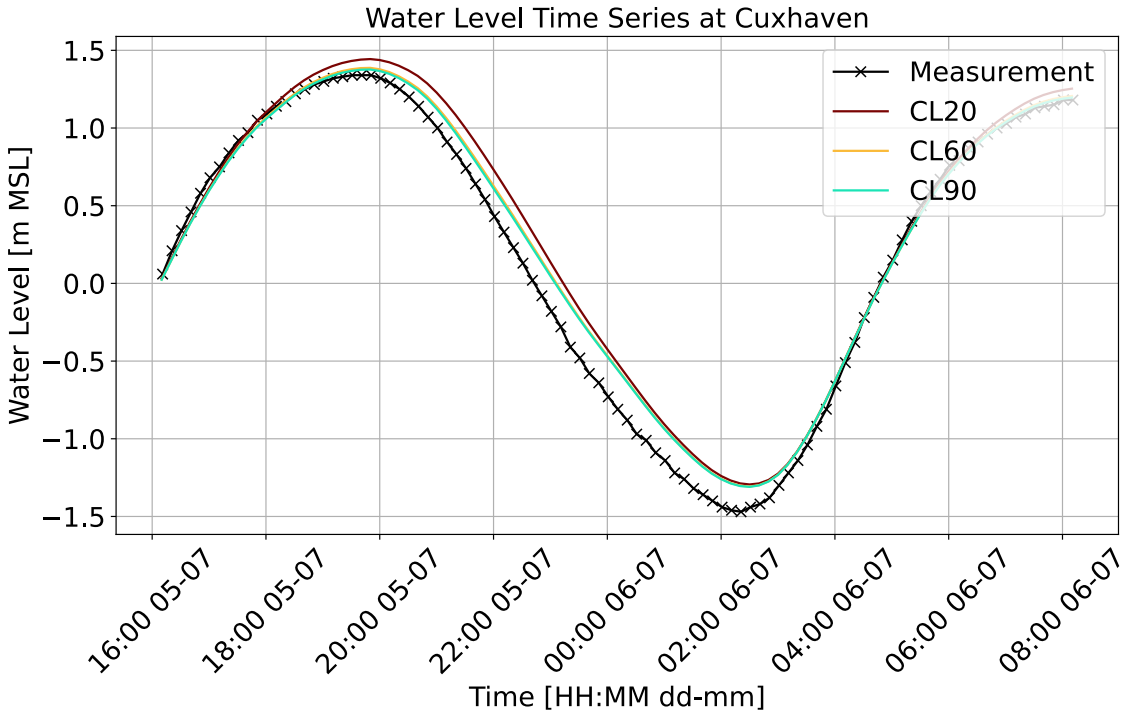

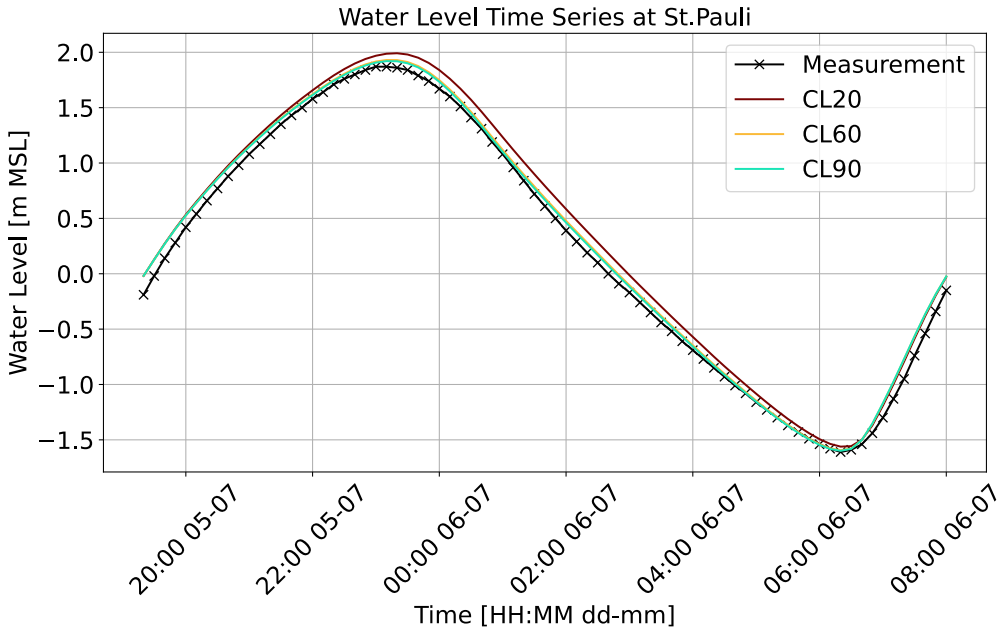

B.2.3 Flow velocity results

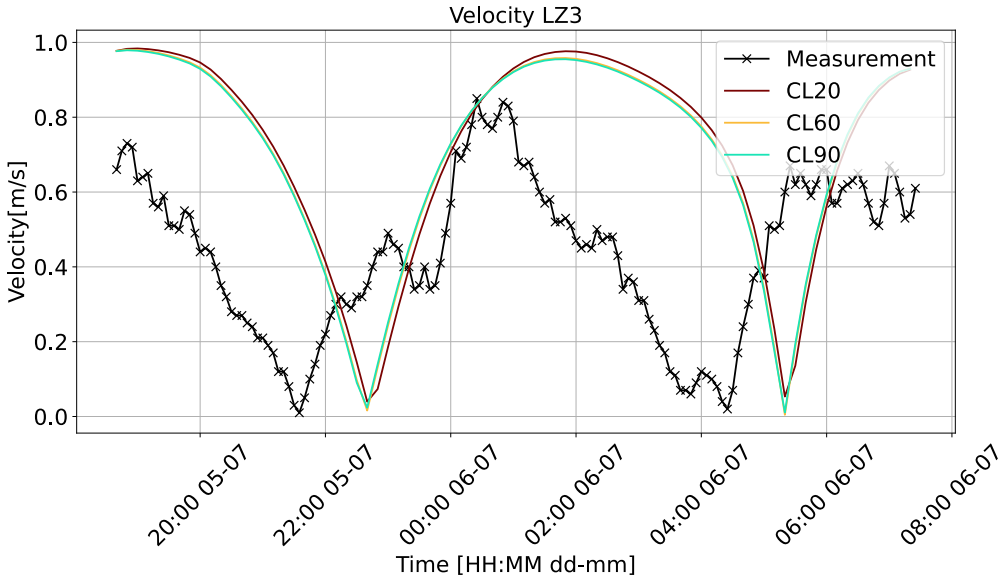

B.3 Performance check on applied boundaries

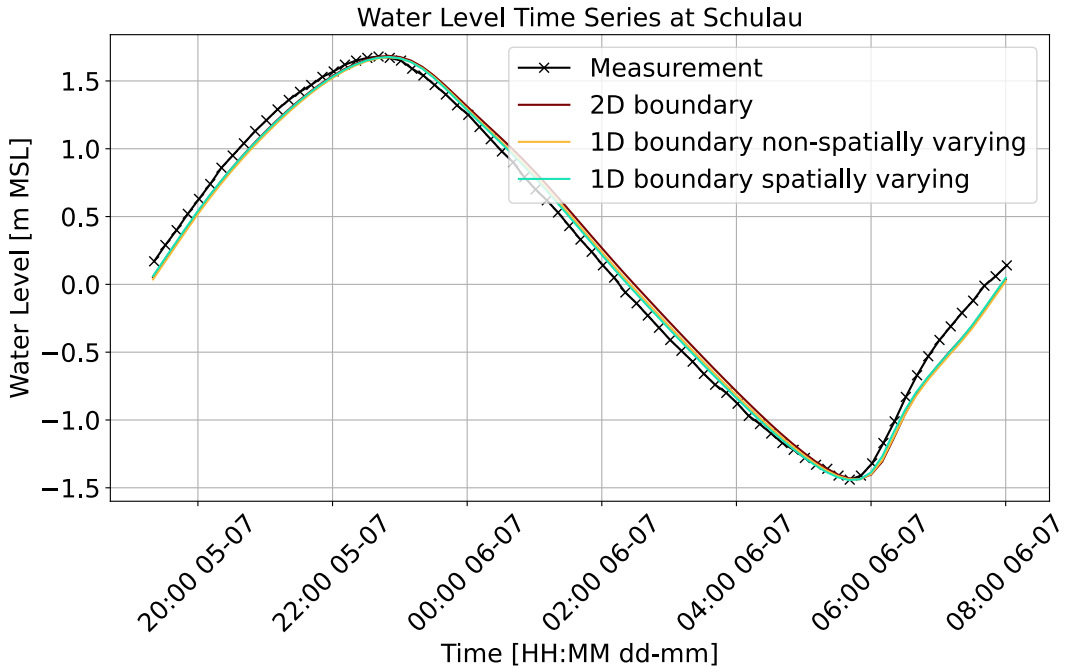

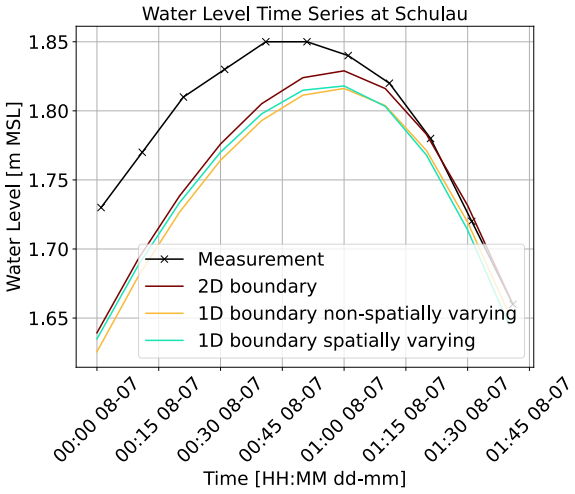

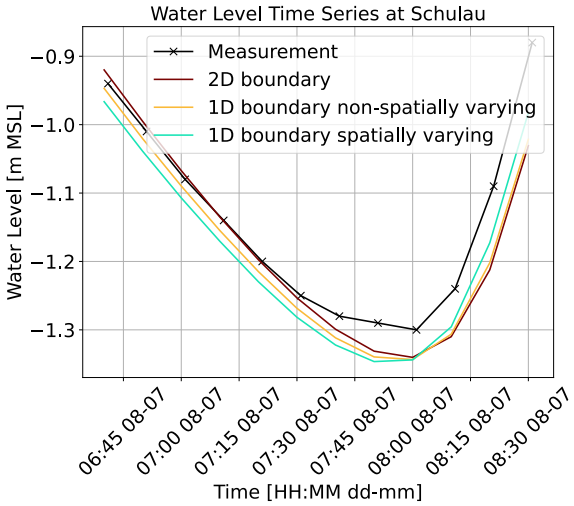

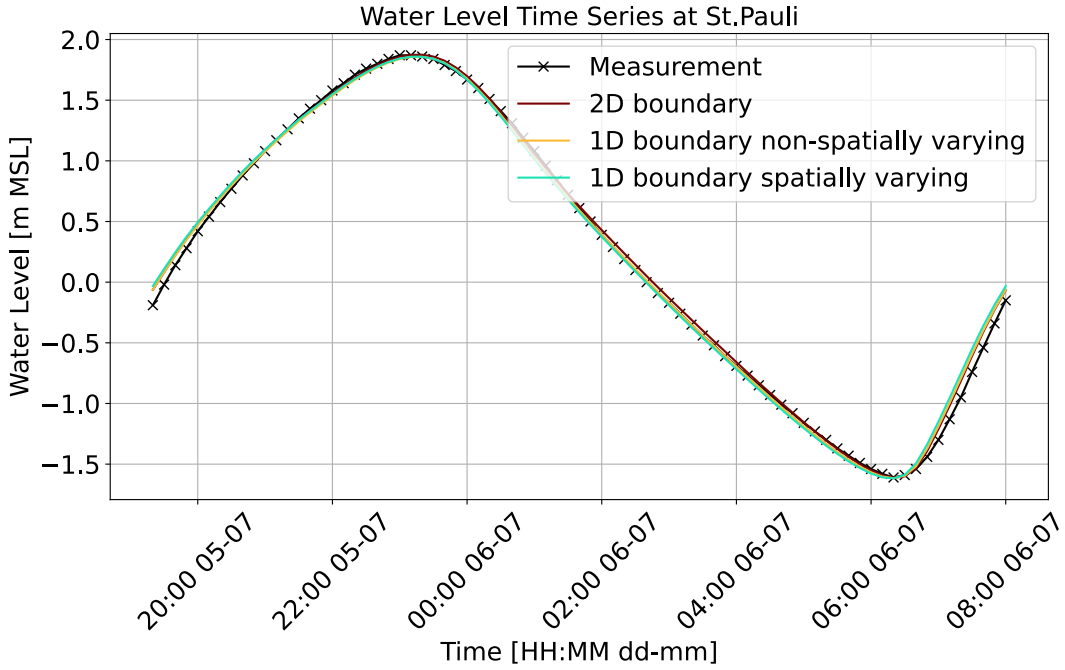
Water Level Time Series at St.Pauli
Measurement
2D boundary
1D boundary non-spatially varying
1D boundary spatially varying
Water Level [m MSL]
2.0
1.5
1.0
0.5
0.0
−0.5
−1.0
−1.5
20:00 05-07
22:00 05-07
00:00 06-07
02:00 06-07
04:00 06-07
06:00 06-07
08:00 06-07
Time [HH:MM dd-mm]

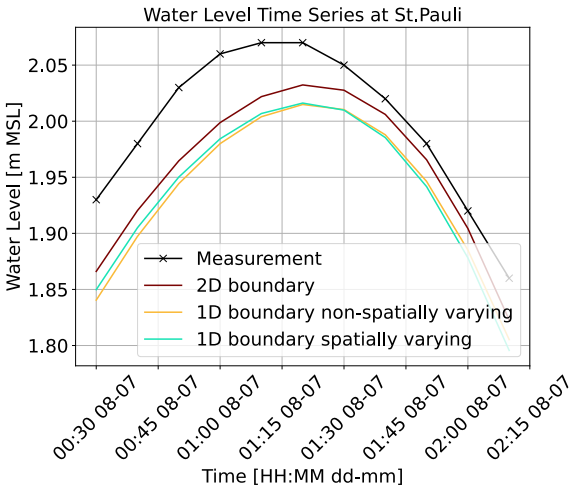
Water Level Time Series at St.Pauli
Measurement
2D boundary
1D boundary non-spatially varying
1D boundary spatially varying
Water Level [m MSL]
2.05
2.00
1.95
1.90
1.85
1.80
00:30 08-07
00:45 08-07
01:00 08-07
01:15 08-07
01:30 08-07
01:45 08-07
02:00 08-07
02:15 08-07
Time [HH:MM dd-mm]

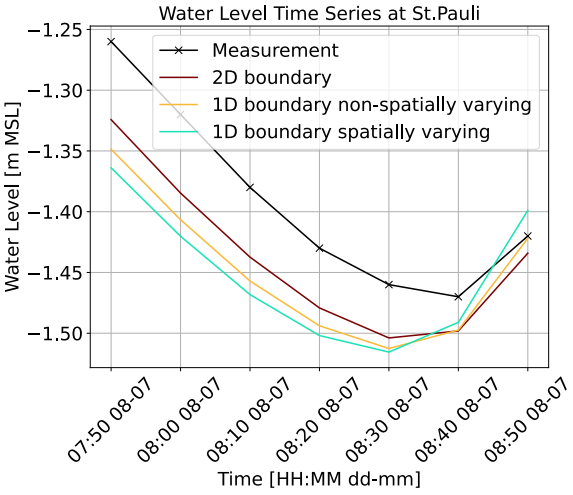
Water Level Time Series at St.Pauli
Measurement
2D boundary
1D boundary non-spatially varying
1D boundary spatially varying
Water Level [m MSL]
−1.25
−1.30
−1.35
−1.40
−1.45
−1.50
07:50 08-07
08:00 08-07
08:10 08-07
08:20 08-07
08:30 08-07
08:40 08-07
08:50 08-07
Time [HH:MM dd-mm]

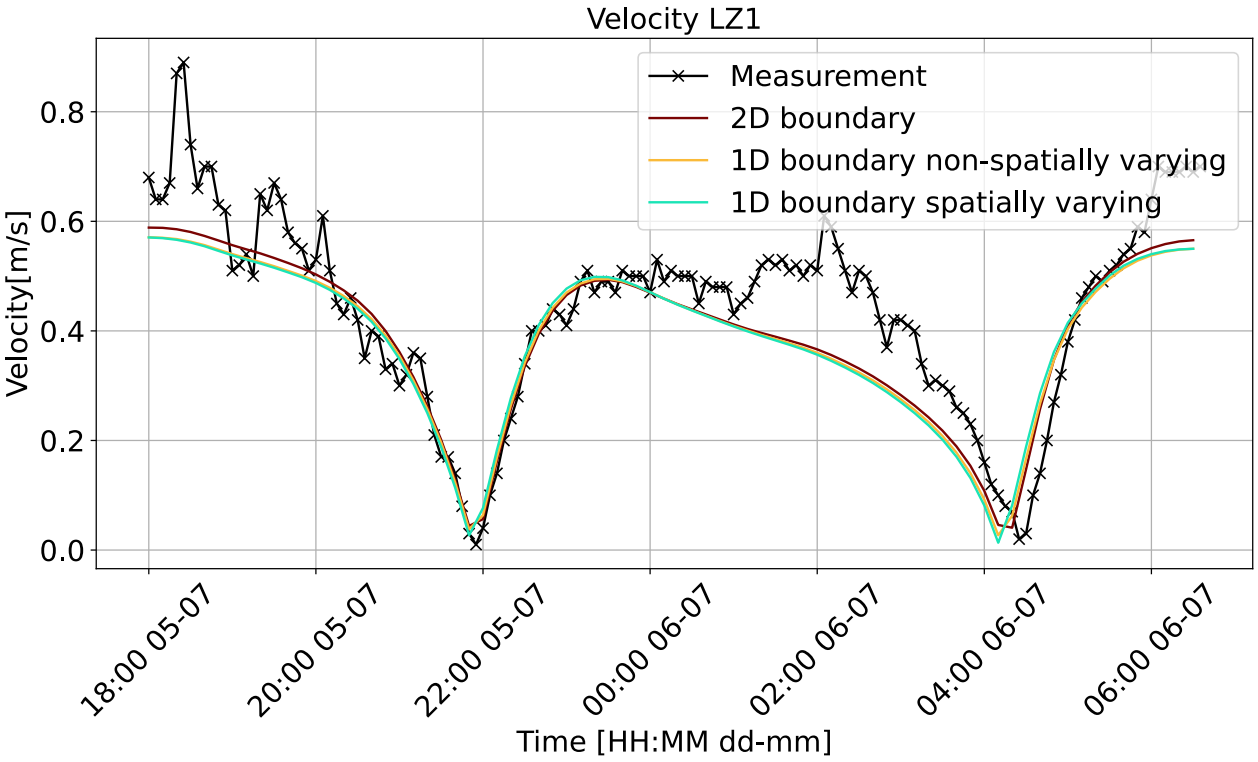
Velocity LZ1
Measurement
2D boundary
1D boundary non-spatially varying
1D boundary spatially varying
Velocity[m/s]
0.0
0.2
0.4
0.6
0.8
18:00 05-07
20:00 05-07
22:00 05-07
00:00 06-07
02:00 06-07
04:00 06-07
06:00 06-07
Time [HH:MM dd-mm]

Appendix C

Q2: grid width and time step analysis

C.1 grid width

C.1.1 Boundary in and outflow

Table C.1: Boundary in and outflow for different grid widths

grid width [m]	Computational time [min]	Boundary inflow [$10^{11} m^3$]	Boundary outflow [10^{11} m^3]
200	164	1.88	1.88
300	78	1.87	1.87
400	45	1.91	1.91
500	29	1.88	1.88
750	14	1.85	1.85
1000	8	1.98	1.98
1500	4	1.94	1.94

C.1.2 Water level results

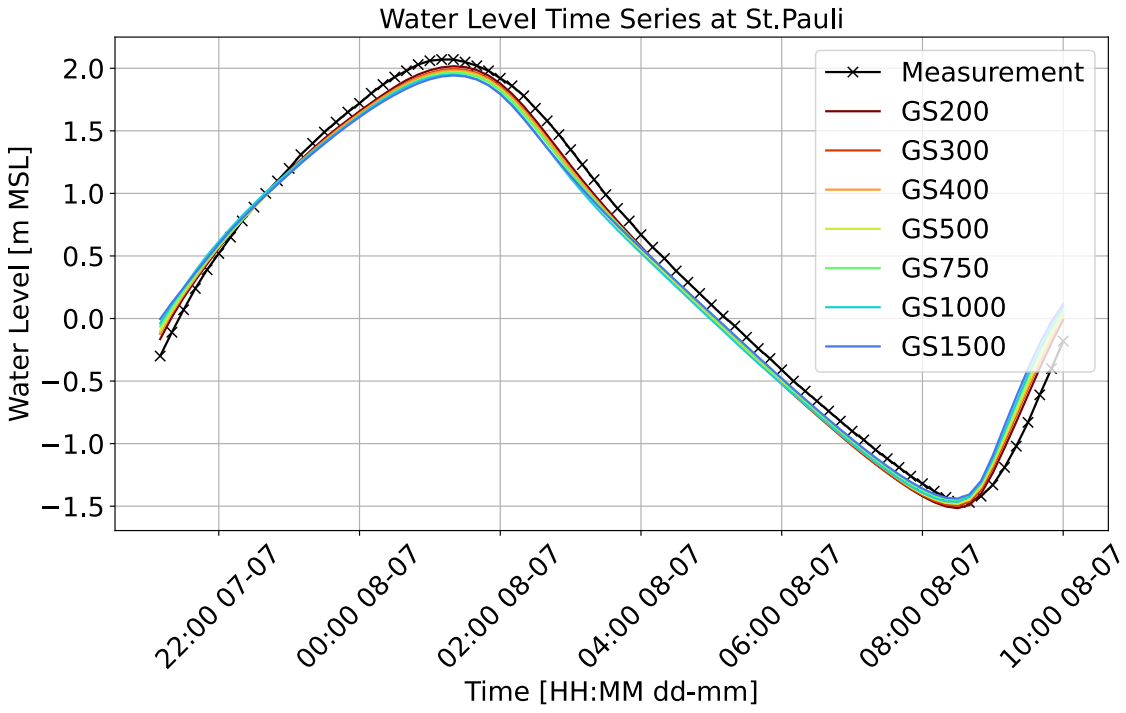

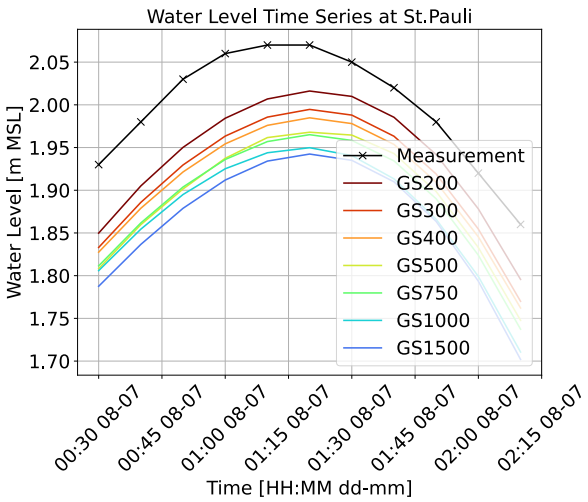

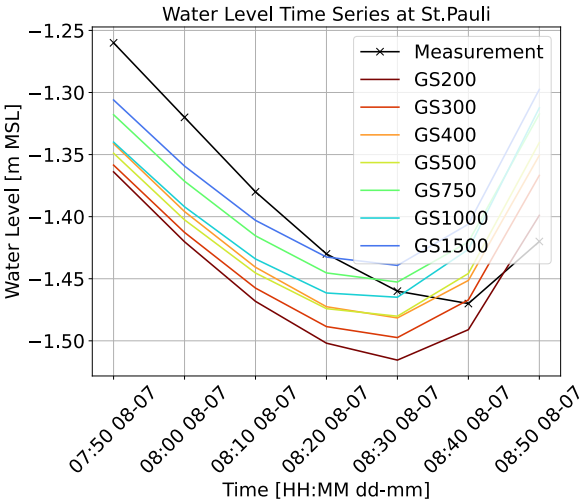

C.1.3 Flow velocity results

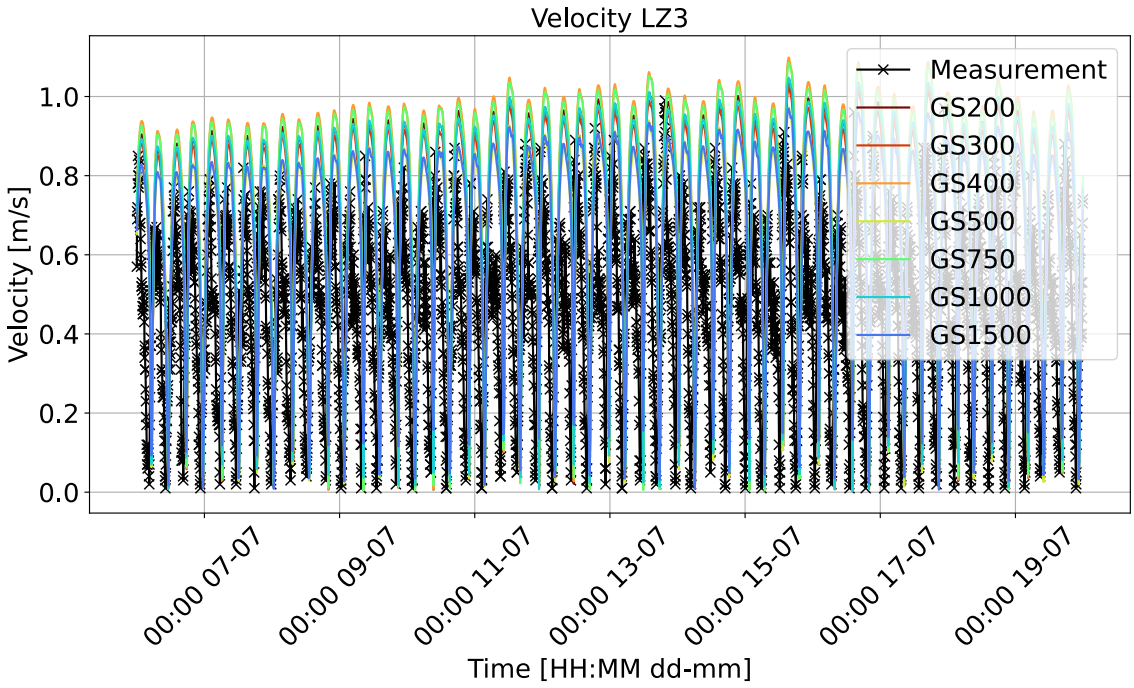

C.2 Time step

C.2.1 Water level results

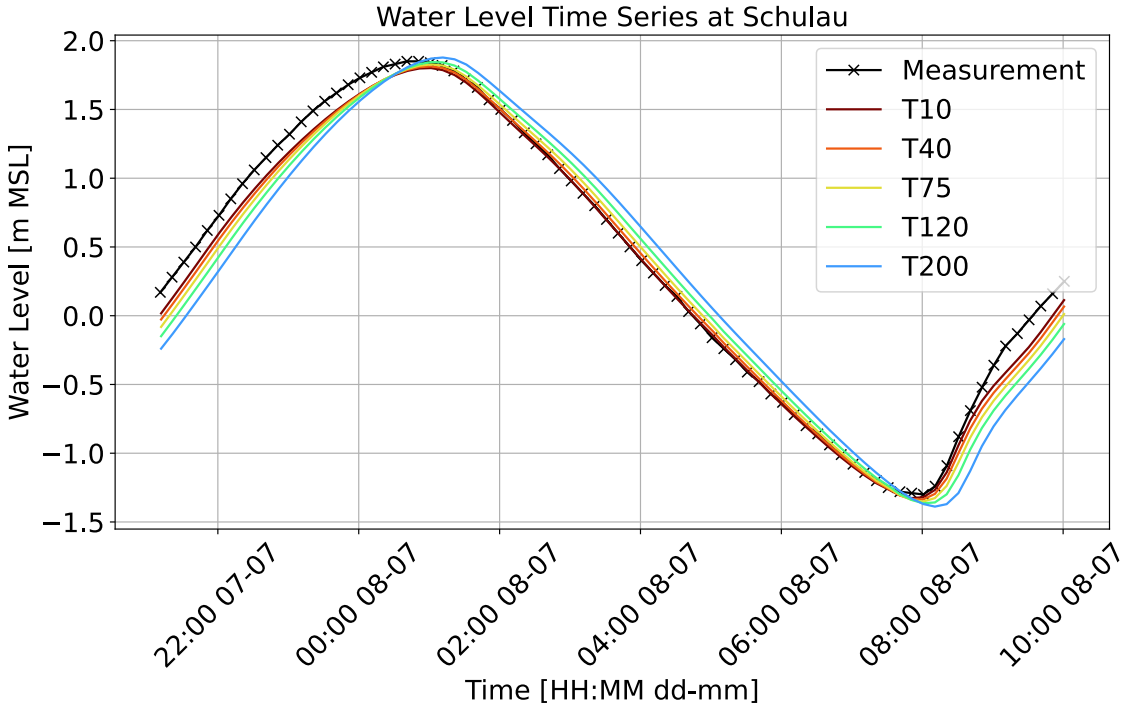

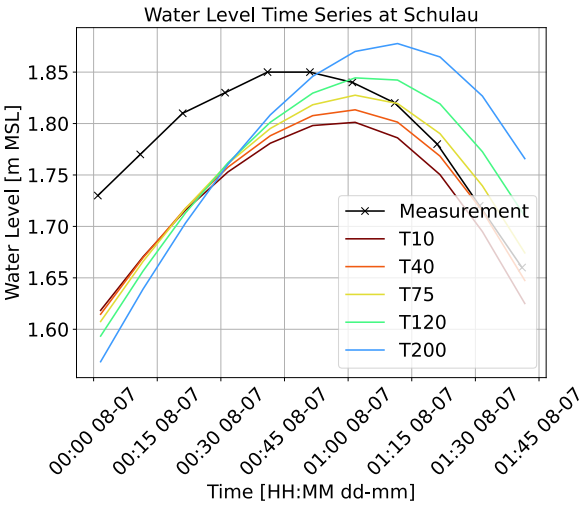
Water Level Time Series at Schulau
Water Level [m MSL]
1.85
1.80
1.75
1.70
1.65
1.60
Measurement
T10
T40
T75
T120
T200
00:00 08-07
00:15 08-07
00:30 08-07
00:45 08-07
01:00 08-07
01:15 08-07
01:30 08-07
01:45 08-07
Time [HH:MM dd-mm]

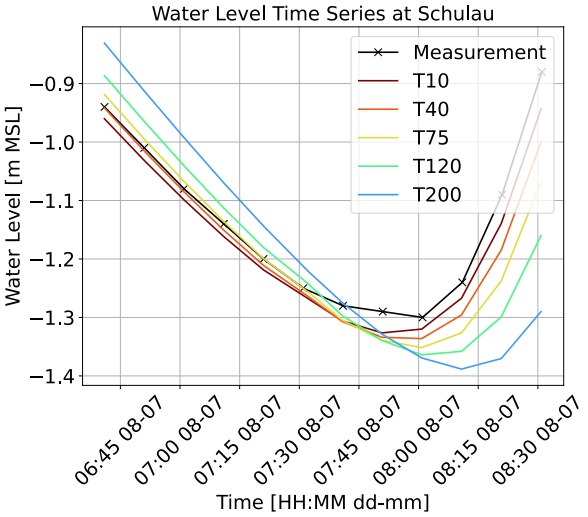
Water Level Time Series at Schulau
Water Level [m MSL]
−0.9
−1.0
−1.1
−1.2
−1.3
−1.4
Measurement
T10
T40
T75
T120
T200
06:45 08-07
07:00 08-07
07:15 08-07
07:30 08-07
07:45 08-07
08:00 08-07
08:15 08-07
08:30 08-07
Time [HH:MM dd-mm]

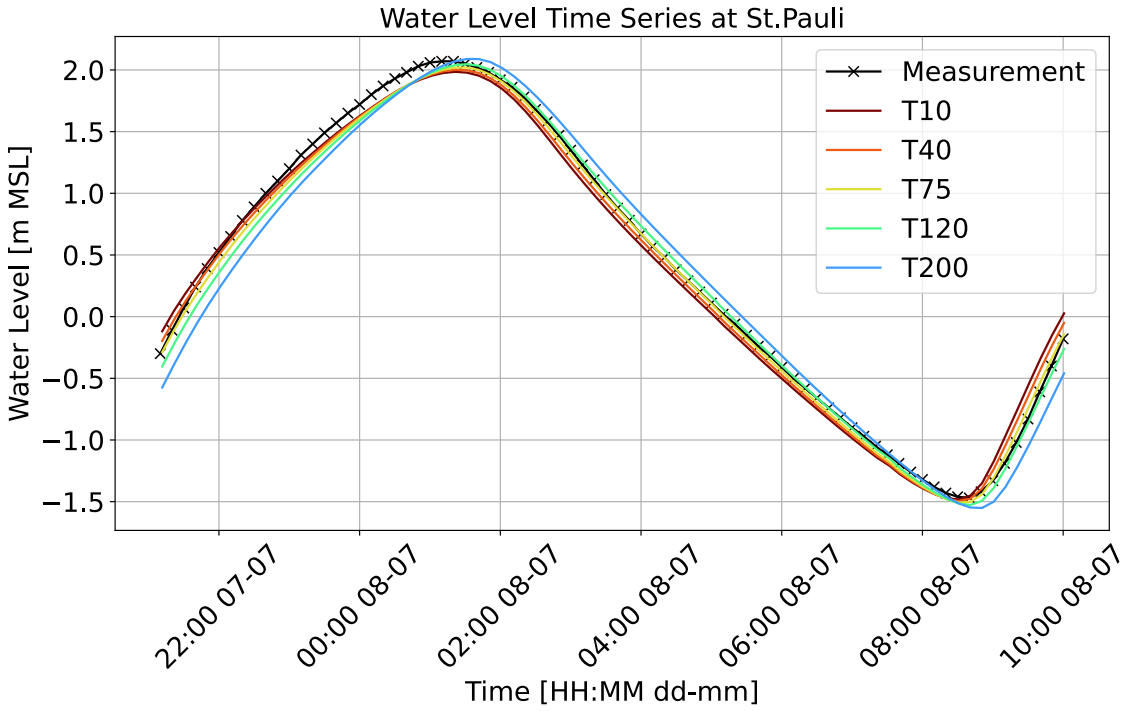
Water Level Time Series at St.Pauli
Water Level [m MSL]
2.0
1.5
1.0
0.5
0.0
−0.5
−1.0
−1.5
Measurement
T10
T40
T75
T120
T200
22:00 07-07
00:00 08-07
02:00 08-07
04:00 08-07
06:00 08-07
08:00 08-07
10:00 08-07
Time [HH:MM dd-mm]

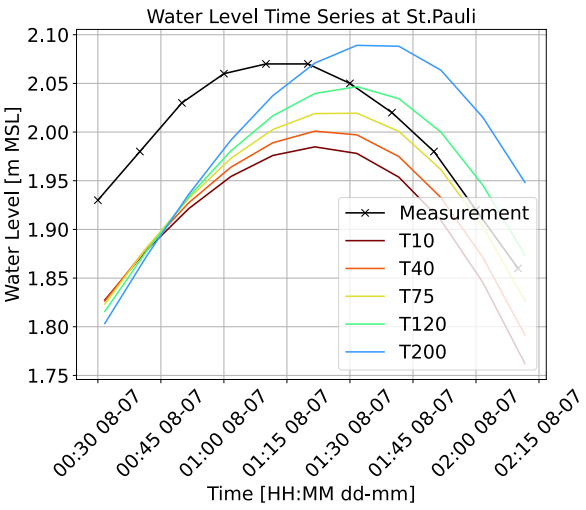

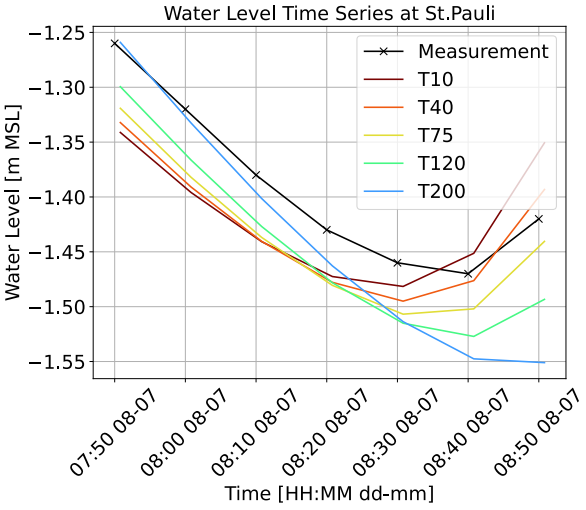

C.2.2 Flow velocity results

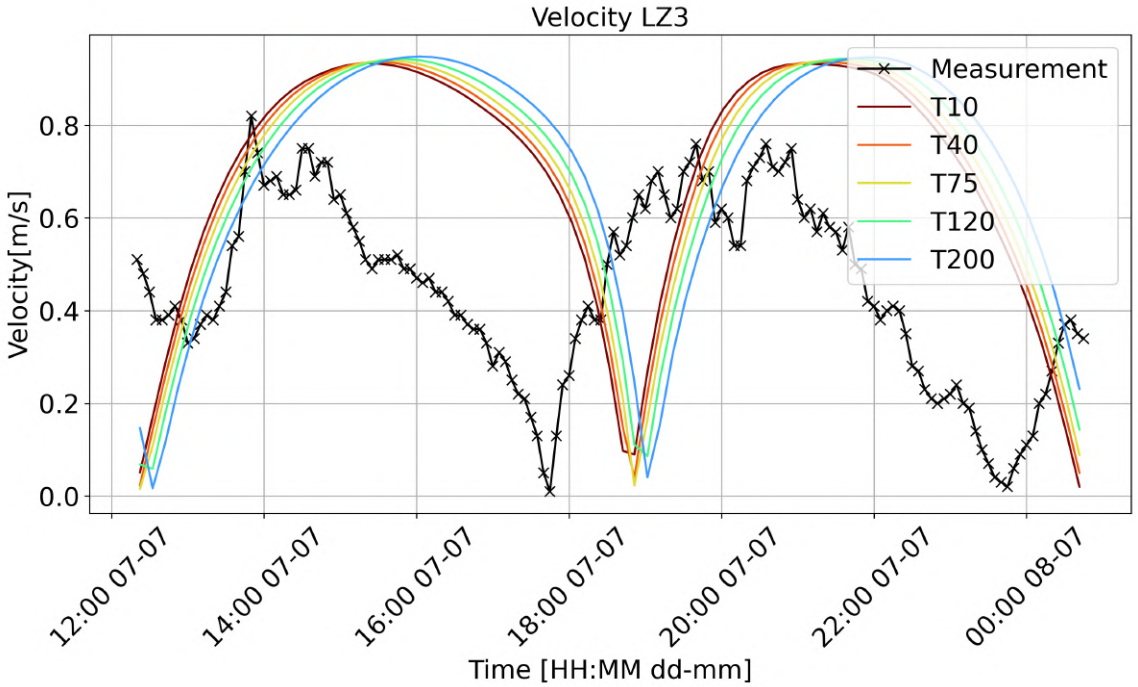

Appendix D

Q3: Local grid refinements

D.1 Port of Hamburg

D.1.1 Water level results

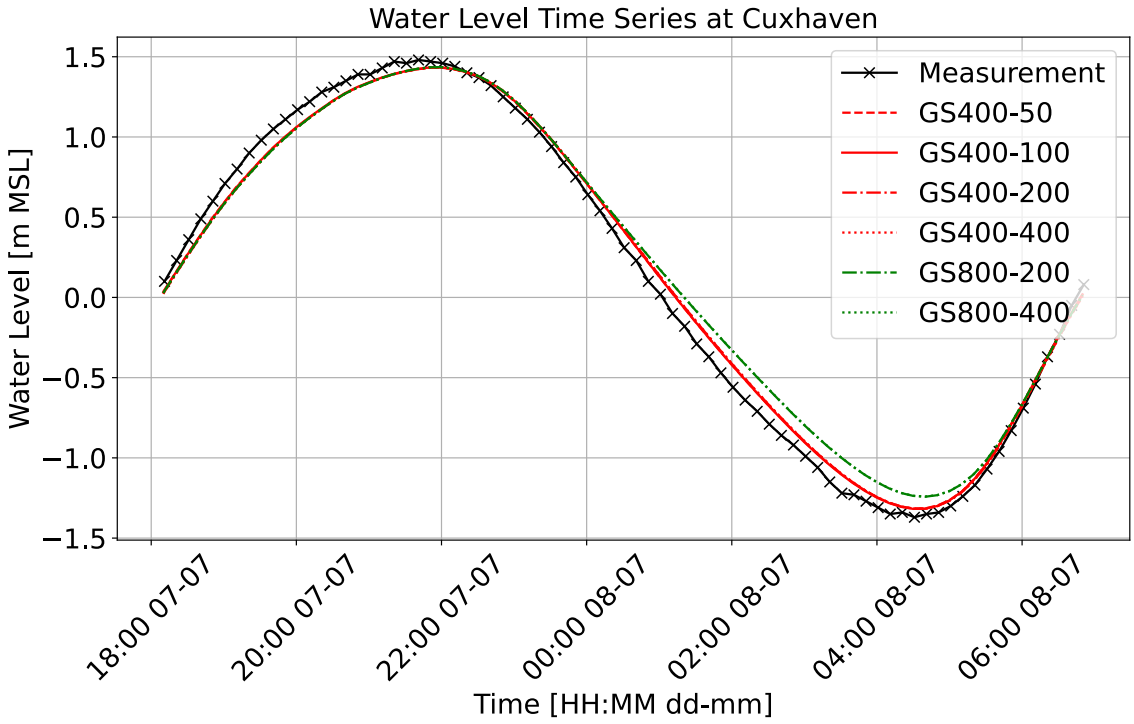

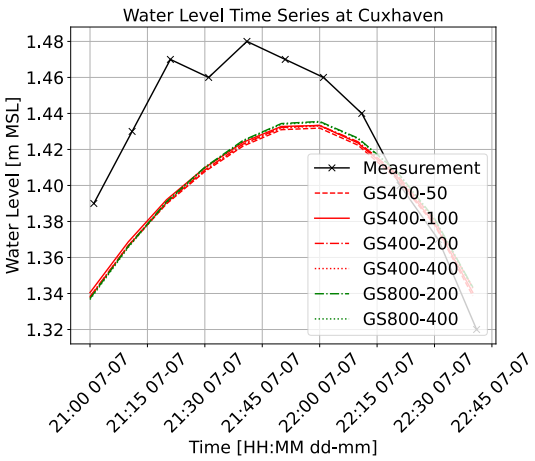

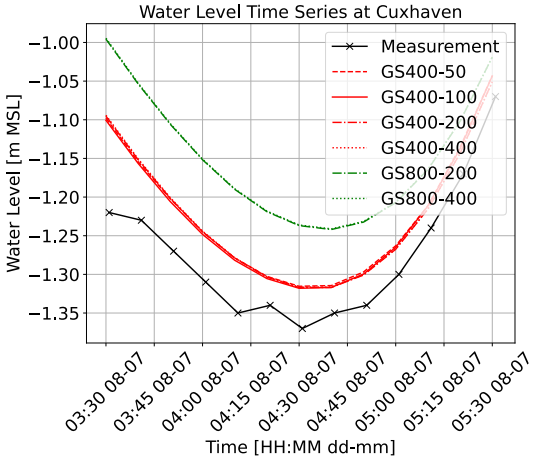

D.1.2 Flow velocity results

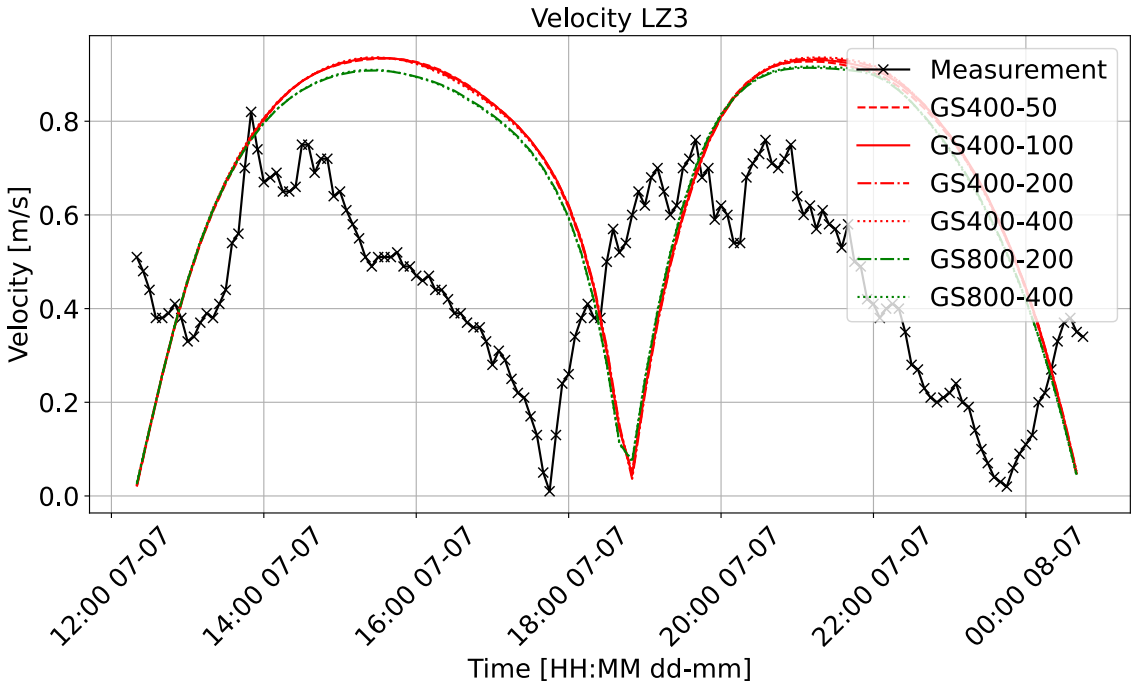

D.2 River widening

D.2.1 Water level results

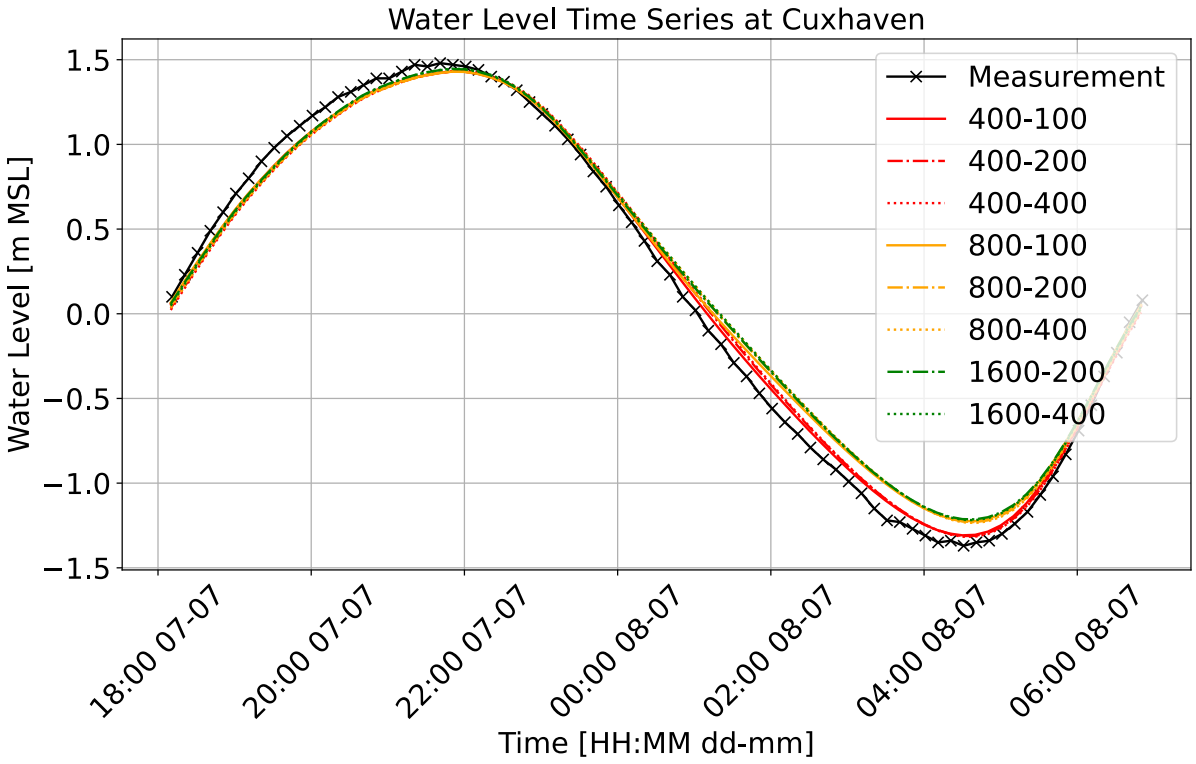

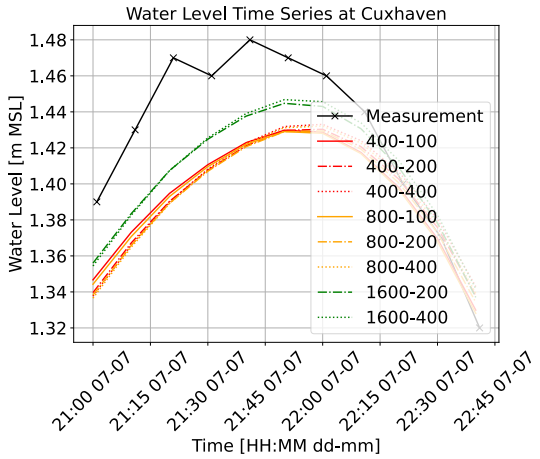

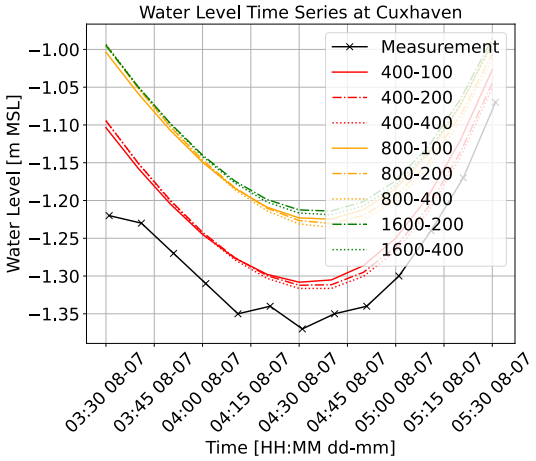

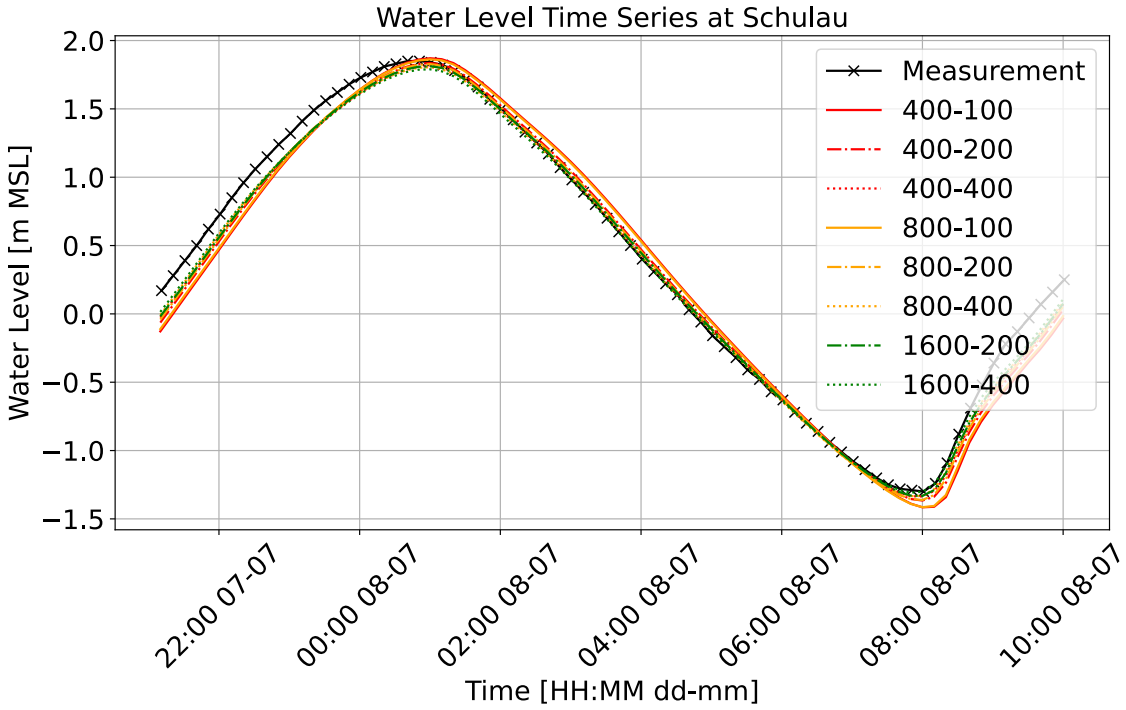
Water Level Time Series at Schulau
Water Level [m MSL]
Time [HH:MM dd-mm]
Measurement
400-100
400-200
400-400
800-100
800-200
800-400
1600-200
1600-400
22:00 07-07
00:00 08-07
02:00 08-07
04:00 08-07
06:00 08-07
08:00 08-07
10:00 08-07

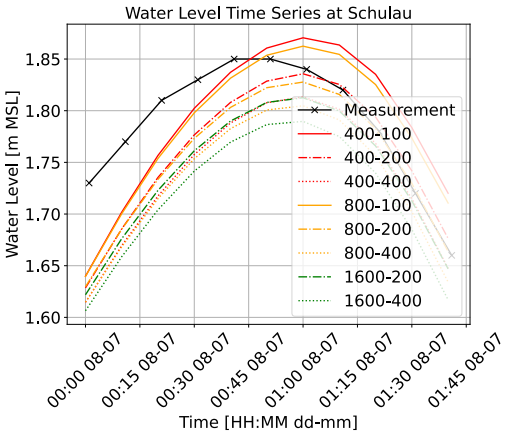
Water Level Time Series at Schulau
Water Level [m MSL]
Time [HH:MM dd-mm]
Measurement
400-100
400-200
400-400
800-100
800-200
800-400
1600-200
1600-400

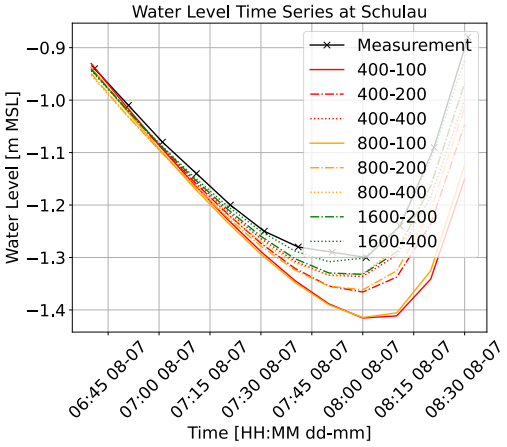
Water Level Time Series at Schulau
Water Level [m MSL]
Time [HH:MM dd-mm]
Measurement
400-100
400-200
400-400
800-100
800-200
800-400
1600-200
1600-400

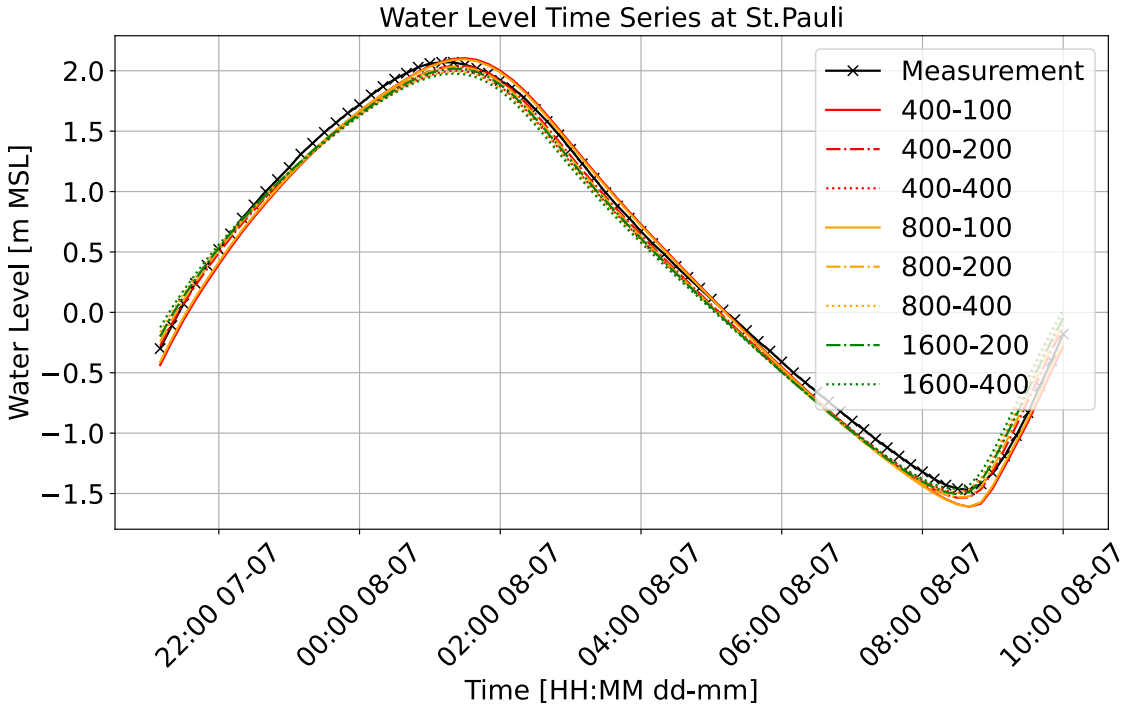
Water Level Time Series at St.Pauli
Water Level [m MSL]
2.0
1.5
1.0
0.5
0.0
−0.5
−1.0
−1.5
22:00 07-07
00:00 08-07
02:00 08-07
04:00 08-07
06:00 08-07
08:00 08-07
10:00 08-07
Time [HH:MM dd-mm]
Measurement
400-100
400-200
400-400
800-100
800-200
800-400
1600-200
1600-400

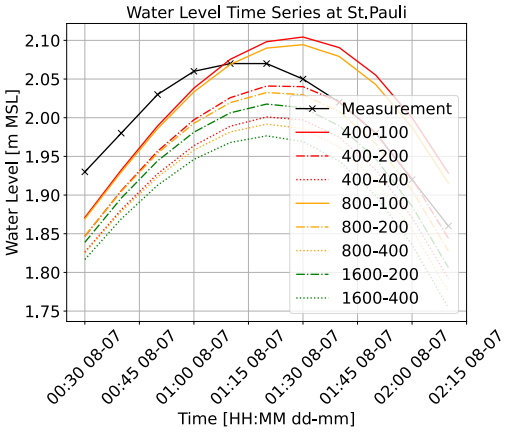
Water Level Time Series at St.Pauli
Water Level [m MSL]
2.10
2.05
2.00
1.95
1.90
1.85
1.80
1.75
00:30 08-07
00:45 08-07
01:00 08-07
01:15 08-07
01:30 08-07
01:45 08-07
02:00 08-07
02:15 08-07
Time [HH:MM dd-mm]
Measurement
400-100
400-200
400-400
800-100
800-200
800-400
1600-200
1600-400

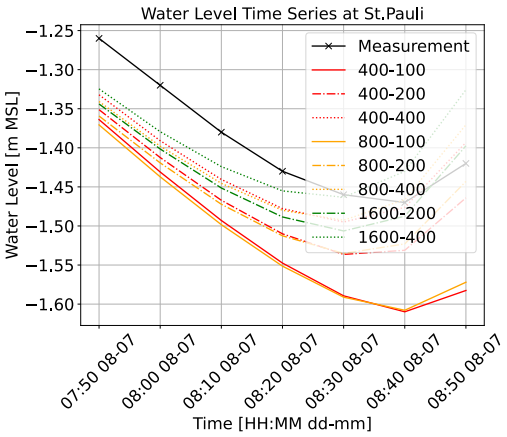
Water Level Time Series at St.Pauli
Water Level [m MSL]
−1.25
−1.30
−1.35
−1.40
−1.45
−1.50
−1.55
−1.60
07:50 08-07
08:00 08-07
08:10 08-07
08:20 08-07
08:30 08-07
08:40 08-07
08:50 08-07
Time [HH:MM dd-mm]
Measurement
400-100
400-200
400-400
800-100
800-200
800-400
1600-200
1600-400

D.2.2 Flow velocity results

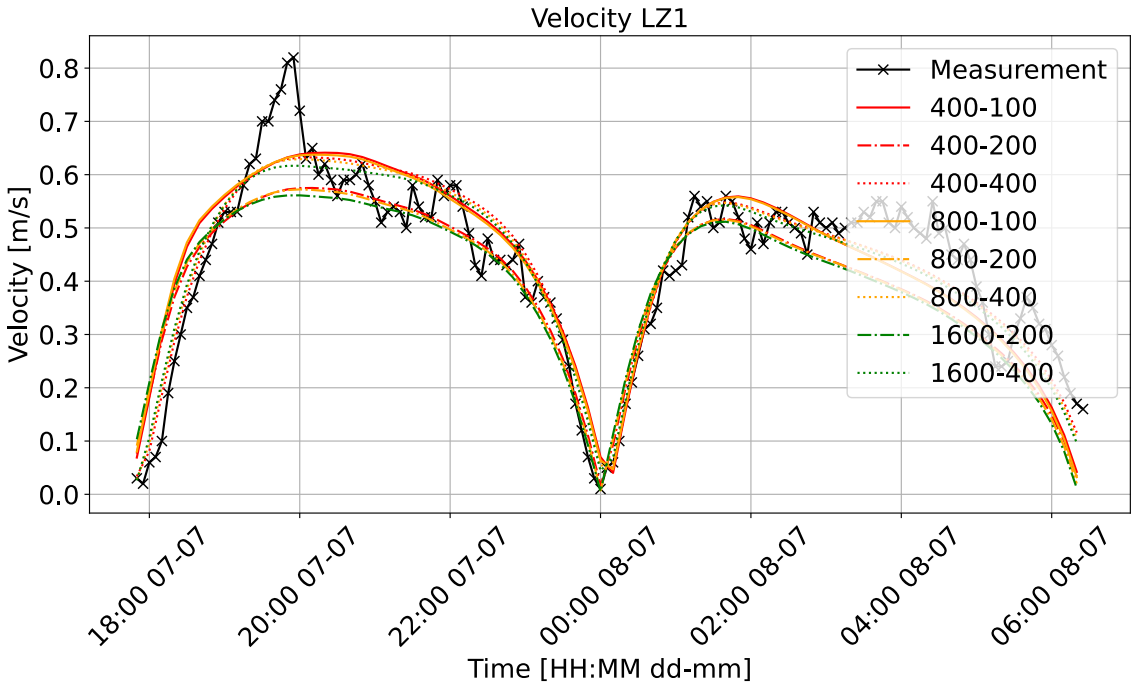

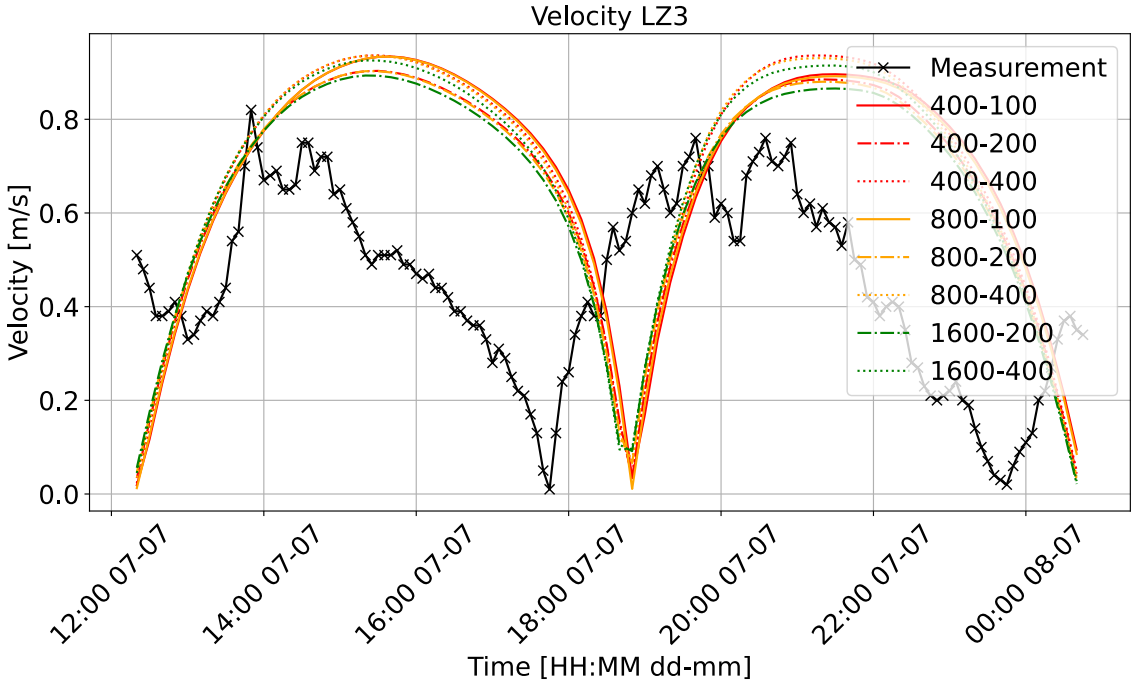

D.3 River sea connection

D.3.1 Water level results

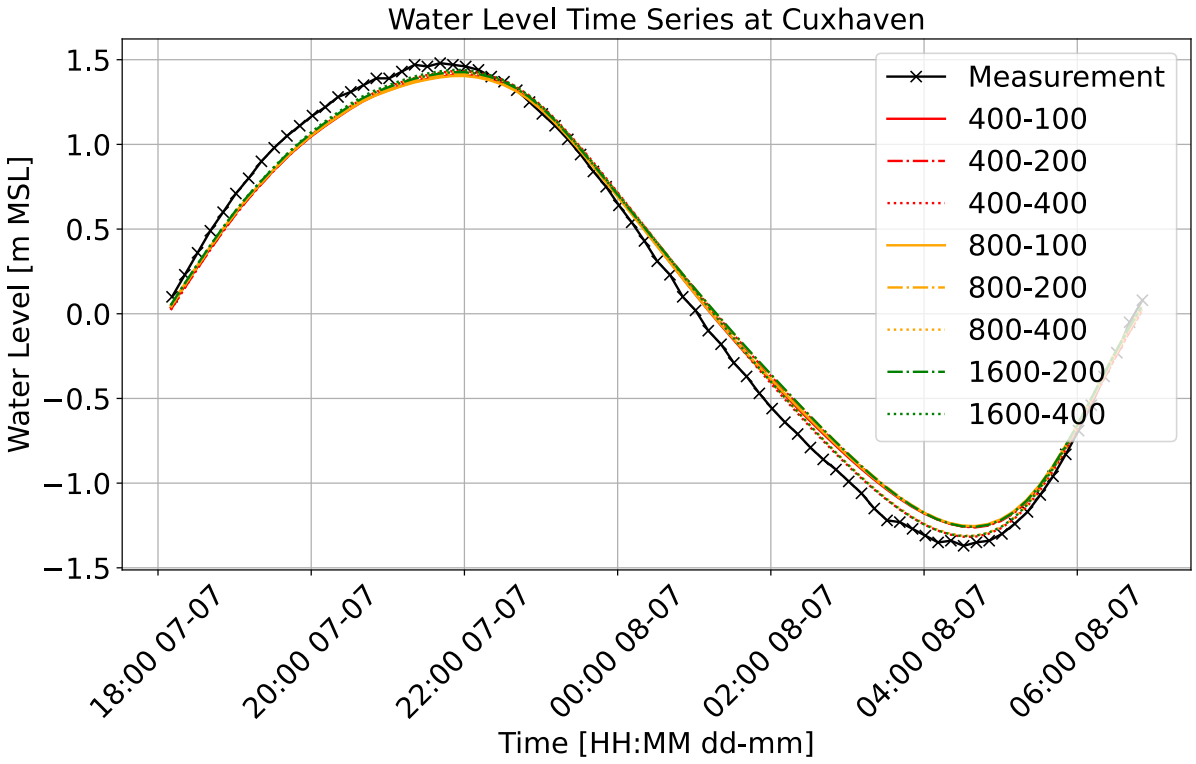

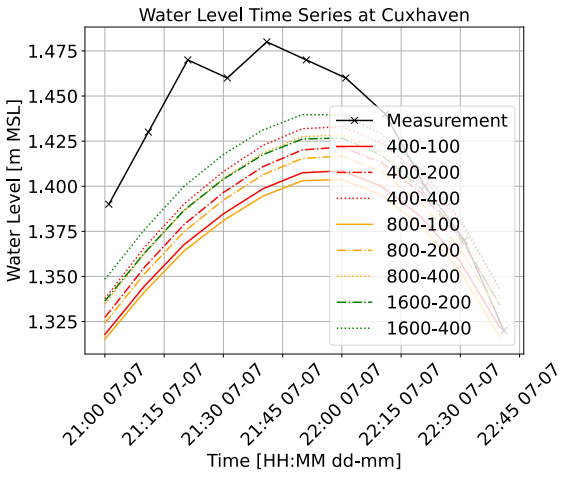

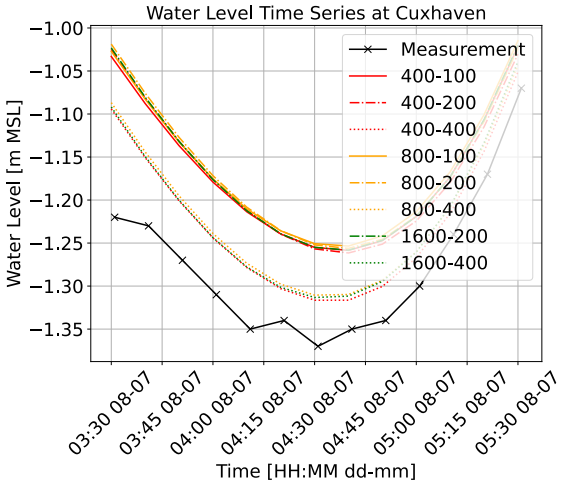

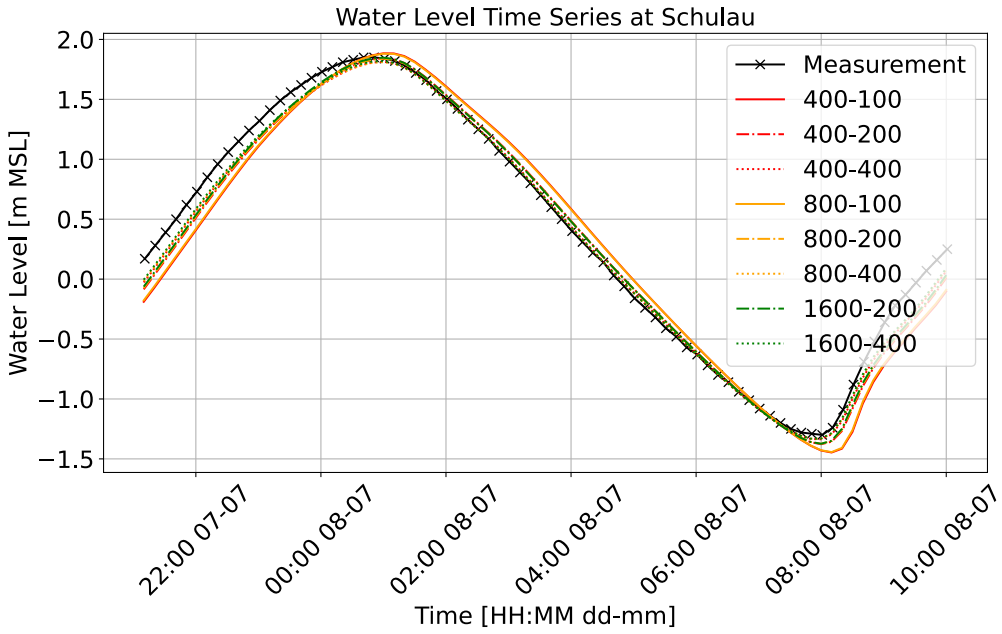
Water Level Time Series at Schulau
Water Level [m MSL]
2.0
1.5
1.0
0.5
0.0
−0.5
−1.0
−1.5
22:00 07-07
00:00 08-07
02:00 08-07
04:00 08-07
06:00 08-07
08:00 08-07
10:00 08-07
Time [HH:MM dd-mm]
Measurement
400-100
400-200
400-400
800-100
800-200
800-400
1600-200
1600-400

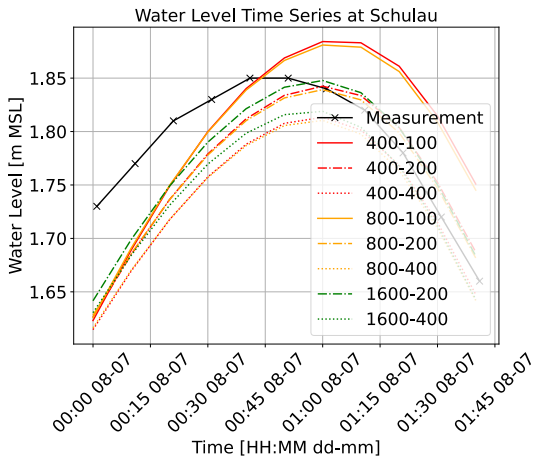
Water Level Time Series at Schulau
Water Level [m MSL]
1.85
1.80
1.75
1.70
1.65
00:00 08-07
00:15 08-07
00:30 08-07
00:45 08-07
01:00 08-07
01:15 08-07
01:30 08-07
01:45 08-07
Time [HH:MM dd-mm]
Measurement
400-100
400-200
400-400
800-100
800-200
800-400
1600-200
1600-400

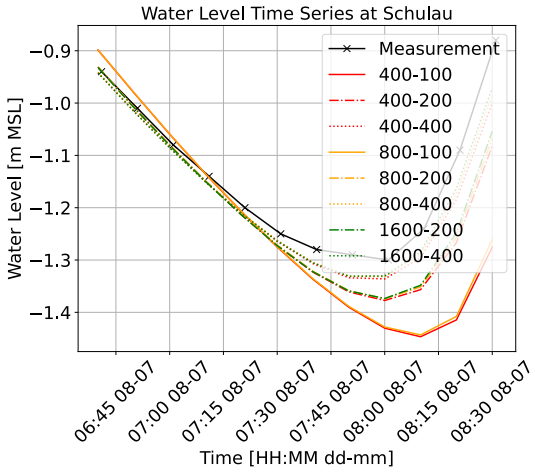
Water Level Time Series at Schulau
Water Level [m MSL]
−0.9
−1.0
−1.1
−1.2
−1.3
−1.4
06:45 08-07
07:00 08-07
07:15 08-07
07:30 08-07
07:45 08-07
08:00 08-07
08:15 08-07
08:30 08-07
Time [HH:MM dd-mm]
Measurement
400-100
400-200
400-400
800-100
800-200
800-400
1600-200
1600-400

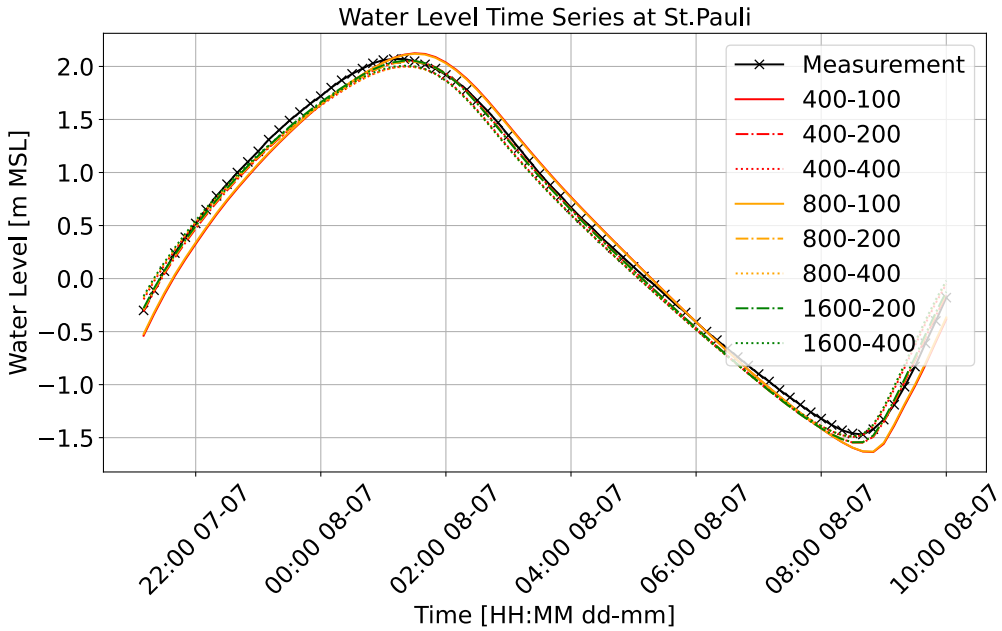
Water Level Time Series at St.Pauli
Water Level [m MSL]
2.0
1.5
1.0
0.5
0.0
−0.5
−1.0
−1.5
22:00 07-07
00:00 08-07
02:00 08-07
04:00 08-07
06:00 08-07
08:00 08-07
10:00 08-07
Time [HH:MM dd-mm]
Measurement
400-100
400-200
400-400
800-100
800-200
800-400
1600-200
1600-400

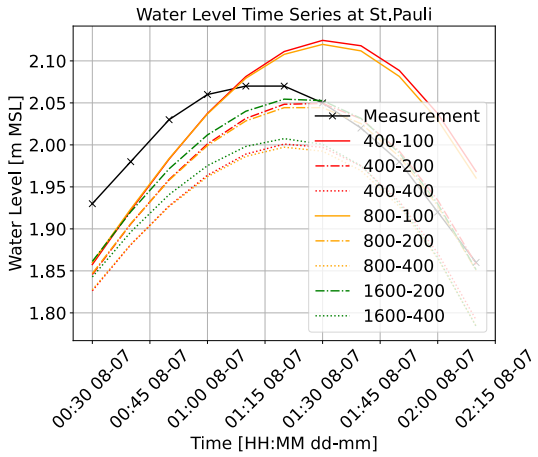
Water Level Time Series at St.Pauli
Water Level [m MSL]
2.10
2.05
2.00
1.95
1.90
1.85
1.80
00:30 08-07
00:45 08-07
01:00 08-07
01:15 08-07
01:30 08-07
01:45 08-07
02:00 08-07
02:15 08-07
Time [HH:MM dd-mm]
Measurement
400-100
400-200
400-400
800-100
800-200
800-400
1600-200
1600-400

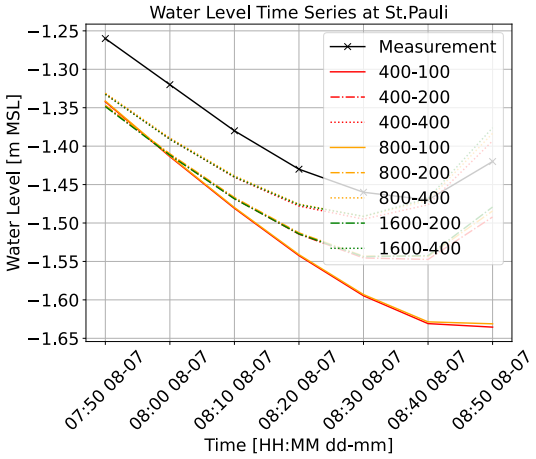
Water Level Time Series at St.Pauli
Water Level [m MSL]
−1.25
−1.30
−1.35
−1.40
−1.45
−1.50
−1.55
−1.60
−1.65
07:50 08-07
08:00 08-07
08:10 08-07
08:20 08-07
08:30 08-07
08:40 08-07
08:50 08-07
Time [HH:MM dd-mm]
Measurement
400-100
400-200
400-400
800-100
800-200
800-400
1600-200
1600-400

D.3.2 Flow velocity results

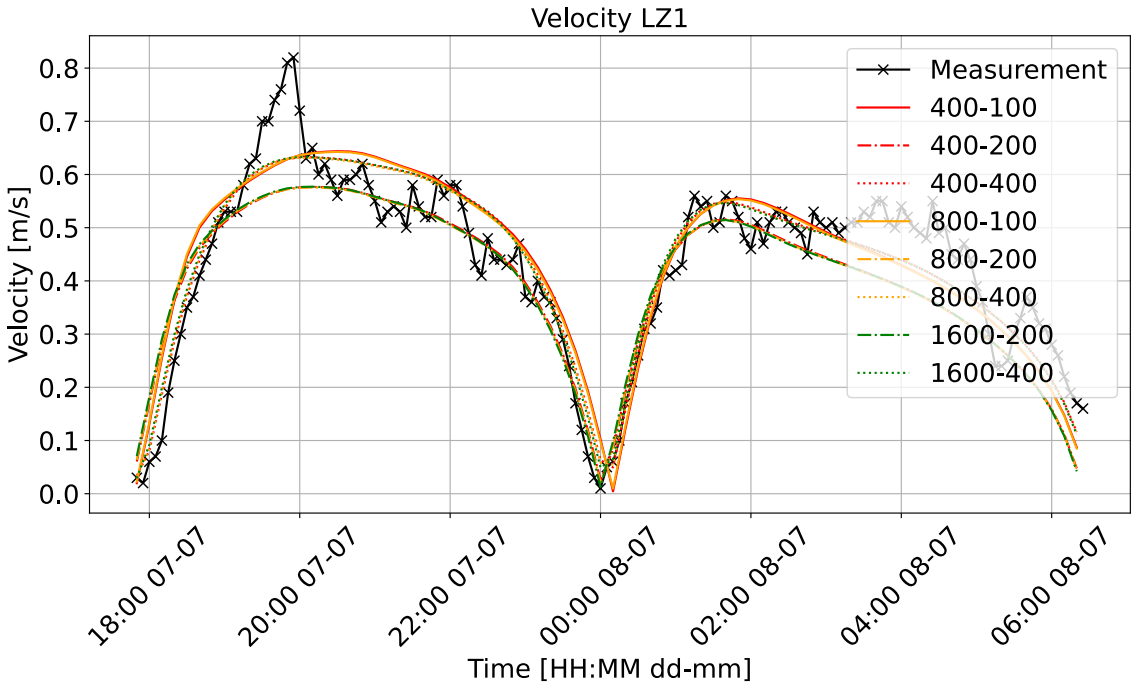

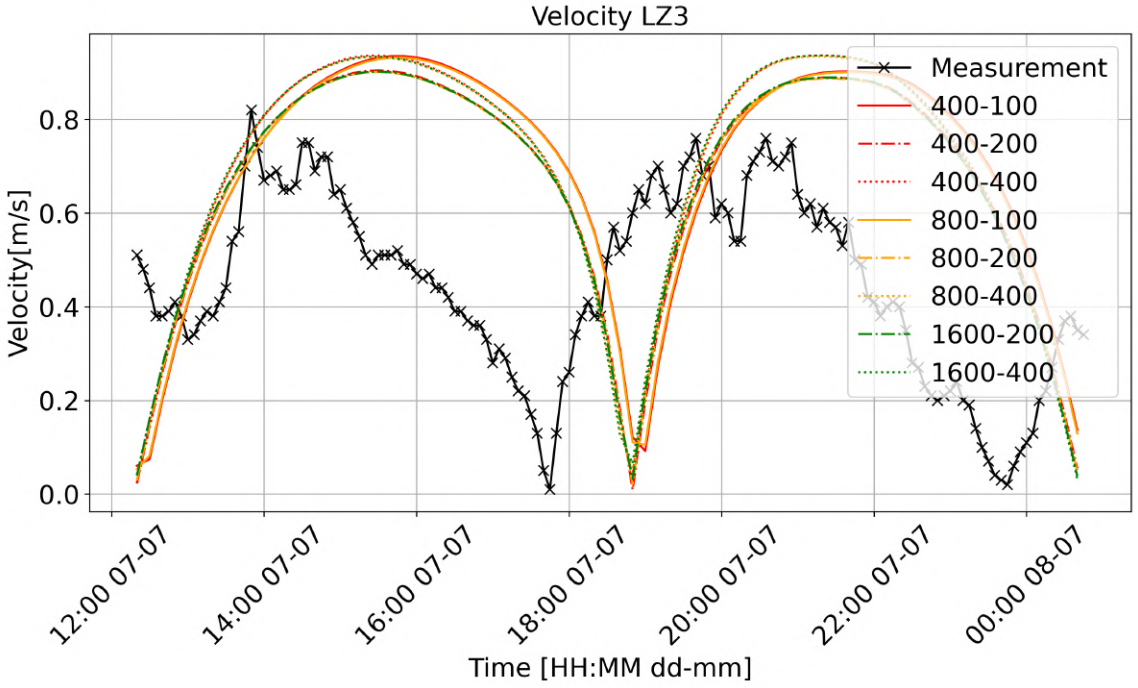

D.3.3 RMSE values

Table D.1: Comparison RMSE local grid refinement river/sea division cases to base case

grid width	Computational time	Cuxhaven			Schulau			St.Pauli		
[m]	[min]	T	H	L	T	H	L	T	H	L
Base case: 400-400	16	12.5	5.1	4.7	14.7	7.2	5.2	9.4	8.9	4.5
400-100	+121	+1.0	+2.2	+6.4	+10.5	-1.7	+9.9	+7.0	-1.8	+12.6
400-200	+18	+2.0	+1.1	+6.1	+3.1	-2.4	+3.1	-1.1	-4.1	+4.1
800-100	+101	+1.0	+2.8	+6.8	+9.8	-2.0	+9.6	+6.2	-2.2	+12.3
800-200	+8	+2.1	+1.6	+6.6	+2.5	-2.3	+2.9	-1.4	-3.9	+3.9
800-400	-8	-0.1	+0.5	+0.5	-0.6	+0.2	-0.2	+0.2	+0.3	-0.1
1600-200	+7	+1.6	+0.4	+6.4	+1.8	-2.7	+2.8	-1.9	-4.4	+3.9
1600-400	-11	-0.6	-0.8	+0.3	-1.3	-0.7	-0.3	-0.1	-0.7	-0.1

D.4 Navigation channel

D.4.1 Water level results

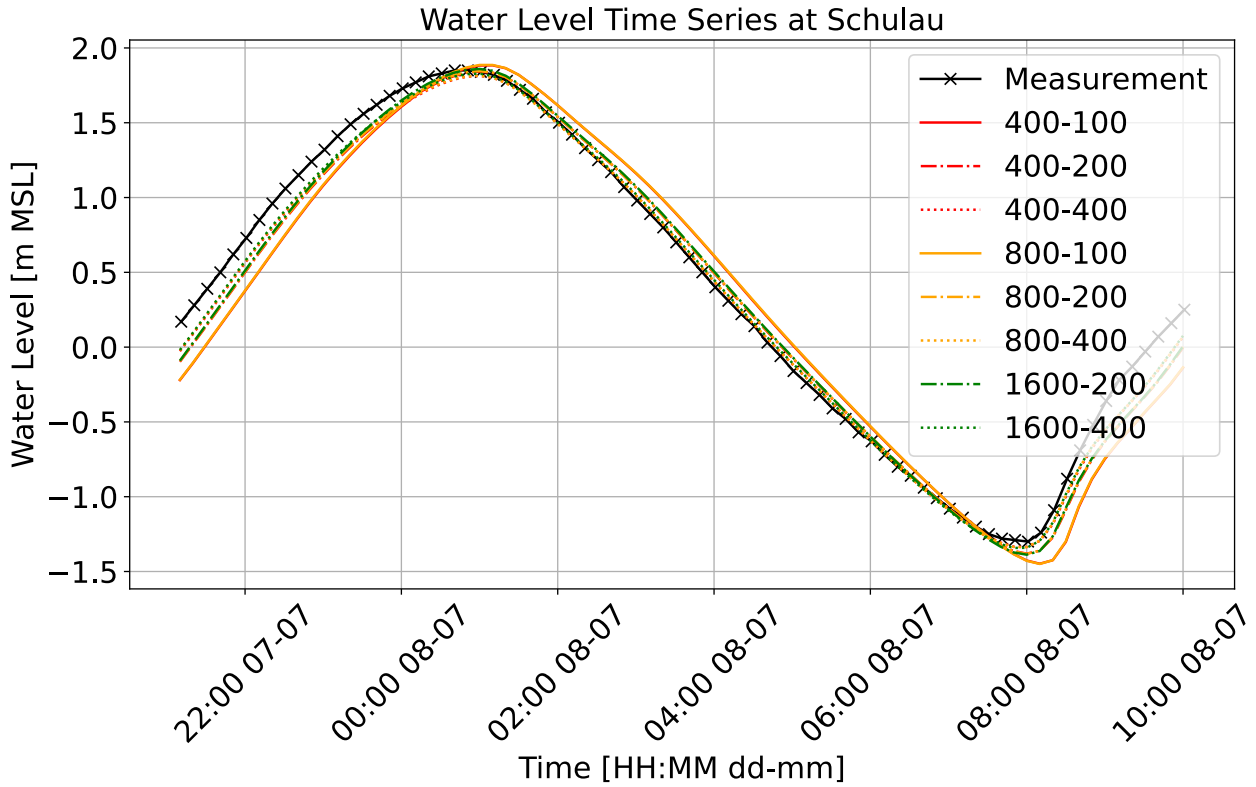

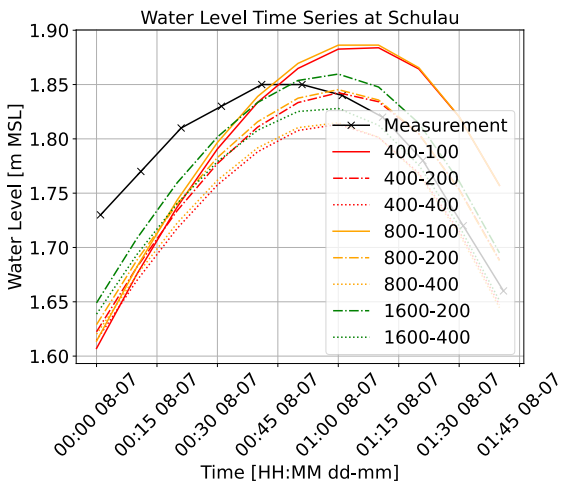
Water Level Time Series at Schulau
Water Level [m MSL]
1.90
1.85
1.80
1.75
1.70
1.65
1.60
Measurement
400-100
400-200
400-400
800-100
800-200
800-400
1600-200
1600-400
00:00 08-07
00:15 08-07
00:30 08-07
00:45 08-07
01:00 08-07
01:15 08-07
01:30 08-07
01:45 08-07
Time [HH:MM dd-mm]

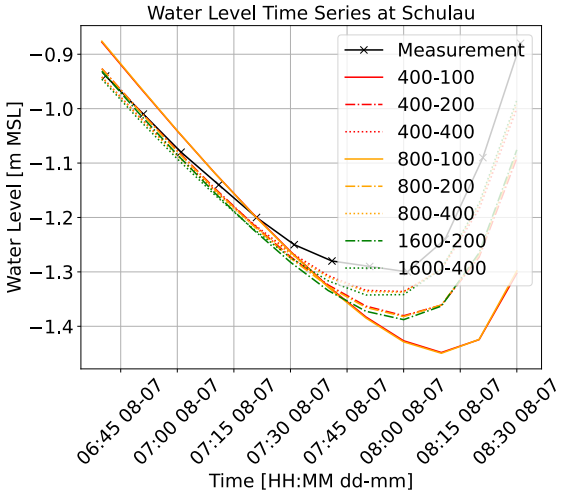
Water Level Time Series at Schulau
Water Level [m MSL]
−0.9
−1.0
−1.1
−1.2
−1.3
−1.4
Measurement
400-100
400-200
400-400
800-100
800-200
800-400
1600-200
1600-400
06:45 08-07
07:00 08-07
07:15 08-07
07:30 08-07
07:45 08-07
08:00 08-07
08:15 08-07
08:30 08-07
Time [HH:MM dd-mm]

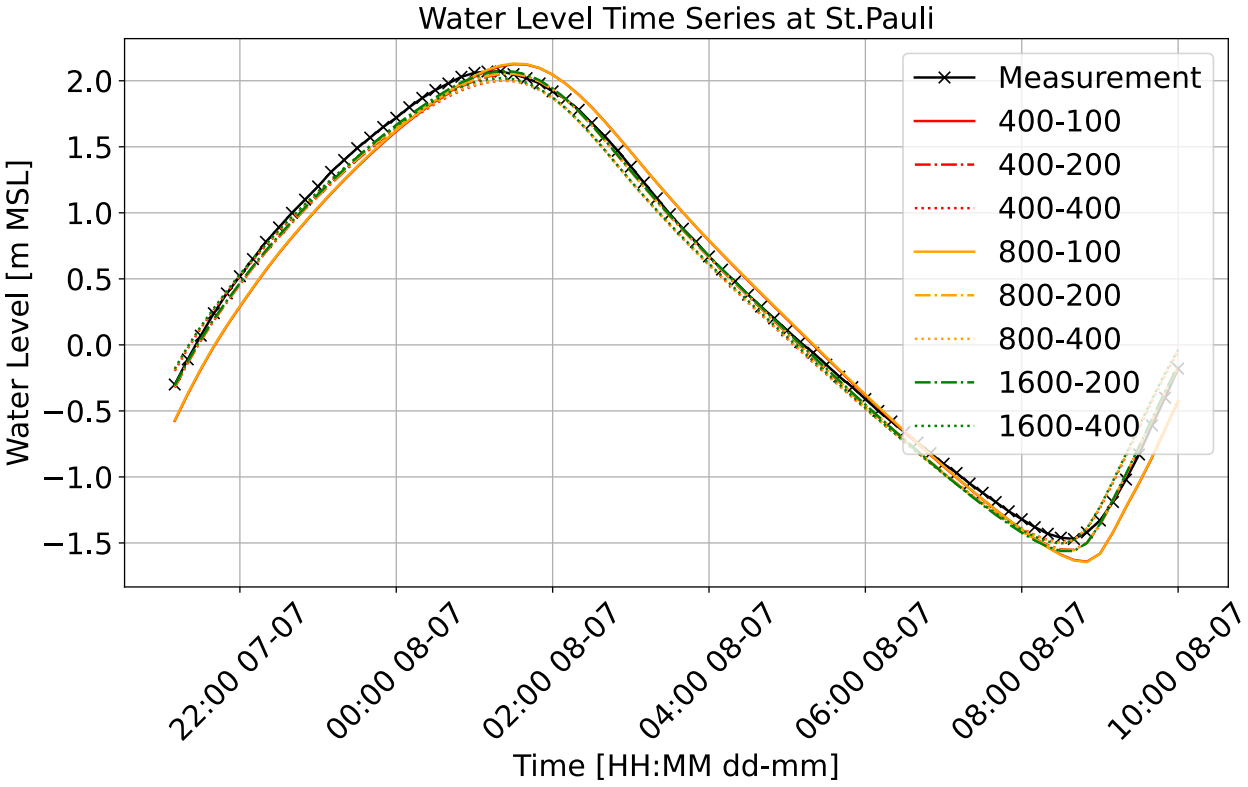
Water Level Time Series at St.Pauli
Water Level [m MSL]
2.0
1.5
1.0
0.5
0.0
−0.5
−1.0
−1.5
Measurement
400-100
400-200
400-400
800-100
800-200
800-400
1600-200
1600-400
22:00 07-07
00:00 08-07
02:00 08-07
04:00 08-07
06:00 08-07
08:00 08-07
10:00 08-07
Time [HH:MM dd-mm]

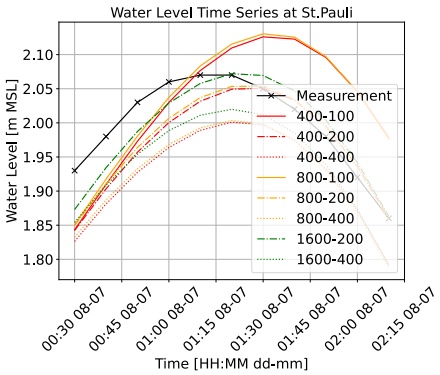

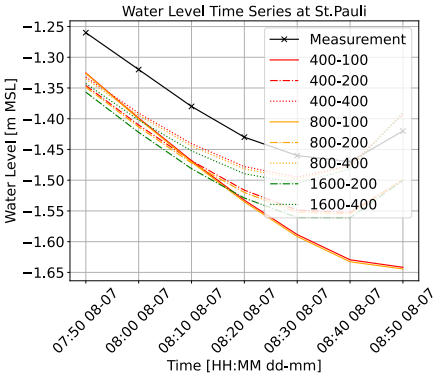

D.5 Combination

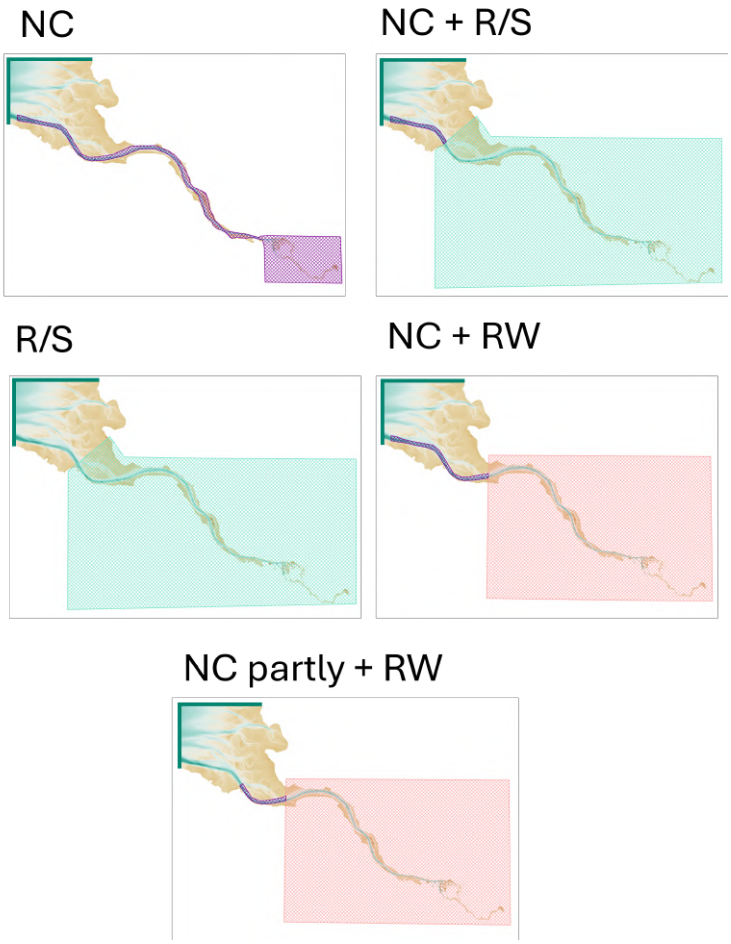

D.5.1 Water level results

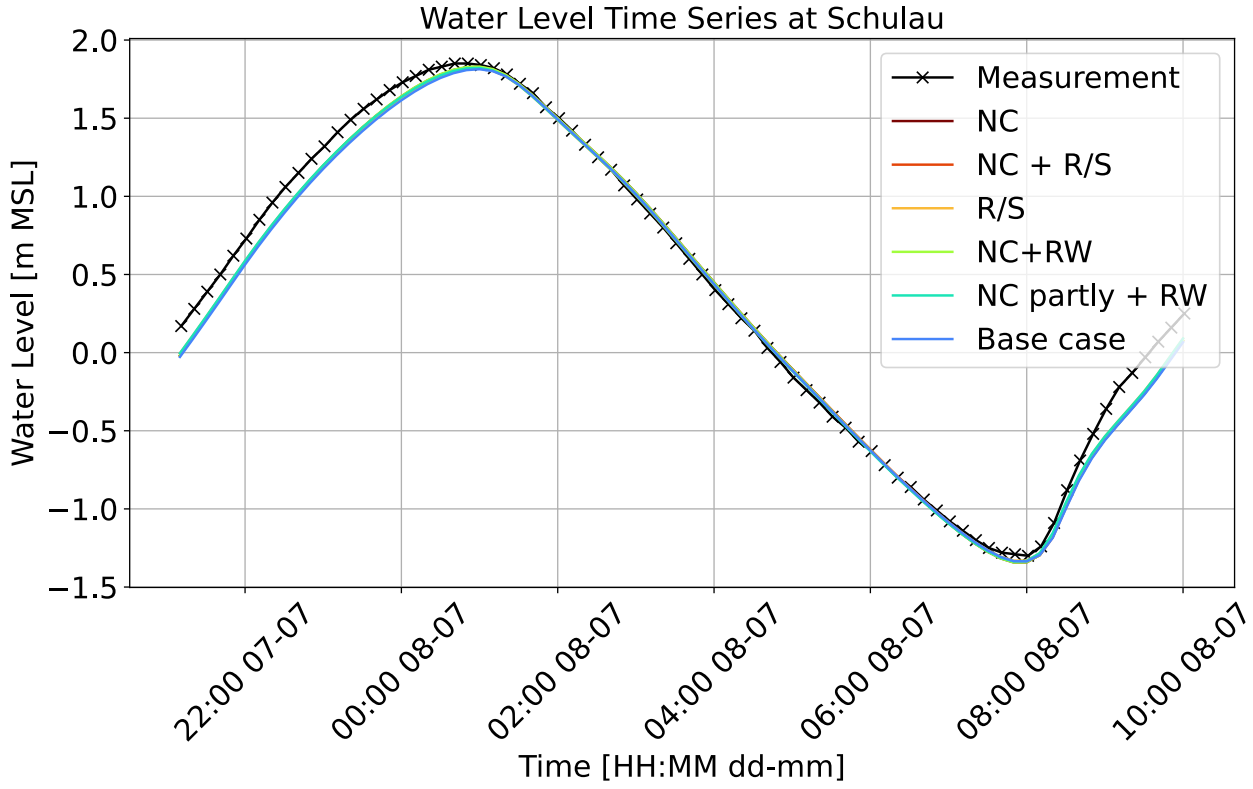

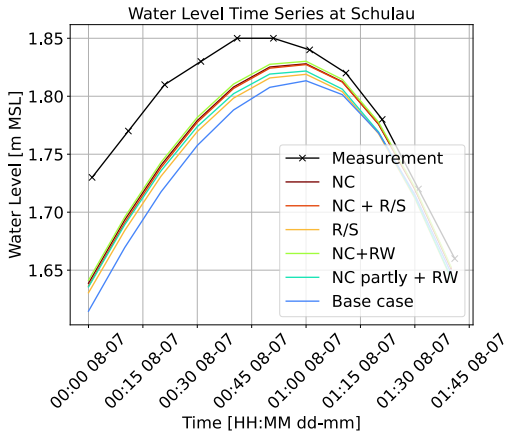

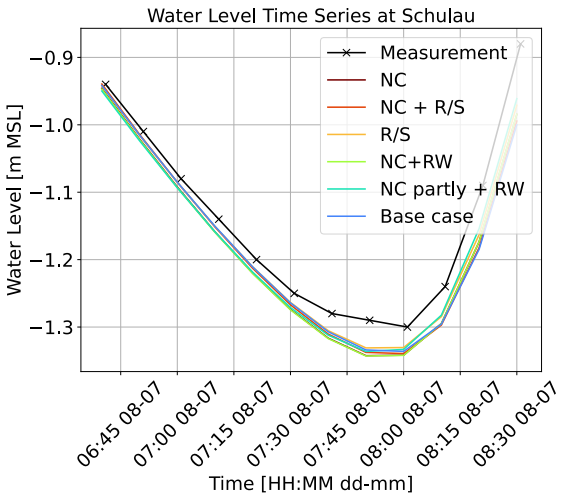

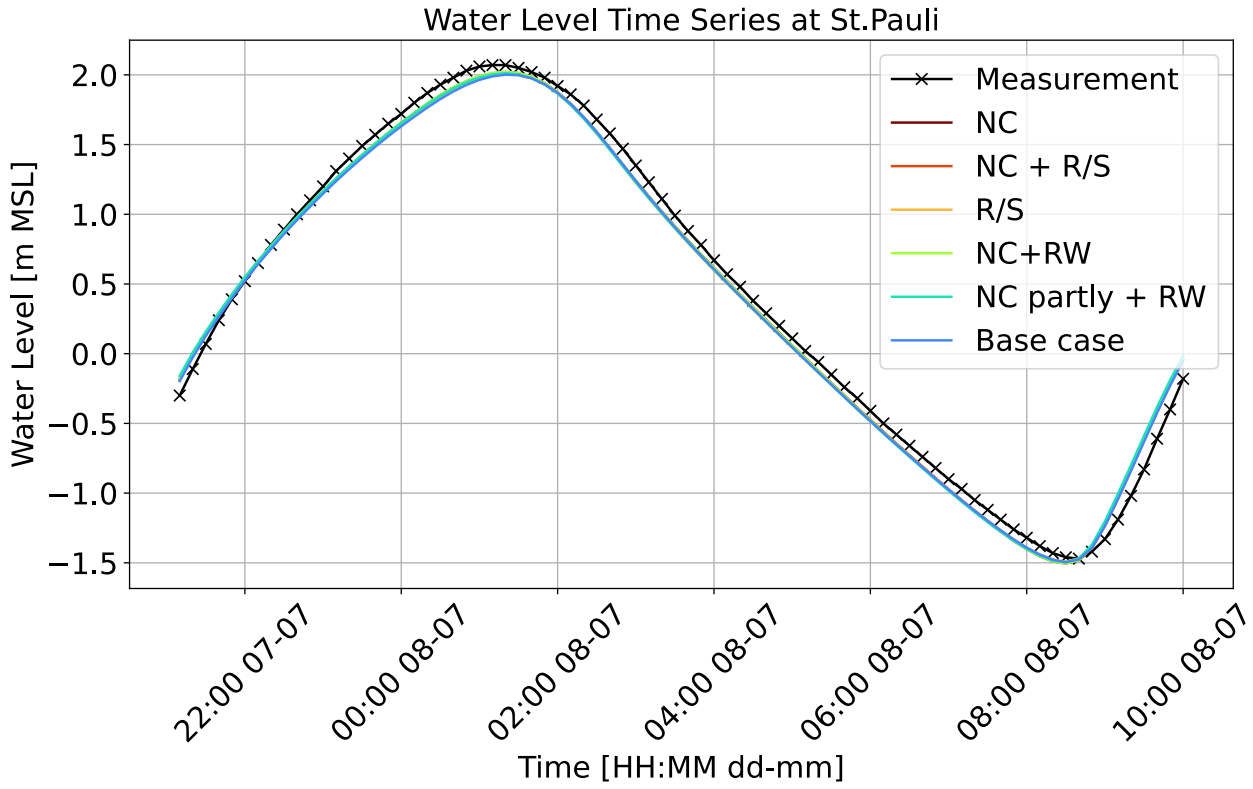
Water Level Time Series at St.Pauli
Water Level [m MSL]
2.0
1.5
1.0
0.5
0.0
−0.5
−1.0
−1.5
22:00 07-07
00:00 08-07
02:00 08-07
04:00 08-07
06:00 08-07
08:00 08-07
10:00 08-07
Time [HH:MM dd-mm]
Measurement
NC
NC + R/S
R/S
NC+RW
NC partly + RW
Base case

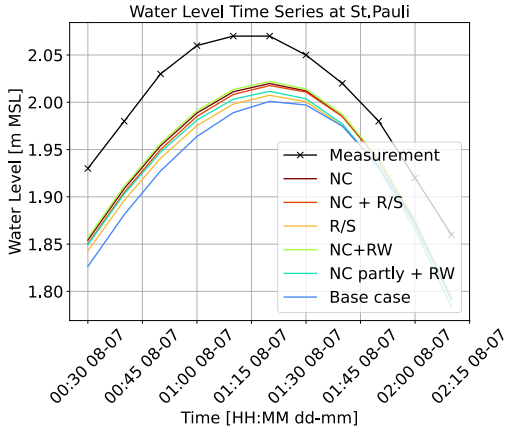
Water Level Time Series at St.Pauli
Water Level [m MSL]
2.05
2.00
1.95
1.90
1.85
1.80
00:30 08-07
00:45 08-07
01:00 08-07
01:15 08-07
01:30 08-07
01:45 08-07
02:00 08-07
02:15 08-07
Time [HH:MM dd-mm]
Measurement
NC
NC + R/S
R/S
NC+RW
NC partly + RW
Base case

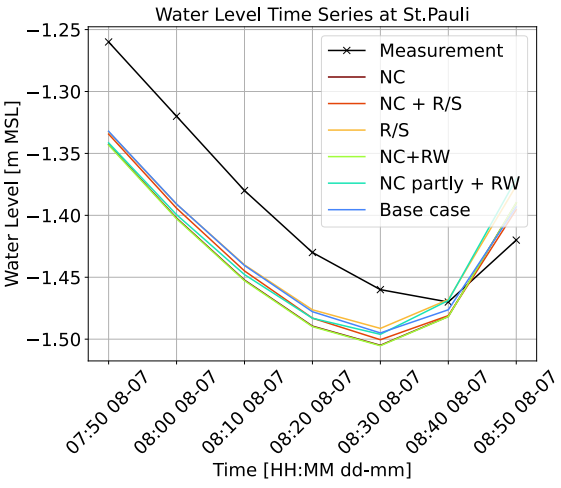
Water Level Time Series at St.Pauli
Water Level [m MSL]
−1.25
−1.30
−1.35
−1.40
−1.45
−1.50
07:50 08-07
08:00 08-07
08:10 08-07
08:20 08-07
08:30 08-07
08:40 08-07
08:50 08-07
Time [HH:MM dd-mm]
Measurement
NC
NC + R/S
R/S
NC+RW
NC partly + RW
Base case

D.5.2 Flow velocity results

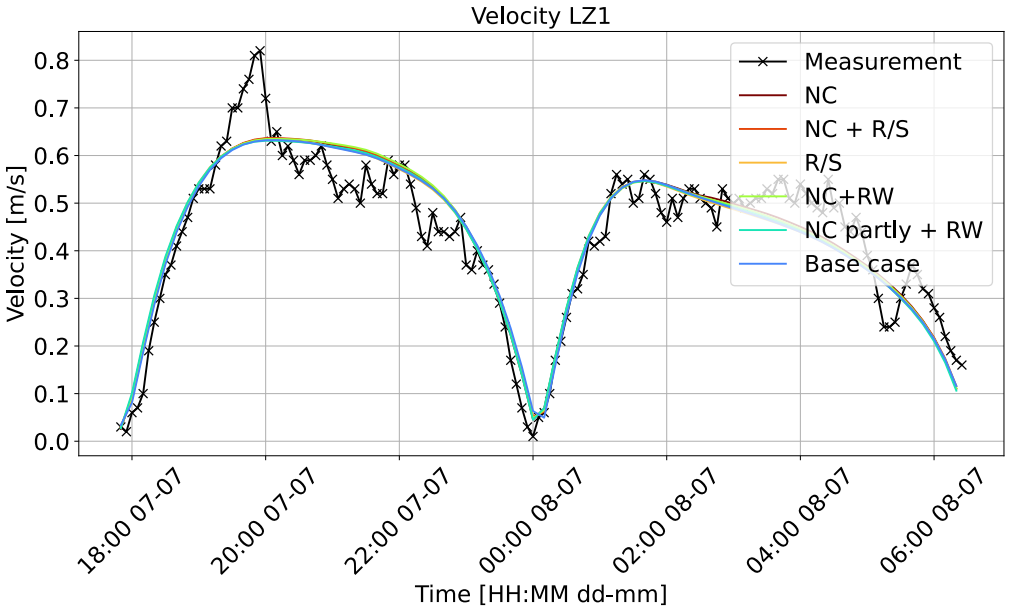

Appendix E

Q4: Roughness values and river discharge

E.1 Roughness values

E.1.1 Water level results

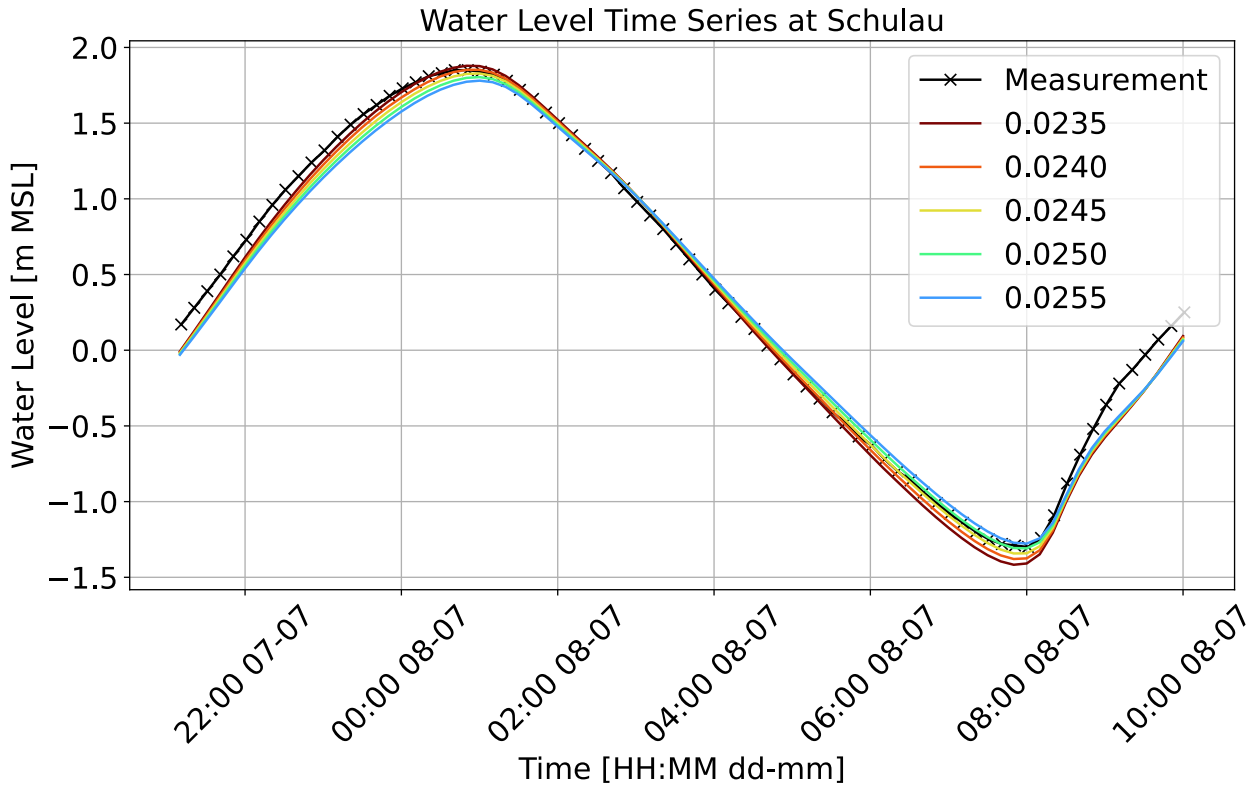

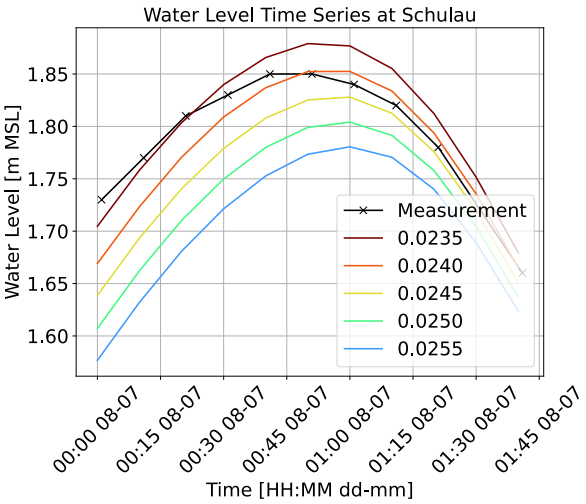
Water Level Time Series at Schulau
Water Level [m MSL]
1.85
1.80
1.75
1.70
1.65
1.60
Measurement
0.0235
0.0240
0.0245
0.0250
0.0255
00:00 08-07
00:15 08-07
00:30 08-07
00:45 08-07
01:00 08-07
01:15 08-07
01:30 08-07
01:45 08-07
Time [HH:MM dd-mm]

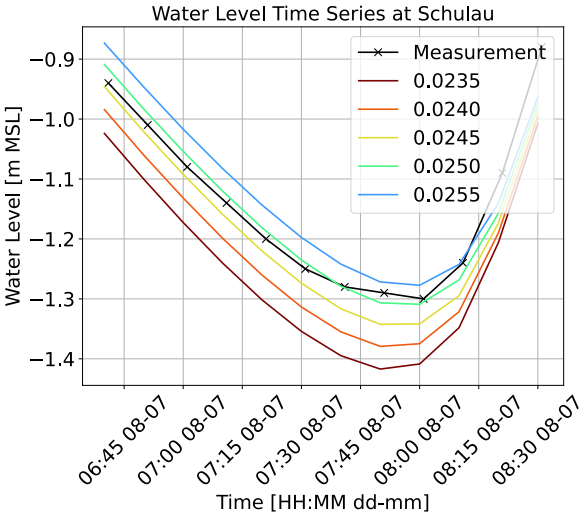
Water Level Time Series at Schulau
Water Level [m MSL]
−0.9
−1.0
−1.1
−1.2
−1.3
−1.4
Measurement
0.0235
0.0240
0.0245
0.0250
0.0255
06:45 08-07
07:00 08-07
07:15 08-07
07:30 08-07
07:45 08-07
08:00 08-07
08:15 08-07
08:30 08-07
Time [HH:MM dd-mm]

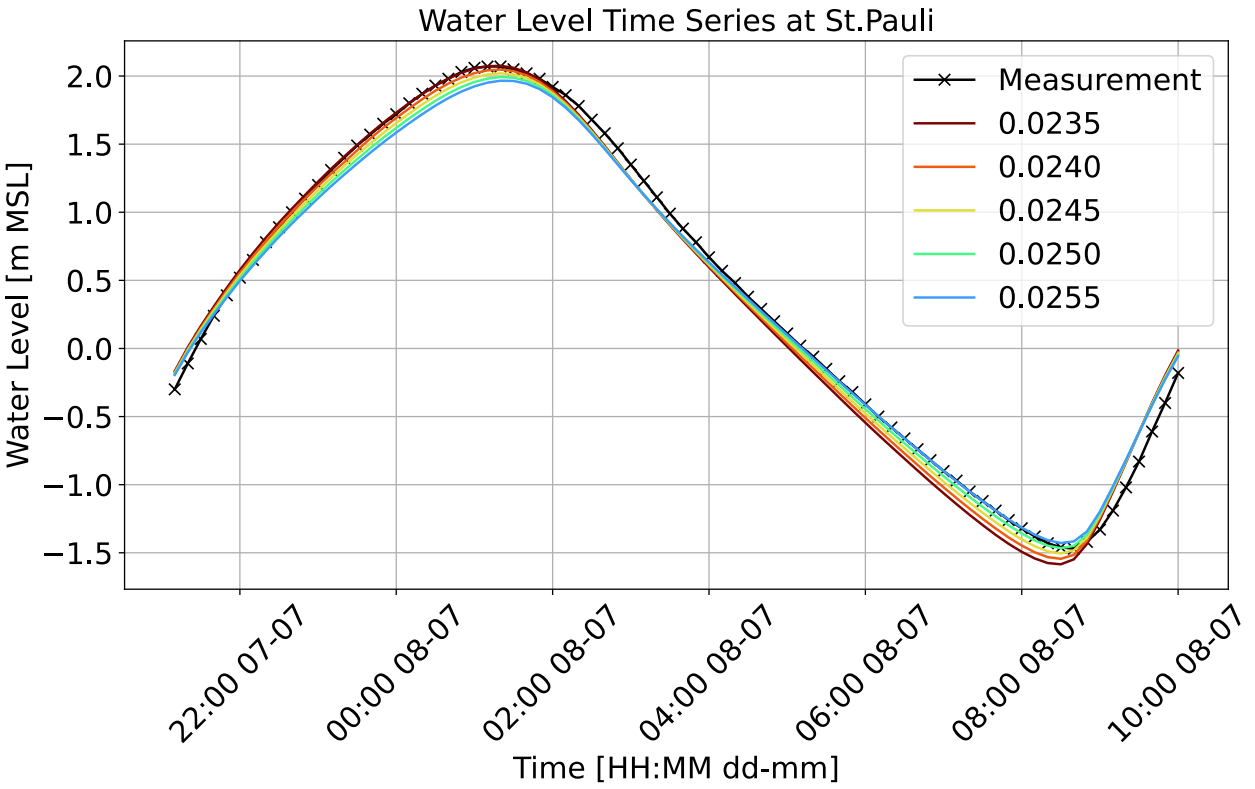
Water Level Time Series at St.Pauli
Water Level [m MSL]
2.0
1.5
1.0
0.5
0.0
−0.5
−1.0
−1.5
Measurement
0.0235
0.0240
0.0245
0.0250
0.0255
22:00 07-07
00:00 08-07
02:00 08-07
04:00 08-07
06:00 08-07
08:00 08-07
10:00 08-07
Time [HH:MM dd-mm]

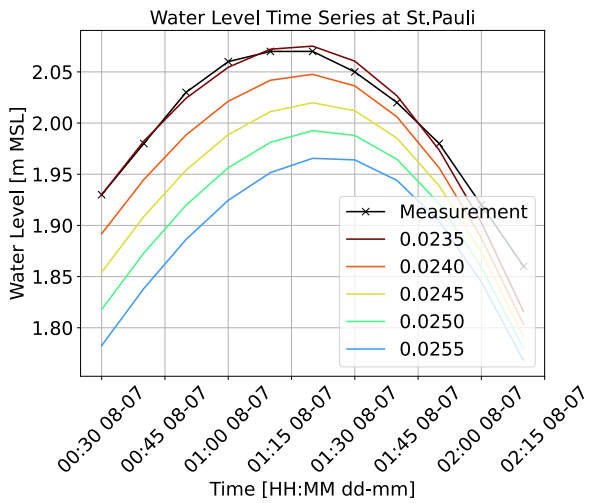

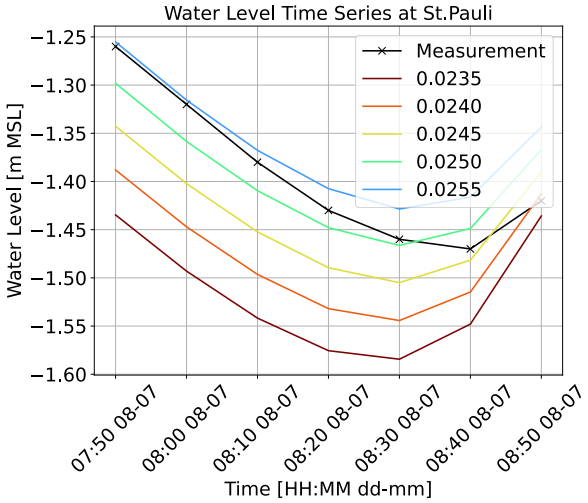

E.1.2 Flow velocity results

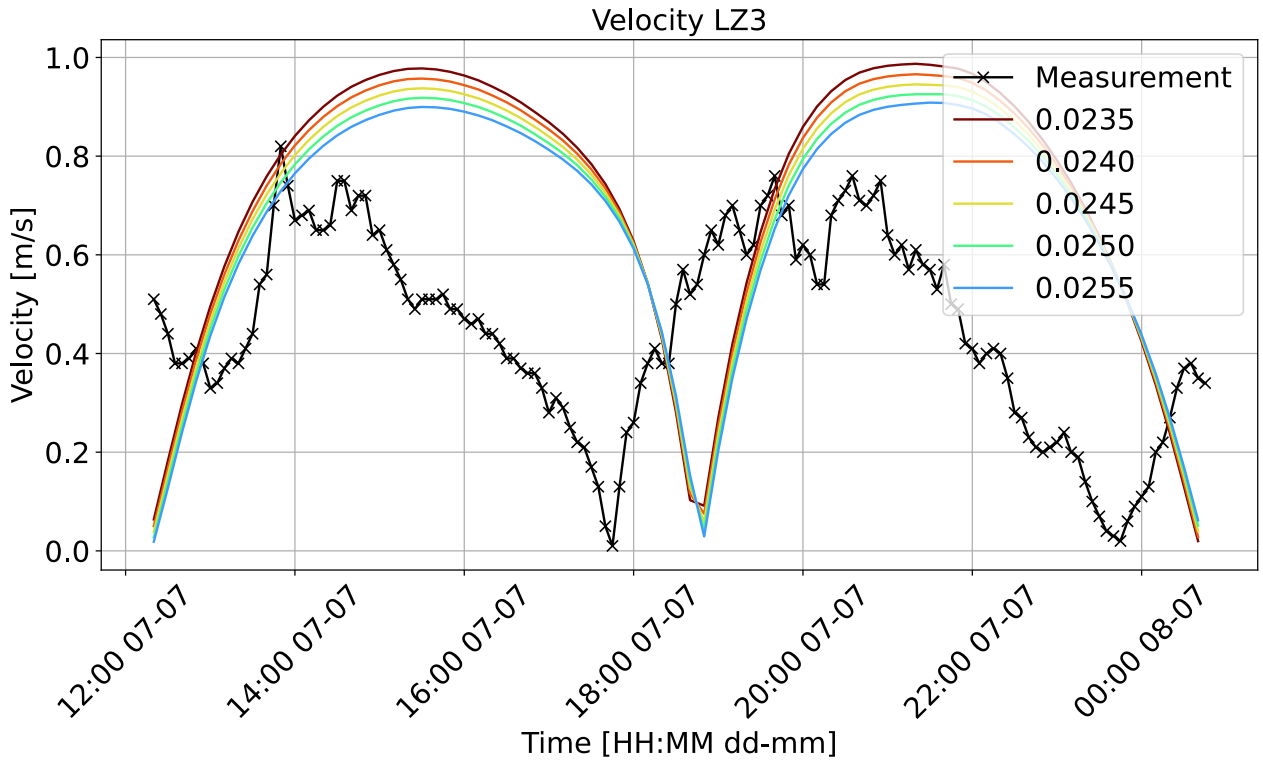

E.2 river discharge

E.2.1 Water level results

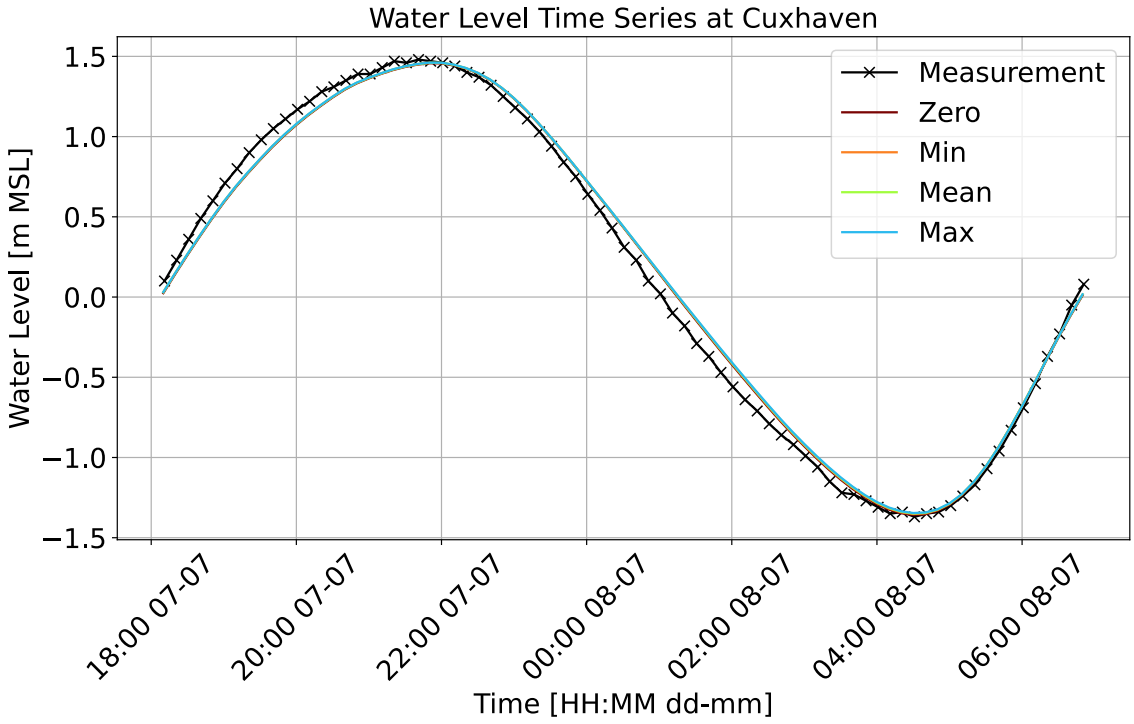

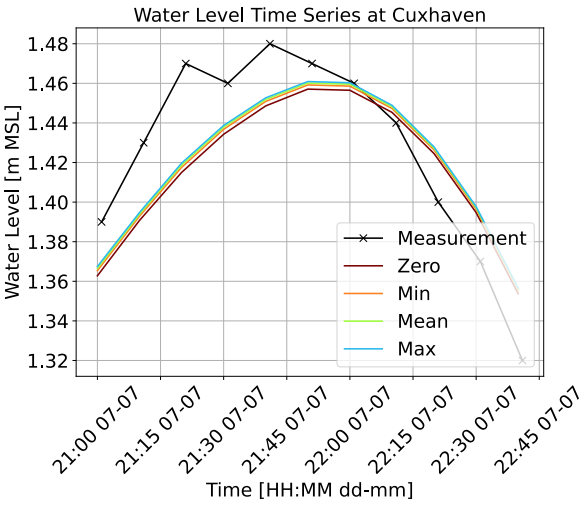
Water Level Time Series at Cuxhaven
Water Level [m MSL]
1.48
1.46
1.44
1.42
1.40
1.38
1.36
1.34
1.32
Measurement
Zero
Min
Mean
Max
21:00 07-07
21:15 07-07
21:30 07-07
21:45 07-07
22:00 07-07
22:15 07-07
22:30 07-07
22:45 07-07
Time [HH:MM dd-mm]

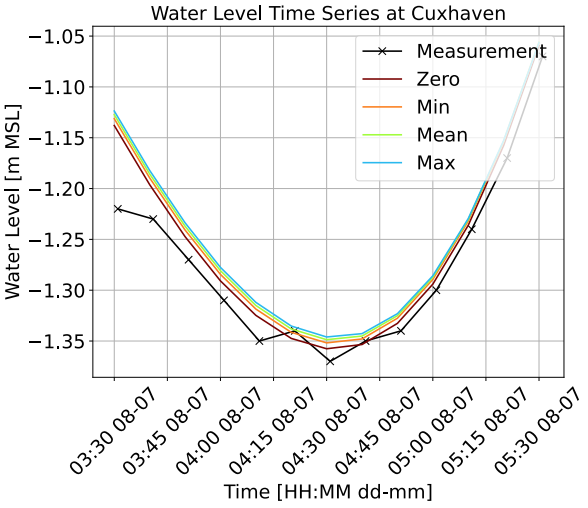
Water Level Time Series at Cuxhaven
Water Level [m MSL]
−1.05
−1.10
−1.15
−1.20
−1.25
−1.30
−1.35
Measurement
Zero
Min
Mean
Max
03:30 08-07
03:45 08-07
04:00 08-07
04:15 08-07
04:30 08-07
04:45 08-07
05:00 08-07
05:15 08-07
05:30 08-07
Time [HH:MM dd-mm]

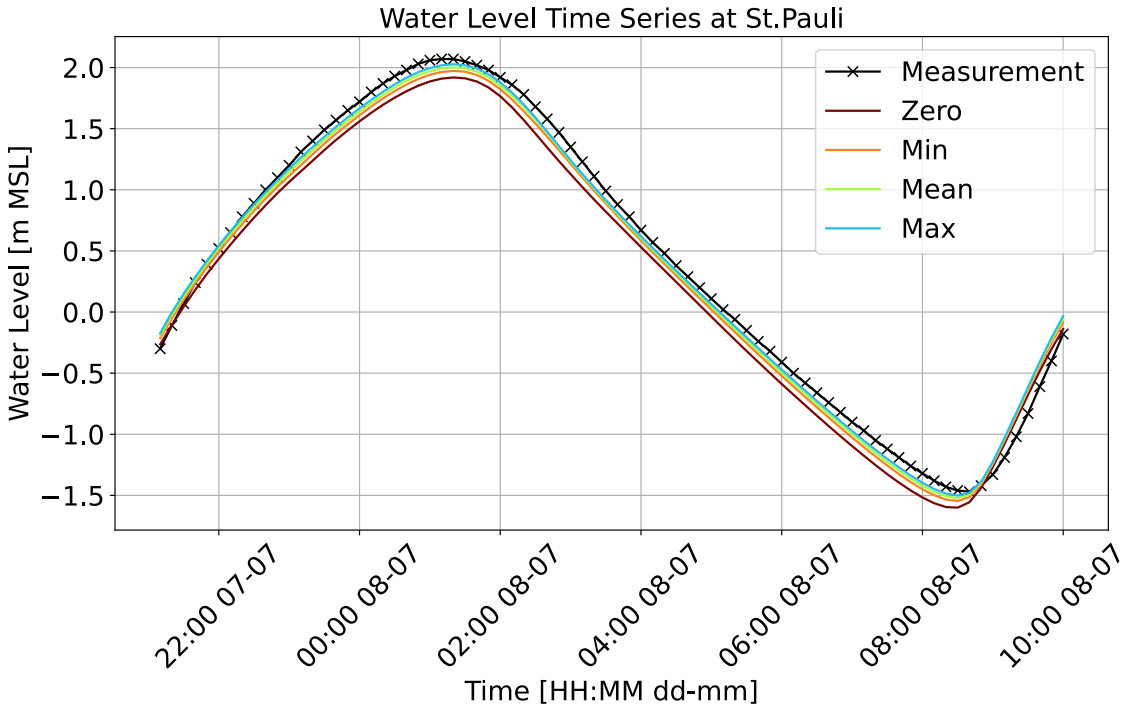
Water Level Time Series at St.Pauli
Water Level [m MSL]
2.0
1.5
1.0
0.5
0.0
−0.5
−1.0
−1.5
Measurement
Zero
Min
Mean
Max
22:00 07-07
00:00 08-07
02:00 08-07
04:00 08-07
06:00 08-07
08:00 08-07
10:00 08-07
Time [HH:MM dd-mm]

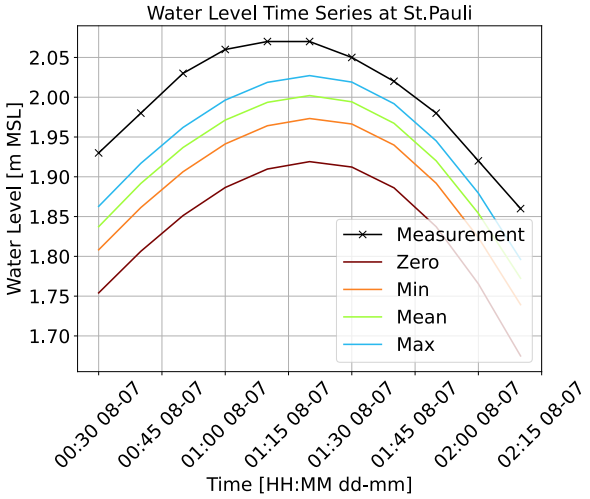

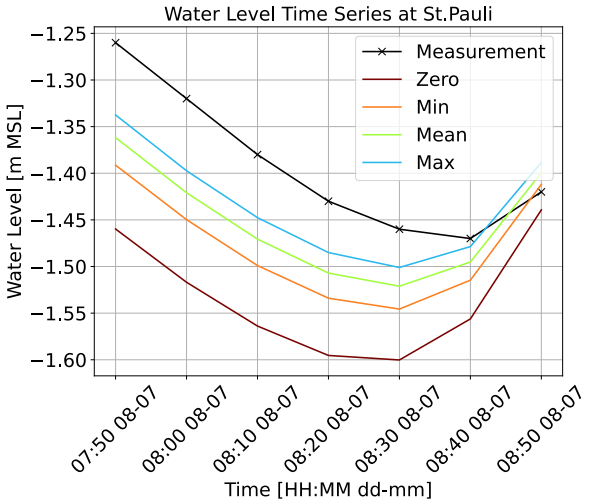

E.2.2 Flow velocity results